THE UNIVERSITY of ADELAIDE

HYDROGEN PRODUCTION VIA METHANE PYROLYSIS: MODELLING OF A SINGLE RISING AND PYROLYSING METHANE BUBBLE WITHIN A MOLTEN CATALYST BATH

A Dissertation submitted in partial satisfaction of the requirements for the degree of

Master of Philosophy

in

Mechanical Engineering

Candidate

Nazgol Mehrabian

Supervisors

Dr Mehdi Jafarian

Professor Graham ‘Gus’ Nathan

Dr Ahmad Seyfaee

School of Mechanical Engineering, Centre for Energy Technology

The University of Adelaide, AUSTRALIA

November 2022

DECLARATION OF AUTHORSHIP

I certify that this work contains no material which has been accepted for the award of any other degree or diploma in my name, in any university or other tertiary institution and, to the best of my knowledge and belief, contains no material previously published or written by another person, except where due reference has been made in the text. In addition, I certify that no part of this work will, in the future, be used in a submission in my name, for any other degree or diploma in any university or other tertiary institution without the prior approval of the University of Adelaide and where applicable, any partner institution responsible for the joint award of this degree.

The author acknowledges that copyright of published works contained within the thesis resides with the copyright holder(s) of those works.

I give permission for the digital version of my thesis to be made available on the web, via the University's digital research repository, the Library Search and also through web search engines, unless permission has been granted by the University to restrict access for a period of time.

I acknowledge the support I have received for my research through the provision of an Australian Government Research Training Program Scholarship.

Nazgol Mehrabian

Date: 20/11/2022

SUMMARY

The global targets for carbon-neutral hydrogen production by 2050 demonstrate the need to develop methods to produce a low-cost, low-emission form of hydrogen. Methane pyrolysis within a molten metal bath is currently a potential technique to meet this need. Despite having great techno-economic potential, this technique has not yet been demonstrated at an industrial scale, partly because of the lack of understanding of the mechanism. Molten metals are typically opaque, corrosive, and hard to maintain and handle, especially at temperatures over 1300 K, as is needed in pyrolysis reactors. Moreover, the presence of explosive and combustible gases such as hydrogen and methane, make it technically very challenging to perform in-situ measurements. To optimise the methane pyrolysis within bubble column reactors and hence minimise the cost of their scaling up, there is a need to develop both understanding about the multi-way coupling phenomenon of methane pyrolysis in a molten bath and reliable mathematical models. The present investigation aims to meet these needs.

In doing so, a dynamic one-dimensional numerical model of methane pyrolysis within a rising and pyrolysing bubble in a column of molten $Ni_{0.27}Bi_{0.73}$, as a molten catalyst, has been developed. The model predicts both the behaviour of the rising bubble in the column and the chemical reactions within it, accounting for any variations in the bubble radius and rising velocity, which have previously been assumed to be constant. A systematic sensitivity analysis was also undertaken. The reliability of the model was assessed through comparing its predictions with the experimental data available from the literature and a reasonable agreement was found. Furthermore, the results attained from the current calculations show that for the assessed conditions, more than 97% of the overall conversion of methane occurs at the bubble-molten bath interface. Furthermore, the bubble size and rising velocity inversely influence the methane conversion.

ACKNOWLEDGEMENTS

This work would not be possible without the academic support with which I have been provided. First and foremost, thanks to my supervisors, Dr Mehdi Jafarian, Professor Graham ‘Gus’ Nathan, and Dr Ahmad Seyfaee, for the deep care they have given to this project.

Without the aid of excellent academic staff, completing this project would have been infinitely more difficult. Special thanks also go to Professor Anthony Zander (Head of the School of Mechanical Engineering), Professor Andrei Kotousov (Chair of HDR Assessment at the School of Mechanical Engineering), Dr Lei Chen (Postgraduate Coordinator at the School of Mechanical Engineering), and Dr Alison-Jane Hunter (Technical English Editor at the School of Mechanical Engineering).

Also, many thanks go to all the professional staff in the school of Mechanical Engineering (especially Paula Billington and Terry Utting) at the University of Adelaide.

Special thanks to Professor Kazem Abhary and Professor Tahereh Ziaian for all their encouragement and support throughout my study.

I would like to express my gratitude to my husband, lovely daughter, and parents who supported and encouraged me to achieve my M.Phil. degree.

I am also thankful that this work has been funded by the Future Fuels CRC, supported through the Australian Government’s Cooperative Research Centres Program. I gratefully acknowledge the financial and in-kind support from all our research, government and industry participants.

LIST OF JOURNAL AND CONFERENCE PAPERS

1. Nazgol Mehrabian, Ahmad Seyfaee, Graham J. Nathan, Mehdi Jafarian, A Numerical Investigation of Methane Pyrolysis in a Molten Catalyst Bath–A Single Bubble Approach, Submitted to the International Journal of Hydrogen Energy.
2. Nazgol Mehrabian, Ahmad Seyfaee, Graham J. Nathan, Mehdi Jafarian, Hydrogen production via Methane Pyrolysis, CET event, 2021.
3. Nazgol Mehrabian, Ahmad Seyfaee, Graham J. Nathan, Mehdi Jafarian, Solar pyrolysis of methane, CET Research Day, Adelaide, 2020.

CONTENTS

LIST OF TABLES

LIST OF FIGURES

NOMENCLATURE

A_0 : pre-exponential factor [$1/s$]

A_c : Nozzle cross-sectional area [m]

Ar : Archimedes number [-]

a, b : Numerical parameters [-]

C : Concentration [$\mathrm{mole/m^3}$]

C_d : Drag coefficient [-]

c_p : Specific heat capacity [$\mathrm{J/kg.K}$]

E_a : Activation energy [$\mathrm{J/mol}$]

g : Gravity [$\mathrm{m/s^2}$]

h : Convective heat transfer coefficient [$\mathrm{W/m^2.K}$]

H : Height [mm]

ΔH : Reaction enthalpy [$\mathrm{J/mol}$]

k : Conductive heat transfer coefficient [$\mathrm{W/m.K}$]

Mo : Morton number [-]

Nu : Nusselt number [-]

p : Pressure [Pa]

P_c : Critical pressure of gas [Pa]

p_s : Nozzle perimeter [m]

r : Bubble radius [mm]

Re : Reynolds number [-]

R_g : Universal gas constant [$\mathrm{J/mol/K}$]

T : Temperature [K]

t : Time [s]

U : Rise velocity [$\mathrm{m/s}$]

V : Volume [$\mathrm{m^3}$]

X : Conversion of methane [-]

y_i : Mol fraction of species [-]

Z : Compressibility factor of gas [-]

z_B : Axial distance from the bottom of the column [mm]

z_P : Axial distance through the nozzle pipe [mm]

Greek letters

μ : Dynamic viscosity [$\mathrm{Pa.s}$]

ρ : Density [$\mathrm{kg/m^3}$]

σ : Surface tension [$\mathrm{N/m}$]

Ω : Collision integral [-]

τ : Residence time of the bubble [s]

Subscripts

B : Bubble

c : Critical

equ : Equilibrium

f : Final

$form$: Formation

g : Gas

$intf$: Interface

m : mean

mix : Mixture

nz : Nozzle

rxn : Reaction

ABBREVIATIONS

AC	Activated Carbon
CB	Carbon Black
DRM	Dry Reforming of Methane
HS	Headspace
MB	Molten Bath
MM	Molten Metals
POM	Partial Oxidation of Methane
PSA	Pressure Swing Adsorption
SMR	Steam Methane Reforming
WGS	Water-Gas Shift

CHAPTER 1

INTRODUCTION

1.1 Background and motivation

The threat of global warming, and its adverse physical impacts on the environment [1], has led to significant interest and attempts both to capture and sequestrate/reutilise emissions resulting from fossil-based fuels, and to use low emission/clean energy fuels such as hydrogen (H_2) [2]. Carbon dioxide (CO_2)emissions were ~6 billion tonnes in 1950, reaching 22 billion tonnes by 1990. Growth has continued until recent years, and it reached the highest ever level, 36.3 billion tonnes, in 2021 [3]. In this regard, the industrial sectors contribute to approximately a quarter of the world's CO_2 emissions [4]. By using zero-emission hydrogen in industries and automobiles instead of fossil fuels and the subsequent replacement of common internal combustion engines with fuel cells, a potential source of CO_2 emissions could be mitigated [2]. That is because combustion of hydrogen (H_2) produces water and therefore is a promising substitute for the current fossil fuels if it can be produced either from renewable resources or with CO_2 capture at a reasonable price [4-6]. However, hydrogen does not exist as a single molecule in nature. It is typically found in compounds such as

hydrocarbons and water. Hence, hydrogen must be produced from other materials, which requires both cost and energy [7].

According to the IEA report [8], the world's hydrogen demand in 2020 was approximately 90 Mt. Of this, ~78% of hydrogen was used in the form of pure hydrogen and the rest was mixed with carbon-containing gases, which were mainly used in steel manufacturing and methanol production industries. For example, Figure 1.1 shows the global hydrogen demand by industry sectors for chemical production in 2020.

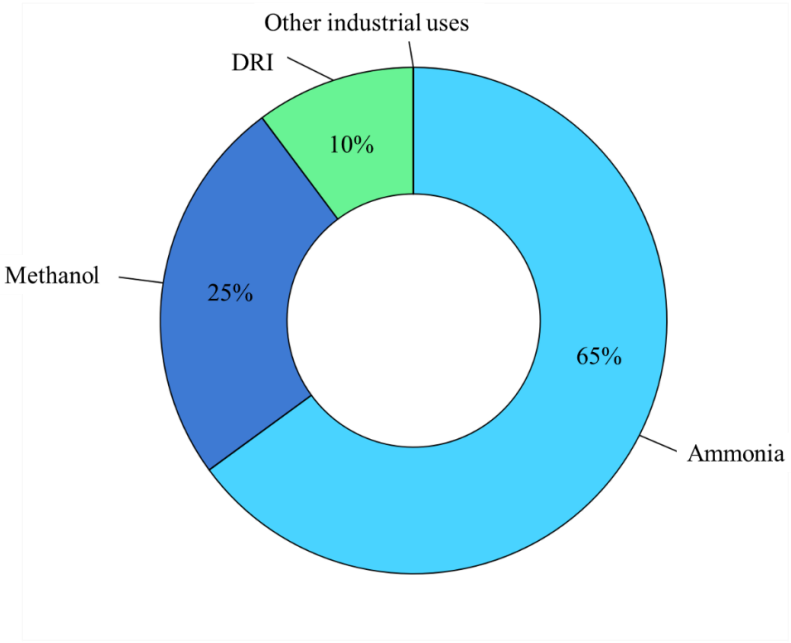

Figure 1.1. A presentation of global hydrogen demand for chemical production by industry sectors, in 2020 (IEA report: key indicators to track clean energy progress on hydrogen [8]).

Currently, about 96% of the world's hydrogen demand (i.e., ~76 Mtonnes/year) is produced via fossil fuel-based technologies, and only 4% is generated via renewable sources, i.e., electrolysis of water. Annually, nearly 900 Mt CO_2 is emitted to the environment (Figure 1.2 shows the share of fossil fuels in hydrogen production) [8].

By increasing the worldwide demand for hydrogen fuel, especially for industrial applications and automobiles [9], hydrogen production technologies without or with lower CO_2 emissions should be developed to replace the available technologies such as steam methane reforming (SMR) [10]. At present, as Figure 1.2 shows, around 50% of H_2 is produced via SMR, as the most cost-effective method for industrial-scale H_2 production at a cost of ~ \$1.5 $(kg\ H_2)^{-1}$ [11, 12]. SMR accounts for the chemical bonds breakage of methane molecules by reacting with high-temperature steam [11-14], which is an endothermic reaction and requires ~206 kJ/mol energy. To further enhance the yield of hydrogen, the carbon monoxide (CO) product in the reforming reaction is also reacted with steam, producing CO_2 and H_2. This exothermic reaction is called the water-gas shift (WGS) reaction and releases ~41 kJ/mol energy. The main drawback of SMR is the level of CO_2 emissions, which is 9-11 kg CO_2/kg H_2 [15, 16].

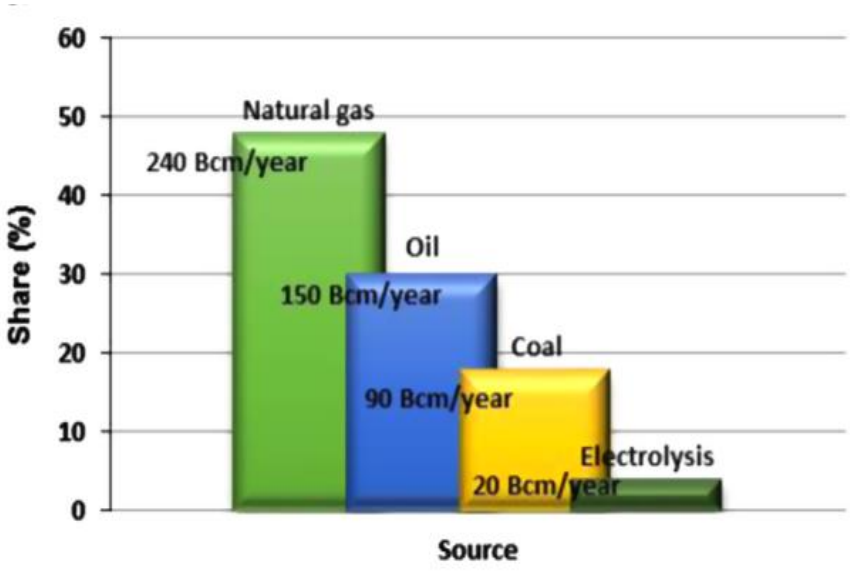

Figure 1.2. Worldwide hydrogen production by source (adapted from previous work [17] with permission).

Methane pyrolysis (Eq. 1.1) is a newly emerging, under-development technology for hydrogen production that has received significant attention due to its potential for low-cost H_2 production with minimal CO_2 emissions. It has manifested itself as a promising technology of hydrogen production without direct CO_2 emissions [4]. However, methane pyrolysis has not yet been demonstrated at industrial-scale [18-24], which is mainly attributed to the uncertainties associated with the optimisation of the reactor and material compatibility. It needs to be understood and used on a large scale as a substitute for the current pollutant commercial methods for hydrogen production [25]. Thermal decomposition of hydrocarbons has been studied since the 1900s [26-32]. Methane pyrolysis reaction is simpler than SMR as it does not need a water-gas shift reaction [7].

$$CH_4 \rightarrow C(s) + 2H_2 \quad \Delta H = +74.9\ \mathrm{kJ/mol} \tag{1.1}$$

Carbon black is a by-product of methane pyrolysis (Eq. 1.1). The conditions of the process are important as they have an effect on the type of produced carbon, its revenue, and hence the cost of the hydrogen production [33, 34]. Depending on the physical and chemical properties of the product carbon, it can have various applications as a raw material for manufacture of several products, such as paints [35], rubber [36], tyres, and fertilizers [37, 38].

Methane pyrolysis can be more favourable than SMR, not only because of its by-product revenue, but also because it requires about 50% less energy than SMR [39]. If the use of the pyrolysis of methane develops to an industrial scale, then there is a chance of a huge reduction in CO_2 emissions by industry [40]. Notwithstanding the abovementioned advantages, the conversion of methane in pyrolysis requires temperatures in excess of ~1200 K to achieve a conversion rate of more than 90%.

Methane decomposition reaction is kinetically controlled, needing a catalyst to achieve an appropriate reaction rate. To date, many solid-state catalysts, such as iron/nickel-based catalysts, have been assessed for methane pyrolysis [7, 41]. Nonetheless, these types of catalysts are deactivated after a short period of time, mainly due to the coking within their pore structure as a result of the solid carbon product from the pyrolysis reaction (Eq. 1.1). To address this challenge, the use of a molten metal catalyst bath in a bubble column reactor has been proposed, in which methane is dispersed as bubbles from submerged nozzles [16, 42]. Advantageously, the carbon product floats to the surface of the molten bath due to the huge density differences between the carbon and the molten bath. Moreover, gas bubbling flow in a molten metal bath enables a high rate of heat and mass transfer [43]. This not only provides a means for continuous separation of carbon from the molten bubble column, but also enables the significantly high heat and mass transfer rates relevant to gas-bubbling flow regimes (Figure 1.3a and b) [43-46]. In one estimate [47], about 250 reactions for methane pyrolysis were reported. Some studies [15, 20, 47-49] have considered a stepwise transformation to simplify the methane conversion reaction, as is briefly shown in Eq. 1.2:

$$CH_4 \rightarrow C_2H_6 \rightarrow C_2H_4 \rightarrow C_2H_2 \rightarrow H_2 + C\,. \qquad (1.2).$$

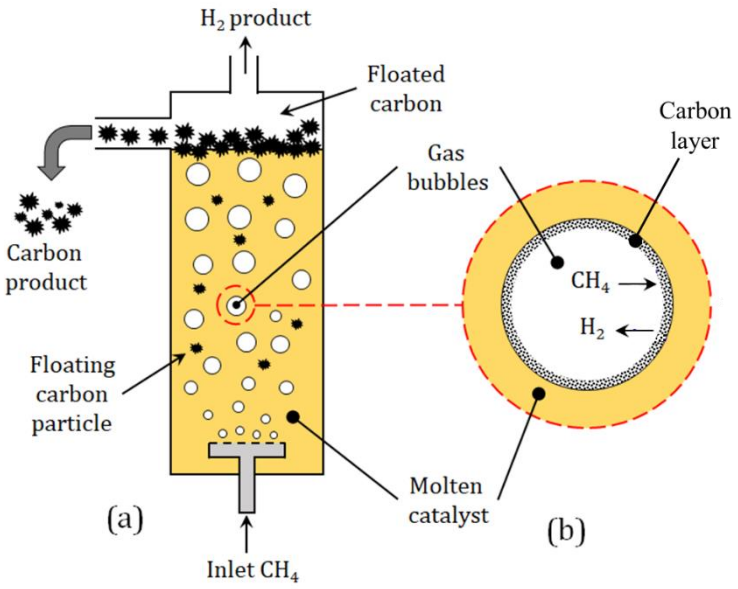

Figure 1.3. A schematic representation of, (a) a molten catalyst methane pyrolysis bubble column reactor, and (b) a single rising and pyrolysing bubble within the molten metal bath [15, 49].

The design and optimisation of methane pyrolysis in a molten metal bath requires a deep understanding of the kinetics of the reactions, hydrodynamics of the molten metal bubble columns and the interaction between the multi-way coupling mechanisms. To save time and resources for the scale-up of methane pyrolysis within a molten catalyst bath, one potential approach is to develop mathematical models of the underlying transport phenomena and reaction kinetics. This enables a better understanding of the phenomena needed to optimise the reactor. Fundamental understanding of the methane pyrolysis reaction under a gas-bubbling flow regime could mitigate not only the risks and cost of upscaling and commercialisation of the technology but also the amount of trial-and-error testing that is historically employed in this process.

1.2 Research objectives

This project aims to develop a fundamental understanding of methane pyrolysis within a single rising and pyrolysing bubble in a molten catalyst bubble column reactor. Accordingly, the following objectives were considered:

1. Develop a numerical model of a bubble, whilst it is rising and pyrolysing within a molten bath. This step will be performed through simultaneously solving the principle governing equations of mass, momentum, and energy. This method will determine the impact of changes in the bubble size, bubble rise velocity, liquid height, pressure, temperature of the gas and molten bath, and initial bubble composition on methane conversion.
2. Use the model to perform a comprehensive sensitivity analysis according to the independent factors to identify the parameters with the greatest impact on the methane conversion.

1.3 Structure of thesis

This thesis is designed using the by-publication format, containing four chapters as follows:

In Chapter 2 of the thesis a literature review was conducted to determine the key questions and gaps in the existing knowledge to establish a detailed framework for the current study. There is a discussion about research and extant studies, which investigated hydrogen production, as a clean fuel, via various catalytic/noncatalytic methods, including steam methane reforming (SMR), water splitting, and

coal/biomass gasification. Furthermore, methane pyrolysis as a potential technique for hydrogen production is discussed and investigated in this chapter.

In Chapter 3, a 1-D model of a rising and pyrolysing bubble in a molten catalyst bath is presented. The methodology and results of the current project are presented as a research paper in Chapter 3. It is of note that this manuscript has been submitted to the *International Journal of Hydrogen Energy*. The current status is under revision.

Chapter 4 includes the key conclusions and the main findings of the study, together with some suggestions for future work.

CHAPTER 2

LITERATURE REVIEW

2.1 Hydrogen as a clean fuel

Hydrogen is a potential clean fuel, as it burns without the emission of carbon products [5, 10]. In order to use hydrogen as a clean fuel efficiently in a range of industrial sectors, several developments need to be applied throughout the various steps of production, storage, distribution, and utilization [5, 50]. At the end of the 1960s, the first studies were undertaken on clean hydrogen production [12]. Even though hydrogen is very simple and plentiful in the universe, it is mainly found in combination with other elements, such as carbon or oxygen, in the form of compounds. Therefore, pure hydrogen needs to be produced via endothermic decomposition of other compounds, such as hydrocarbons or water [7].

Figure 2.1 shows a summary of the potential hydrogen production pathways and their applications. As shown, hydrogen can be produced via various technologies, including steam methane reforming [51], methane decomposition (pyrolysis) [49], coal/biomass gasification [52, 53], CO_2 reforming of methane [54], partial oxidation of oil/methane

[51, 55], and water splitting [56]. However, steam methane reforming, coal/biomass gasification, and partial oxidation of oil/methane have the big drawback of CO_2 emission. Methane pyrolysis and water splitting inherently have no direct CO_2 emissions. The need to address the increasing demand for hydrogen in various streams (Figure 2.1), including transportation [29], power generation [57], oil refining [58], metallurgy [59-61], and buildings [62], necessitates the development of zero-emission technologies for hydrogen production if the target for CO_2 emissions mitigation is to be met. In the following section a brief description of each technology is provided.

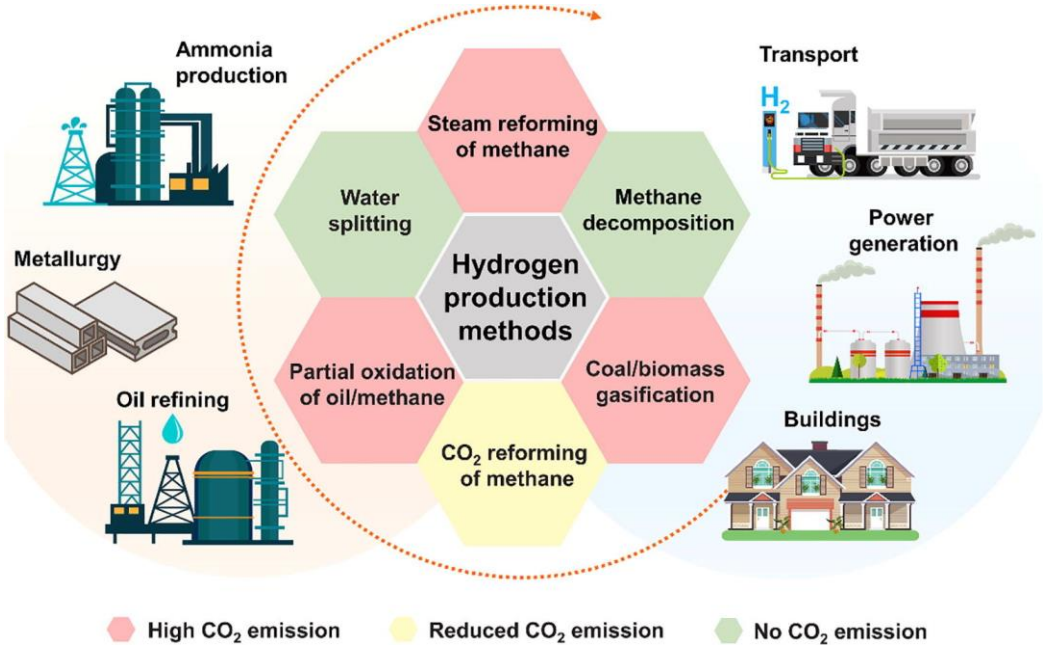

Figure 2.1. A schematic diagram of conventional hydrogen production technologies and uses of hydrogen. Adapted from previous work [63] with permission.

2.1.1 Water splitting

Electrolysis of water, as a pathway for hydrogen production, is an electrochemical process in which an electrical potential is employed to break the water molecule into O_2 and H_2. The associated reactions in the anode and cathode of a water electrolyser system are as follows (Eq. 2.1-2.3) [7, 12, 64]:

Anode: $H_2O \rightarrow \frac{1}{2} O_2 + 2H^+ + 2e^-$ (2.1).

Cathode: $2H^+ + 2e^- \rightarrow H_2$ (2.2).

Overall: $H_2O \rightarrow H_2 + \frac{1}{2} O_2 \qquad \Delta H^0_{form} = +235\ \text{kJ}$ (2.3).

As shown in Eq. 2.3, pure oxygen is the by-product of the water electrolysis reaction and can be utilized in industries such as steel making [65, 66]. The water splitting reaction is thermodynamically unfavorable because it needs some 235 kJ/mol of energy, which increases the price of hydrogen production via this technique [4]. It theoretically needs a voltage of 1.23 V; however, practically it is ~1.8 V to overcome the over-potential, including the Ohmic, activation and concentration losses. These depend on the wettability of the electrocatalyst with electrolyte, the bubble desorption over the electrodes, covering the active site of the electrocatalyst, and the hydrophilicity and aerophobicity of the electrode [67].

Figure 2.2 shows a schematic representation of a water electrolysis cell and water splitting. A variety of designs for the production of H_2 has been developed, which are summarized in Figure 2.2b, including two-electrode electrolysis of water (e.g., electrolysers), water splitting driven by green energy resources, such as photoelectrodes, solar cells, thermoelectrics, and triboelectrics, and pyroelectrics [67]. In the case of using green driving energy – as shown in Figure 2.2b - the total process

can be considered as a clean pathway for hydrogen production, such as via photo-electrochemicals [9], photo-chemicals, photo-biologicals, and solar thermochemical [1] means.

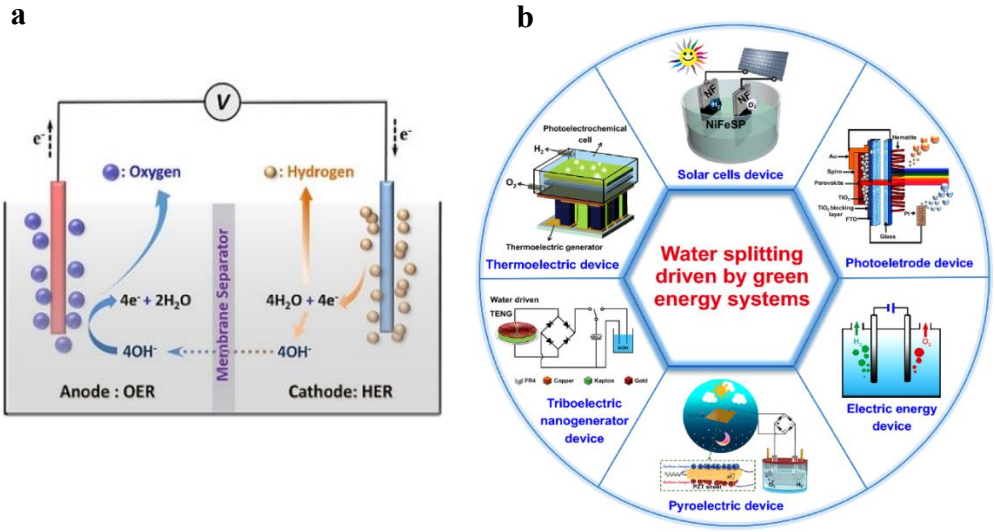

Figure 2.2. A schematic representation of, a) a water electrolysis cell under alkaline conditions, adapted from previous work [68], and b) water splitting techniques, from previous work [67] with permission.

Based on the 2020 IEA report [10], the contribution of water electrolysis to hydrogen production was ~0.03%. The cost of the electricity results in an expensive product hydrogen, with a cost of \$4.98 $(\text{kg } H_2)^{-1}$ for photocatalytic water splitting [11]. This key factor needs to be addressed for the dominant commercial hydrogen technologies, such as steam methane reforming (SMR), which is further discussed in section 2.1.4.

2.1.2 CO_2 reforming of methane

Dry (CO_2) reforming of methane (DRM) is a reaction to use of carbon dioxide and produces hydrogen as the product [69]. The reaction of carbon dioxide reforming reaction is presented in Eq. 2.4:

$$CH_4 + CO_2 \rightarrow 2H_2 + 2CO \quad \Delta H_{298K} = 247 \text{ kJ/mol} \qquad (2.4).$$

A reverse water-gas shift reaction occurs as a side reaction according to Eq. 2.5:

$$H_2 + CO_2 \rightarrow H_2O + CO \qquad \Delta H_{298K} = 41 \text{kJ/mol} \qquad (2.5).$$

Furthermore, carbon deposition is created under the Boudouard reaction as follows [70]:

$$2CO \rightarrow CO_2 + C \qquad \Delta H_{298K} = -172 \text{kJ/mol} \qquad (2.6).$$

This is an endothermic reaction and needs temperatures of > 1073 K to prevent carbon deposition and to achieve high equilibrium conversion of CH_4 and CO_2 to H_2 and CO [69]. In this method, Ni-based catalysts are used to facilitate the conversion reaction, even though the deactivation due to the carbon deposition is their main problem. Nobel metals (e.g., Rh, Ru, Pt, and Pd) can be used to promote the performance of the Ni-based catalysts; however, the process makes them uneconomical [69].

2.1.3 Gasification (Coal/Biomass)

Gasification is defined as a process in which the carbonaceous (carbon-based) raw material, for instance coal, can be converted into fuel gas or synthetic gas, called syngas.

In this process, the interactions between oxygen (typically from the air), steam, and coal or other feedstock (biomass) occur in a high temperature/pressure vessel, namely a gasifier. Under a series of chemical reactions, the feed is converted into syngas and residual ash/slag [71]. As shown in Eq. 2.7, CO_x is the by-product of this reaction:

$$\text{Biomass} \rightarrow \text{Char} + C_6H_6 + CO + H_2 + CO_2 + N_2 + CH_4 + H_2O + H_2S \quad (2.7).$$

To enhance the hydrogen production, CO is further reacted with water in a reaction called a water-gas shift (WGS) (Eq. 2.8) [53, 72]:

$$CO + H_2O \leftrightarrow CO_2 + H_2 \qquad \Delta H = -41\ kJ/mol \quad (2.8).$$

Using biomass, due to the high ratio of hydrogen to carbon, can address dependency on hydrocarbons for hydrogen production [73].

Despite the advantages of coal/biomass gasification in production of H_2, it has the drawback of CO_2 emission, especially if coal is used as the feedstock.

2.1.4 Steam methane reforming (SMR)

SMR is a commercial pathway for hydrogen production in which natural gas (e.g., methane, CH_4) is used as the feedstock of the process [7, 74]. It consists of two reactions: methane reforming and water-gas shift. Methane reforming (Eq. 2.9) is an endothermic reaction, which accounts for the chemical bonds' breakage of methane molecules by reacting with high-temperature steam [11-14]:

$$CH_4 + H_2O \leftrightarrow CO + 3H_2 \qquad \Delta H = +206\ kJ/mol \quad (2.9).$$

To further enhance the yield of hydrogen, the CO product from the reforming reaction is reacted with steam, producing CO_2 and H_2 through the water-gas shift reaction (Eq. 2.8). While reforming is a highly endothermic reaction, the water-gas shift reaction is slightly exothermic. In total, SMR is an endothermic process, and it requires high temperatures up to 1100 K [11-13]. Several conditions and parameters have been evaluated, based on the type of fuel employed [18, 75-78], the temperature [18, 79, 80], pressure [18, 81], etc. [82-84].

Currently, SMR is the most cost-effective technology for H_2 production, meeting some 48% of the world's H_2 demand [11, 12, 85]. As shown in Figure 2.3, a simplified SMR plant consists of three main process sections: methane reforming, water-gas shift (WGS), and CO_2 removal (pressure swing adsorbtion-PSA). Furthermore, the process plant requires two extra stages namely steam regeneration, to heat the cooled steam, and desulphurization, in order to make the poisoned catalyst reusable [7].

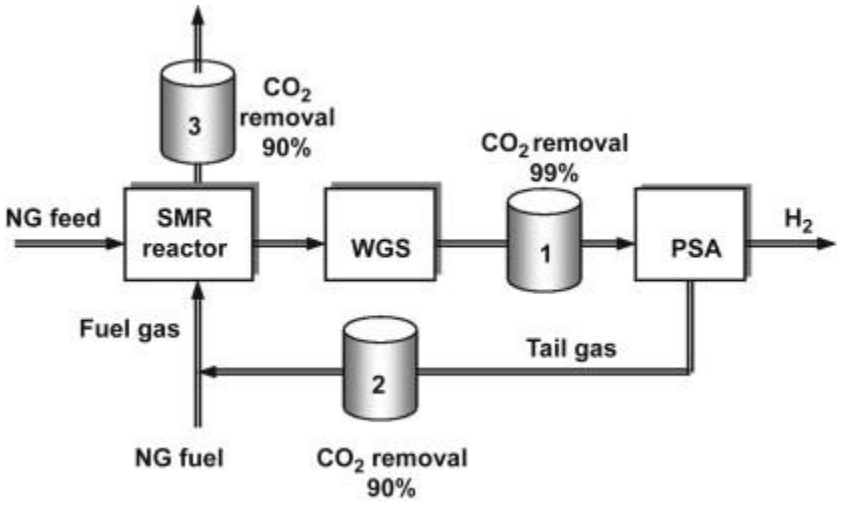

Figure 2.3. A simplified representation of a steam methane reforming (SMR) plant. Adapted from previous work [86], with permission.

As Eqs. 2.8 and 2.9 depict, CO_2, as a by-product of SMR, is the main drawback of this process. The whole process produces between 8-10 kg of CO_2 per kg of H_2. Out of this, CO_2 emissions, ~83%, are produced from the oxidation of carbon in the SMR process, and the rest derives from the fuel consumed to supply the process heat [18]. Even though the CO_2 product in SMR can be separated via carbon capture and storage techniques (CCS), it is an expensive process, with a cost of about $10-90 per ton of CO_2 for capture and separation [39, 40, 87-89], plus $3 to $12 per ton of CO_2 per 100 km for transportation through pipelines [12]. Furthermore, the storage of CO_2 needs specific geological reservoirs, which can be a limiting factor, and its technology still is not fully developed at a large scale [90]. Further to the CO_2 emissions, around 79.2 litres of water are used to process each kilogram of methane [91]. The application of methane in SMR is mainly restricted by the associated risks and costs of the CO_2 which is released into the atmosphere. If CO_2 emission can be mitigated, the use of hydrocarbons (e.g., CH_4) as a fuel for hydrogen production can continue until it reaches a competitive price and level of availability compared with the alternative feedstocks and fuels [40]. Hence, even though SMR is a mature technology, it suffers from significant environmental disadvantages [18, 85]. The polluting outcomes of the SMR method emphasise the requirements for a process with fewer or zero environmental challenges [92].

2.1.5 Partial oxidation of Methane

Partial oxidation of methane (POM) is another method for hydrogen production. Through POM, methane is partially combusted with oxygen in a non-stoichiometric ratio, which results in yielding CO and H_2 (Eq. 2.10) [93, 94]:

$$CH_4 + \frac{1}{2} O_2 \rightarrow 2H_2 + CO \quad \Delta H_{298K} = -36 \text{ kJ/mol} \qquad (2.10).$$

In contrast with highly endothermic steam methane reforming, POM is an exothermic process. Moreover, POM needs lower cost. However, it produces more CO_2 with an H_2 to CO ratio of 2 (Eq. 2.10) [94]. In this technique, catalysts are not mandatory at high temperature conditions; however, the use of catalysts increases the production of hydrogen [95].

The hydrogen production plant via POM, in addition to partial oxidation reactor, needs a shift reactor and hydrogen purification equipment. This technique needs no heat exchanger; thus a partial oxidation reactor is more compact than a steam reformer. The POM units provide a relatively high efficiency of 70 to 80%; however, POM systems are typically less energy efficient than steam reforming due to their requirement for the higher temperature condition [95].

2.1.6 Pyrolysis of methane

Pyrolysis is a combination of two Greek words, pyro (πυρο), which means fire, and lysis (λύσις), which means separation. This reaction occurs in the absence of oxygen and is mainly based on the thermal cracking of large hydrocarbon molecules into smaller ones [19, 96], using molecular vibrations created by high temperature [96].
Thermal decomposition of large hydrocarbon molecules is not a new method and has been used since the 1900s [30, 44, 47, 52, 97, 98]. In 1908, Bone *et al*. [30] discussed the thermal decomposition of a range of hydrocarbons, including methane, ethane, ethylene, and acetylene. The methane cracking process has been in use since 1970 to produce carbon black [99]. The results of previous work on methane pyrolysis based

on various factors, such as operation conditions, methods, reactions, and kinetic constants were evaluated and discussed by Khan *et al.* [97], which surveyed the research on methane pyrolysis up to 1970. Pyrolysis of various hydrocarbons such as biomass [52, 100, 101], polyacrylonitrile [102]**,** plastic wastes [103], cellulose [104, 105], coal [106], ceramics [107], and methane [4, 89, 108-111] have been also studied. Methane has the highest ratio of hydrogen to carbon in all hydrocarbon molecules. It is also the main component of natural gas. Therefore, direct cracking of methane for hydrogen production has received significant attention. This reaction is called pyrolysis and produces solid carbon (Eq. 1.1), as a by-product, instead of CO_2 produced through SMR [10]. This is a great advantage because carbon has industrial applications, and it could decrease the cost of hydrogen production. Furthermore, pyrolysis of methane requires less energy than SMR. That is, methane pyrolysis has been revealed as a potential substitute for current CO_2-emitting methods (e.g., SMR) for hydrogen production [112, 113]. Table 2.1 compares some properties of both of these methods.

Table 2.1. A comparison between SMR and pyrolysis of methane for hydrogen production [37].

Item	SMR	Methane pyrolysis
Reaction chemistry	$CH_4 + 2H_2O \rightarrow CO_2 + 4H_2$	$CH_4 \rightarrow 2H_2 + C$
Mols H_2 per mol CH_4	4	2
Endothermic heat of reaction KJ/mol CH_4	165	75.31
Process Thermal Efficiency for H_2 Production-%	75	58
CO_2 emission mol CO_2/mol H_2	0.43	0.05
Process unit operations	1. Reformer 2. Shift 3. Separation	1. pyrolizer 2. CH_4 separation if needed
By-product value	low	High materials potential
Process development	Well developed	Needs development

2.1.6.1 Equilibrium of the methane pyrolysis reaction

Equilibrium thermal decomposition of methane as a function of temperature for various pressures is illustrated in Figure 2.4 [40]. As shown, the temperature required for the full conversion of methane to H_2 depends significantly on pressure, such that the temperature of full conversion of methane to H_2 increases from 1373 K at 0.1 MPa to 1773 K at 3.5 MPa. Since in the methane decomposition reaction (Eq. 1.1) the net number of mols (mols of product - mols of reactant) is positive, it is expected that the bubble expands as the reaction proceeds. Thus, a low-pressure system could increase

methane conversion [16, 108] at the cost of an increase in the size of the reactor [40]. These are in agreement with the observations of Gueret *et al*. [114]; who, for the first time, studied the species distribution at equilibrium versus temperature and the effects of dilution by a hydrogen atom (H/C = 4, 6, and 8) and pressure. They also found that methane conversion increases with temperature, while it decreases with increasing of the pressure, which also increases the concentration of hydrogen-rich products (CH_4 - C_2H_4).

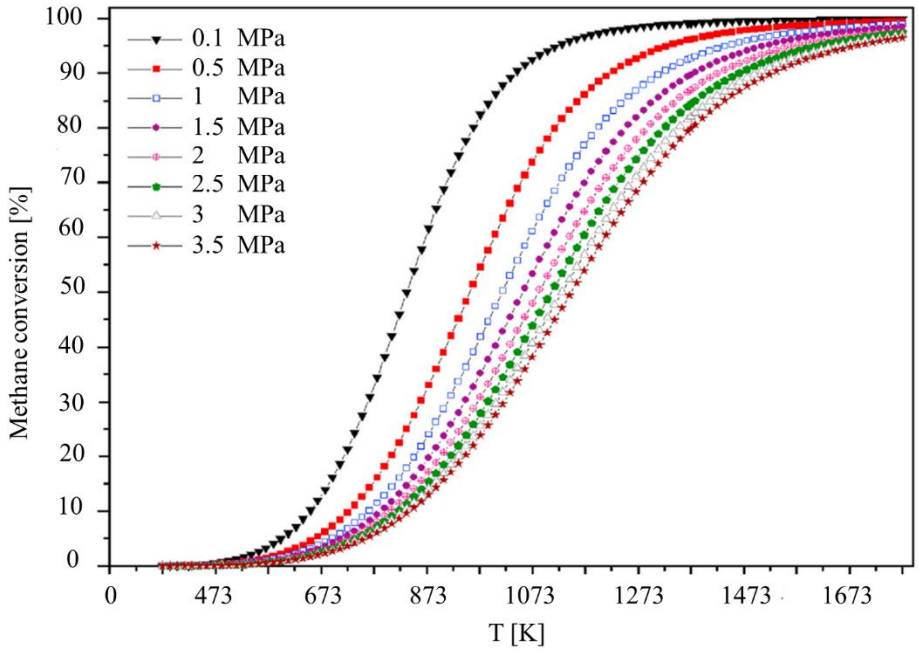

Figure 2.4. Equilibrium thermal decomposition of methane at a range of 0.1-3.5 MPa pressures as a function of temperature. Adapted from previous work [34] with permission.

2.1.7 Catalytic methane pyrolysis

Methane decomposition is found to be a kinetic control reaction with an activation energy of 312-450 kJ/mol, which can be lowered by means of a catalyst [8]. The kinetically controlled step in the methane cracking process is breakage of the bond between carbon and hydrogen (dissociation energy: 436 kJ/mol) [115, 116]. The type and the form of the catalyst may vary from metal-based to carbon-based, and molten to solid, respectively.

2.1.7.1 Solid-based catalysts

Solid-based catalysts, typically made of transition metals (e.g., Fe, Ni, and Co-based catalysts), have been widely used for hydrogen production [2, 10, 25, 74, 117-119]. However, these catalysts, despite having a high catalytic effect on methane pyrolysis, are prone to deactivate due to the deposition of carbon product within their pores [10, 12, 44, 120-123]. Fau *et al.* [124] proposed a mechanism for methane decomposition both in the gas phase (Figure 2.5a) and for solid-based catalysts (Figure 2.5b). However, as schematically shown in Figure 2.5b, the formed solid carbon in methane pyrolysis covers the active sites of the pore structure of the solid catalysts and hence decreases their catalytic effects. This phenomenon is called coking. It has been observed in many efforts that, after a few hours of operation, the catalyst is deactivated [18, 19, 46, 125], even though the carbon produced through the pyrolysis of methane may potentially play a role as a catalyst [15, 19].

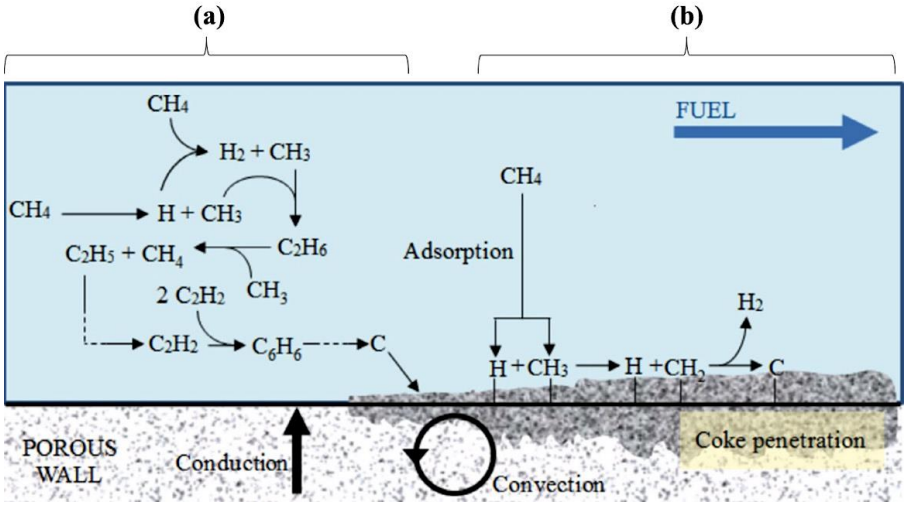

Figure 2.5. A schematic representation of the methane decomposition mechanism, a) within the gas phase, and b) on the surface of the solid-based catalyst. Adapted from previous work [124] with permission.

The use of carbon-based catalysts has been also considered, as they are less expensive than metal-based catalysts and have relatively high temperature tolerance [2, 91]. Moliner *et al*.[126] studied the influence of textural properties and surface chemistry of activated carbons as catalysts on the efficiency of methane decomposition. According to their results, catalysts' surface chemistry, specifically the active sites not the surface area, has a significant impact on the initial rate of the decomposition of methane; however, the catalyst deactivates rapidly. Also, the pore size distribution and surface area are important in carbon deposition on the catalyst and long-term sustainability of the process, such that mesopore carbons with their higher surface area are more stable than microporous carbons. Lee *et al*. [120] studied methane decomposition over several carbon-based catalysts in an air/water-free environment within a fluidized bed made of quartz with 0.055 m inner diameter and a height of 0.65 m. They found that the deactivation rate of the assessed carbon catalysts, due to the carbon deposition, in a fluidized bed, was the same as for a fixed bed reactor.

Another work [2] evaluated different carbon black (CB) catalysts with high external surface areas as an alternative to activated carbons (AC). The results showed that the tested CB samples illustrated a higher sustainability in comparison with the AC. The process continued until most of the surface was covered by a carbon layer produced from methane decomposition. Figure 2.6 shows the evolution of the hydrogen production (as a function of hydrogen concentration in volume within the leaving gas stream exiting the reactor), versus time during an eight-hour run at 1123 K and under a methane flowrate of 20 ml/min. As shown in Figure 2.6, the initial hydrogen productions are different for the studied CB samples, changing from less than 10% for the Carbopack B sample (methane conversion of 5.2%) and up to 70% (methane

conversion of 53.8%) for Fluka 03866 and Norit CG samples. According to the results, the Fluka 05120 sample retains its high activity at the end of the eight-hour run. CBs, owning a high surface area in comparison with AC, provide a relatively greater methane decomposition rate with later deactivation. This could be attributed to the surface chemistry and pore size distribution as the important factors in the initial rate of methane conversion and the long-term sustainability of the catalyst, respectively [2].

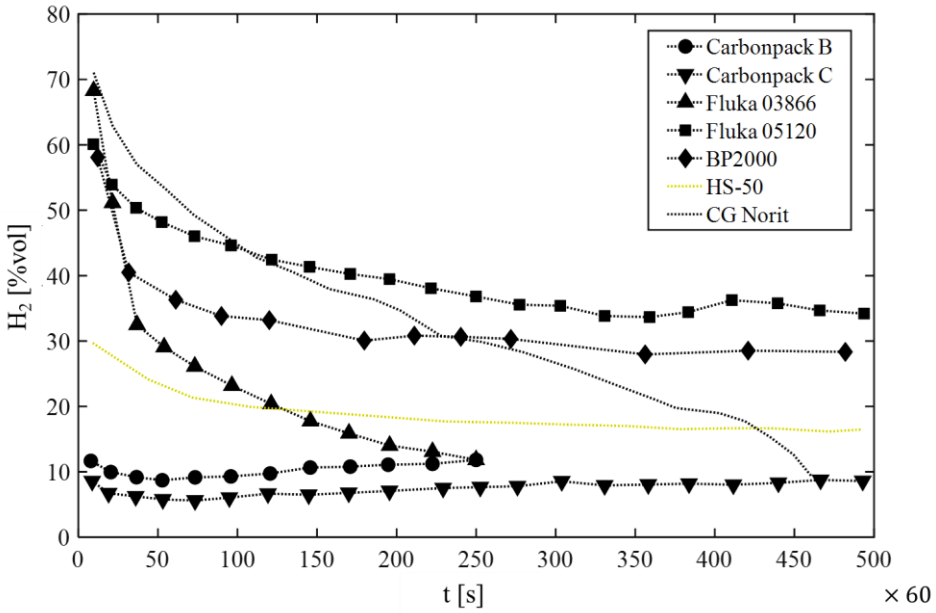

Figure 2.6. The evolution of the hydrogen production (as a function of hydrogen concentration in volume in the leaving gas stream exiting the reactor), versus time during an eight-hour run at 1123 K and under a methane flow of 20 ml/min for a series of carbon black samples. Adapted from previous work [2] with permission.

Qian *et al.* [119] investigated the effects of catalysts on methane pyrolysis in a fluidized bed by using $Ni/Cu/Al_2O_3$ and $Co/Mo/Al_2O_3$. The results showed that the

nickel catalyst achieved higher conversion than the cobalt catalyst. Murata *et al.* [118] studied the performance of various catalysts supported on alumina for methane cracking in a fluidized/molten metal bed. According to their results, the catalysts' activities were ordered as: $Ni/Ca/Al_2O_3 > Ni/Al_2O_3 > Co/Al_2O_3 > Fe/Al_2O_3$. A work [10] used three catalysts, namely $Ni/\gamma Al_2O_3$, $Ni/\alpha Al_2O_3$, and Ni/SiO_2, for catalysed methane cracking in a fluidized bed reactor. The effects of temperature, pressure (P_{CH_4}) and the particle size, and their interactions, on methane conversion, were studied for each catalyst. The temperature was the dominant parameter affecting the hydrogen production rate for all catalysts and the particle diameter had the strongest effect on the total amount of carbon deposited. The maximum methane conversion as a function of support type followed the order $Ni/SiO_2 > Ni/\alpha Al_2O_3 > Ni/\gamma Al_2O_3$.

Bai *et al*. [127] used coal char without any activation as a catalyst for methane decomposition. They studied the kinetics of the reaction as well as the change in properties of the catalyst surface. Their results showed that the initial rate of the reaction over char is almost the same as that of activated carbon under the same conditions. Also, the temperature of the reaction affects the activity and stability of the char catalyst. Previous studies [48, 128] confirmed that methane pyrolysis is a temperature-dependant process, in which, at higher temperatures, a shorter conversion time is required. Rodat *et al*. [125] designed a graphite cavity to assess methane pyrolysis at temperatures around 1940 K. Argon was applied to the system as an inert gas to control the mol fraction of the methane in the system. They reported 100% conversion of methane at a temperature of ~1940 K.

Liu *et al.* [129] investigated the effect of using carbon black (CB) and activated carbon (AC) as a catalyst, which increases the kinetics of the reaction in chemical looping for hydrogen production via methane decomposition (Figure 2.7). They used a chemical looping system with carbon as a circulating component between the reactors. The carbon is used as a catalyst and deactivated due to coking. Then, to activate the carbon, it is retreated with steam, which produces syngas. Based on their results, a part of the catalyst was damaged through the regeneration process. Moreover, CB and AC, as catalysts, showed opposite behaviours regarding the rate of deactivation. The latter showed a higher rate of deactivation than the former. Moreover, the catalytic activity of the CB, despite being lower than AC, was maintained for a longer period of time. The formed and deposited carbon on the surface of the studied catalysts have different orientations and chemical structures, and diverse shapes. In addition, the AC catalyst deactivated after approximately 6 hours of operation, while no variation was observed with the CB catalyst. Based on their investigations, the densely deposited carbon on the surface of the AC covers it thoroughly, mostly having an amorphous structure and deactivating the catalyst. The deposited carbon on the CB is relatively porous. However, the formation rate of active sites is greater than its deformation and it increases the number of exposed active sites: that is, the CB saves its activity over time. The main source of different shapes of deposited carbon on these two catalysts was reported to be the cross-linking graphene layer of AC and the spherical bent graphene layer of CB.

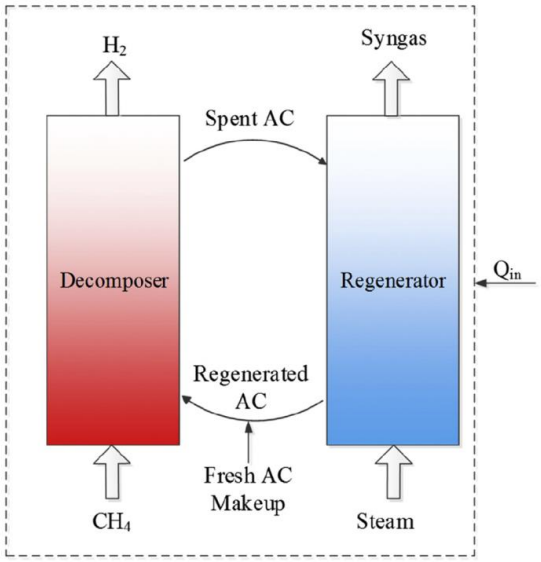

Figure 2.7. A schematic representation of the chemical looping concept applied to methane thermo-catalytic decomposition for continuous high-purity H_2 production using activated carbon (AC) as a catalyst. Adapted from previous work [129] with permission.

Alongside the advantages of the solid-base catalysed methane conversion process, carbon blockage and the cost of catalysts are the two main restricting factors in methane pyrolysis in gas-solid catalytic systems [13, 17, 25, 74]. Catalyst regeneration is practicable through burning off the carbon, gasification, and even acid treatment; however, these techniques are unfavourable as they either result in CO_2 emission or need extra costs [10, 25, 44, 45, 74]. In addition to the CO_2 generation, the hot spots within the catalysts caused by the combustion of the deposited carbon through the regeneration process can alter the morphology of the catalyst structure and decrease their activity [130]. One potential solution to address these challenges is the use of a liquid/fluidized bed catalyst, which will be discussed in subsequent sections.

2.1.7.2 Molten catalyst

The challenge of deactivation of the solid phase catalysts could potentially be addressed through employing a liquid catalyst [44, 45]. In this system, methane is dispersed as bubbles into the liquid catalyst bath [131, 132]. The methane bubbles decompose into H_2 and carbon, as the bubbles rise within the column. The produced carbon floats to the surface of the bath due to its much lower density than that of the molten bath. Subsequently, the challenges associated with the coking of the catalyst are eliminated as the methane content of the gas bubble is continually exposed to a carbon-free molten metal surface [4, 25, 87].

The use of a molten bath has recently garnered more attention as some molten metals, such bismuth (Bi) and iron (Fe) alloys, present a catalytic effect on methane decomposition [133]. The dissolution of the active metal catalysts (e.g., Ni, Pt, Pd) in the inactive low-melting temperature metals (e.g., In, Ga, Sn, Pb) can produce stable molten metal alloy catalysts [87].

Methane decomposition is a complicated mechanism that depends on the conditions of the experiment [134, 135]. Serban *et al.* [44] presented a setup in which either methane or natural gas was bubbled through a bath of either low-melting-point metals (e.g., lead or tin), granular or catalytic materials (e.g., silicon carbide, α-alumina, or NiMo/γ-alumina), or a mechanical mixture of molten metal and solid media. The methane conversions were reported based on the contact time between the methane and the molten bath, along with the methane bubble size. The most efficient systems containing Sn + SiC or Sn, where the natural gas bubbled through Mott porous metal filters, showed the product stream comprised of almost 80 and 70 vol% of hydrogen at 1023 K, respectively.

Plevan *et al.* [16] investigated the catalytic effect of molten tin (Sn) on methane decomposition at a temperature range of 973 to1223 K. According to their results, methane decomposition grows by increasing the temperature of the reactor and decreasing the gas flow rates from 200 to 5 mlN/min. They reported that the catalytic effect of the molten metal in the column needs to be well understood and considered, as it impacts directly on the methane conversion.

Upham *et al.*[87] achieved a methane conversion of 95% at 1338K in a 1.1-meter bubble column (Figure 2.8) and produced pure hydrogen without CO_2 by employing the 27% Ni–73% Bi alloy as a catalyst.

Figure 2.8. A schematic representation of a $Ni_{0.27}Bi_{0.73}$ molten catalyst bubble column for hydrogen production via CH_4 conversion with continuous carbon removal. Adapted from previous work [87].

Rahimi *et al.* [45] have studied carbon production via methane pyrolysis in a two-phase liquid column containing $Ni_{0.27}Bi_{0.73}$, KBr, and NaBr salts. They used a quartz

glass tube as the column to make the bubbles visible during the reactions, in which methane gas was injected through a submerged quartz tube. As with previous observations, their results also illustrated that a higher temperature of the liquid column results in higher methane conversion, while a high flow rate showed a diverse impact on the methane conversion such that a lower flow rate was favourable for higher conversion. The maximum conversion of methane in this setup was reported as approximately 38% at a temperature of 1273 K and a low flow rate of 10 ml/min. Also, they pointed to the formation of a carbon layer at the bubble and molten metal interface.

Kang *et al.* [25] investigated the catalysed methane decomposition via molten $KCl: MnCl_2$ mixtures in a bubble column reactor at a temperature range from 973 to 1323 K. The results showed that the activation energy decreased from approximately 300 kJ/mol for pure KCl to 161 kJ/mol in a 67:33 mol% mixture of $KCl: MnCl_2$. The pyrolysis at 30% methane in the molten $KCl: MnCl_2$ at 1323 K demonstrated a high hydrogen selectivity (~99%) in comparison with pure molten KCl (~90%), which produced multiple hydrocarbon co-products. The pyrolysis activity of the molten $KCl: MnCl_2$ was reported to stay stable for over 30 hours and produced a separable, highly graphitic carbon solid, which accumulated at the surface of the higher-density molten salt. Perez *et al.* [34] studied methane decomposition within a quartz bubble column of molten gallium as a heat transfer agent and catalyst. They achieved 91% methane decomposition at 1392 K for a methane and argon gas mixture, with a ratio of 50-50% and a residence time of 0.5 s within the bubble column. The results showed that the produced carbon is mostly carbon black. According to their estimations, if the product carbon has a revenue and a tax for CO_2 emissions, then methane pyrolysis

within a molten metal bubble column is comparable with the current economic technology (e.g., SMR).

It is noteworthy that methane decomposition within a molten catalyst bath is under investigation [87, 113, 116]. The bubble columns are simple to build and operate, even though the hydrodynamics of these reactors and the interactions between the gas and the liquid in two-phase systems, and gas, liquid, and solid in three-phase systems, are extremely complicated [131, 136]. The pressure of the system controls the bubble size in the column. According to Eq. 2.11, the bubble's radius holds an inverse relationship with the pressure difference between the gas inside the bubble and the liquid in the column [137]:

$$P_{\mathrm{B}} = \frac{2\sigma}{r_{\mathrm{B}}} + P_{\mathrm{MB}} \qquad (2.11).$$

where P_{B} is the pressure inside the bubble, σ is the surface tension, r_{B} is the bubble radius, and P_{MB} is the hydrostatic pressure of the molten bath in the column on top of the bubble.

Other operational parameters are also linked together, and variations in any factor have an impact on the others. For example, the height and type of the molten bath affect the bubble size by changing the pressure due to the molten column height and surface tension at the gas-molten bath interface, respectively. Based on Eq. 2.11, this impacts the bubble pressure and hence methane conversion. Moreover, the bubble size directly affects the bubble rise velocity; which, in turn, influences the bubble residence time within the molten bath [15, 138] and the contact time of the gas with the molten catalyst and hence its conversion. Furthermore, the gas flow rate, the size of the nozzle, the bubble size, and the bubble's superficial velocity also influence the gas hold-up, which is defined as the volume fraction of gas in the mixture of gas-liquid within a

column. The flow rate controls the time in which the bubble grows at the nozzle tip. Once the bubble detaches from the tube, its rise time through the molten bath depends on the depth, the bubble size, the melt density, its viscosity and the gas-bubbling flow regime [38]. By decreasing the diameter of the nozzle [15, 45, 139], the bubble size decreases. A smaller bubble size also decreases the mass transfer limitations inside the bubble, while it increases the surface area per volume of the bubble. Decreasing the bubble size decreases the buoyancy force acting on the bubble, which, in turn, leads to a lower rise velocity of the bubble, leading to a higher residence time [15, 138]. Hence, the contact time between the methane gas inside the bubble and molten bath increases, which can lead to an increase in methane conversion. Furthermore, the residence time affects the formation and decomposition of the heavy hydrocarbon intermediate products, such as acetylene (C_2H_2), which exist only within a short residence time range [15, 16, 125]. Even though there are studies on the effect of the nozzle type and size on the residence time of bubbles in liquid columns, they are not focused on methane pyrolysis in a liquid column [88, 140].

For the development, optimisation, and scale-up of molten metal bubble column reactors, a fundamental understanding of the bubble hydrodynamics and the associated transport phenomena, both inside the reactor and within the bubbles, is required. Because of the lack of in-depth knowledge of the multiphase process inside the columns, the design of these reactors has necessarily been based on empirical correlations and experiments performed in the laboratory- or pilot-scale setups [141]. Specifically for the methane pyrolysis, the effect of the temperature, pressure, gas flow rate, type of molten bath, size of the nozzle, superficial gas velocity within the column and the height of the liquid on the methane conversion need to be better understood if the system is to be optimised and demonstrated at large scales [44, 142, 143].

Table 2.2 summarizes the operational parameters in several studies on methane decomposition in liquid bubble columns. As shown in the first and second rows of Table 2.2 [16, 144], although both experiments were undertaken in a column of tin, they used different column sizes, designs and operational temperatures that made their data incomparable. That is the same for most of the available data in the literature. Hence, experimental data and numerical modelling are required for better identification of the fundamental parameters and the magnitude of their impacts on methane pyrolysis.

Table 2.2. Experimental conditions for methane pyrolysis that have been used by researchers.

Media	Type of column	Column height (mm)	Liquid height (mm)	Column diameter (mm)	Orifice diameter (mm)	T (K)	P (bar)	CH_4 conversion	H_2 yield	Ref
Sn	-	1268	-	40.6	0.5	1203-1448	1.013	-	78% @1448 K	[144]
Sn	Stainless steel	1150	600 and 1000	35.9	1	1023-1173		0-20%	Values for blank tube	[16]
Pb, Sn and Sn+SiC, alumina, NiMo/alumina	Stainless steel 304	355.6	101.6	25.4	6.35-1.58 + porous metal filter	873-1173	-	0-70%	70%- 80%	[44]

Sn and packed bed	Quartz glass in a stainless-steel tube	1268	250 Sn 850 packed bed	40.6	0.5	1093-1273	2	0-35%	0-30%	[15]
NiBi + (NaBr, KBr, and KCl)	Quartz glass tube	-	300, 400, 1000	22	2	1193-1273	-	5-40%	-	[45]
$Ni_{0.27}Bi_{0.73}$, catalyst (Ni, Pt, Pd), Low melting metals (In, Ga, Sn, Pb)	-	1100-1150	150	1100	3	1313-1338	0.01 - 1	0-95%	-	[87]

2.1.7.3 Numerical modelling of methane pyrolysis

Molten metal catalysts are opaque, typically corrosive, and hard to handle in a laboratory, especially at the high temperatures of relevance to methane pyrolysis within bubble column reactors. Hence, in-situ observations and measurements in these systems are technically challenging, time-consuming and expensive. Numerical modelling of these systems is a substantially useful tool to develop the required understanding of the phenomenon to optimise these systems. It minimises the costs, materials, and the risks. Catalan *et al*. [133] developed a non-catalytic kinetic model that is capable of optimisation of the diameter and length of the liquid metal bubble column reactor as well as the inlet pressure. By optimising the column dimensions, it will be possible to minimise the volume of the molten metal and consequently the cost of design and construction of the column. Farmer *et al.* [89] modelled a membrane bubble reactor for methane pyrolysis. This model was investigated to separate product hydrogen from the unreacted methane gases. This process eliminated the need for recycling un-reacted methane, thereby reducing the total equipment dimensions and energy costs. In this design, the product hydrogen can be completely collected via the membrane reactor walls without requiring a post reactor hydrogen separation.

Despite the advantages of modelling methane pyrolysis within a molten bath, reported models are scarce in the literature [15, 141, 145]. Nonetheless, models of a single bubble rising and pyrolysing methane within a molten metal bath have been reported previously. In the available models, the impact of variations of the bubble size and the bubble rise velocity in the column were not considered. This is despite the fact that calculations show that these factors vary significantly as the bubble rises and reacts

within the molten bath. Also, in these models, the effect of surface tension on pressure has been ignored [16, 42, 47]. Plevan *et al.* [16] developed a thermo-chemical model that fitted well with their experimental data obtained from pyrolysis of methane within a blank reactor. However, they reported that their model does not show a good agreement with the experimental results for the case of a system with a temperature of 1173 K and at flow rates lower than 25 mlN/min. This may be attributable to some of the governing simplified assumptions, such as a constant bubble size and rise velocity.

In a molten metal column, the density of the liquid bath is high (e.g. ~7033 kg/m^3 for molten tin [146, 147], and ~6095 kg/m^3 for gallium [34]); hence the hydrodynamic pressure on the bubble changes significantly during the bubble rise within the bath. As a result of decreasing the pressure on the bubble, Eq. 2.11, the bubble enlarges while it rises in the molten bath. Moreover, conversion of methane to H_2 produces 2 mols of H_2 per each consumed mol of CH_4. Consequently, the bubble size, despite the assumptions made in the available models [15, 16, 42], is not constant. Additionally, due to bubble radius changes through the column, the bubble rise velocity varies in practice [15, 16, 42]. Also, the size variation of the bubble in the liquid column directly impacts the mass transfer [148] and the heat transfer, both within the bubble and between the liquid bath and the bubble, which significantly affects the methane pyrolysis within the bubble column [15, 16, 149]. Considering a fixed bubble size and rise velocity in the model is like considering a bubble as a solid sphere, which is far from the reality. Thus, the available models could be improved by relaxing these simplifying assumptions.

2.2 Summary of identified gaps

Based on the literature review, the following gaps in the knowledge of hydrogen production via methane pyrolysis in a molten metal bubble column were identified:

1. Neither the impact of the size variation of the bubble while it rises within the column nor changes to the methane concentration have been considered previously. The bubble size was previously assumed to be constant throughout the column, even though the bubble expands when it rises. This expansion occurs for two reasons. Firstly, the pyrolysis reaction generates two molecules of hydrogen from each molecule of methane within the bubble. Secondly, the hydrostatic pressure on the bubble decreases as it rises within the molten bath.
2. The bubble rise velocity is another factor that has been overlooked in previous studies. This is an important parameter as it affects the residence time of bubbles within the molten bath and consequently the extent of the reaction.

The following chapter presents the results of a fundamental study on the effects of the abovementioned parameters.

2.3 References- Chapter 1 and Chapter 2

[1] K. Keller, Bayesian Decision Theory and Climate Change, Encyclopedia of Energy, Natural Resource, and Environmental Economics, (2013) 1-4.

[2] M.J.L. I. Suelves, R. Moliner, J. L.Pinilla, H. Cubero, Hydrogen production by methane decarbonization: Carbonaceous catalysts, International Journal of Hydrogen Energy, 32 (2007) 3320-3326.

[3] Global CO2 emissions rebound by nearly 5% in 2021, approaching the 2018-2019 peak, Global Energy Review, (2021).

[4] M.S.M. Gregory A. Von Wald, D. Chester Upham, Adam R. Brandt, Optimization-based technoeconomic analysis of molten-media methane pyrolysis for reducing industrial sector CO2 emissions, Sustainable Energy Fuels, (2020).

[5] T.L. Tiina Keipi, Terese Løvås, Henrik Tolvanen, Jukka Konttinen, Jukka Konttinen, Methane thermal decomposition in regenerative heat exchanger reactor: Experimental and modeling study, Energy, (2017) 823-832.

[6] D.P.S. Javier Dufour, José L. Gálvez, Antonio González, Enrique Soria, José L. G. Fierro, Life cycle assessment of alternatives for hydrogen production from renewable and fossil sources, International Journal of Hydrogen Energy, 37 (2012) 1173-1183.

[7] E.C. Ashraf M. Amin, William Epling, , Review of methane catalytic cracking for hydrogen production, International Journal of Hydrogen Energy, 36 (2011) 2904-2935.

[8] Key indicators to track clean energy progress on hydrogen, (2020).

[9] O. Bethoux, Hydrogen Fuel Cell Road Vehicles: State of the Art and Perspectives, Energies, 13 (2020).

[10] E.C. Ashraf M. Amin, Zuhair Malaibari, William Epling, Hydrogen production by methane cracking using Ni-supported catalysts in a fluidized bed, International Journal of Hydrogen Energy, 37 (2012) 10690-10701.

[11] I.R.E. Agency, Hydrogen, (2019).

[12] A.K. N. Ozalp, M. Epstein, Solar decomposition of fossil fuels as an option for sustainability, International Journal of Hydrogen Energy, 34 (2009) 710-720.

[13] A.R. Abánades, Renu Kumar Geißler, Tobias Heinzel, Annette Mehravaran, Kian Müller, George Plevan, Michael Rubbia, Carlo Salmieri, Delia Stoppel, Leonid Stückrad, Stefan Weisenburger, Alfons Wenninger, Horst Wetzel, Thomas,

Development of methane decarbonisation based on liquid metal technology for CO2-free production of hydrogen, International Journal of Hydrogen Energy, 41 (2016) 8159-8167.
[14] B.H. Yutong Qi, Jingli Luo,, Dynamic modeling of a finite volume of solid oxide fuel cell: The effect of transport dynamics, Chemical Engineering Science, 61 (2006) 6057-6076.
[15] M.P. T. Geißler, A. Abánades, A. Heinzel, K. Mehravaran, , C.R. R. K.Rathnam, D. Salmieri, L. Stoppel, S. Stückrad, A. Weisenburger, H. Wenninger, Th. Wetzel, Experimental investigation and thermo-chemical modeling of methane pyrolysis in a liquid metal bubble column reactor with a packed bed, International Journal of Hydrogen Energy, 40 (2015) 14134-14146.
[16] T.G. M. Plevan, A. Abánades, K. Mehravaran, R. K. Rathnam, C. Rubbia, D. Salmieri, L. Stoppel, S. Stückrad, Th. Wetzel, Thermal cracking of methane in a liquid metal bubble column reactor: Experiments and kinetic analysis, International Journal of Hydrogen Energy, 40 (2015) 8020-8033.
[17] W.M.A.W.D. U. P. M. Ashik, Hazzim F. Abbas, , Production of greenhouse gas free hydrogen by thermocatalytic decomposition of methane – A review, Renewable and Sustainable Energy Reviews, 44 (2015) 221-256.
[18] E.R. A. Abánades, E. M. Ferruelo, F. Hernández, A. Cabanillas, J. M. Martínez-Val, J. A. Rubio, C. López, R. Gavela, G. Barrera, C. Rubbia, D. Salmieri, E.Rodilla, D.Gutiérrez, Experimental analysis of direct thermal methane cracking, International Journal of Hydrogen Energy, 36 (2011) 12877-12886.
[19] S.A. Sylvain Rodat, Julien Coulié, Gilles Flamant, Kinetic modelling of methane decomposition in a tubular solar reactor, Chemical Engineering Journal, 146 (2009) 120–127.
[20] G.T.a.S.S. D. C. Toncu, On methane pyrolysis special applications, Materials Science and Engineering, (2015).
[21] T.L. Tiina Keipi, Terese Løvås, Henrik Tolvanen, Jukka Konttinen, Methane thermal decomposition in regenerative heat exchanger reactor: Experimental and modeling study, Energy Conversion and Management, 135 (2017) 823-832.
[22] S.R.b. G. Maag a, G. Flamant b, A. Steinfeld, Heat transfer model and scale-up of an entrained-flow solar reactor for the thermal decomposition of methane, International Journal of Hydrogen Energy 35 (2010) 13232-13241.

[23] S.A. Sylvain Rodat, Gilles Flamant, Experimental Evaluation of Indirect Heating Tubular Reactors for Solar Methane Pyrolysis International Journal of Chemical Reactor Engineering 8(2010).
[24] Y.X. Zhang-Jing Zheng, A novel system for high-purity hydrogen production based on solar thermal cracking of methane and liquid-metal technology: Thermodynamic analysis, Energy Conversion and Management, 157 (2018) 562–574.
[25] N.R. Dohyung Kang, Michael J. Gordon, Horia Metiu, Eric W. McFarland, Catalytic methane pyrolysis in molten MnCl2-KCl, Applied Catalysis B: Environmental, 254 (2019) 659–666.
[26] R.M.R. James E. Funk, Energy Requirements in the Production of Hydrogen from Water, l&EC Process Design and Development, 5 (1966) 336-342.
[27] A.D. C Koroneos, G Roumbas, N Moussiopoulos, Life cycle assessment of hydrogen fuel production processes, International Journal of Hydrogen Energy, 29 (2004) 1443-1450.
[28] R.R. Carney, Slush Hydrogen Production and Handling as a Fuel for Space Projects, Timmerhaus K.D. (eds) Advances in Cryogenic Engineering, 9 (1964).
[29] S.K.G. Sunita Sharma, Hydrogen the future transportation fuel: From production to applications, Renewable and Sustainable Energy Reviews, 43 (2015) 1151-1158.
[30] H.F.C. William A. Bone, The thermal decomposition of Hydrocarbons, Part I. [Methane, Ethane, Ethylene and Acetylene], Journal of the chemical society, (1908) 1198-1225.
[31] M. Ismael, Latest progress on the key operating parameters affecting the photocatalytic activity of TiO2-based photocatalysts for hydrogen fuel production: A comprehensive review, Fuel, 303 (2021) 121-207.
[32] A.G. Mehdi Mehrpooya, S.M. Ali Moosavian, Yasaman Amirhaeri, Optimal design and economic analysis of a hybrid process of municipal solid waste plasma gasification, thermophotovoltaic power generation and hydrogen/liquid fuel production, Sustainable Energy Technologies and Assessments, 49 (2022) 101717.
[33] C.b. pricing, https://m.echemi.com/productsInformation/pd20150901230-carbon-black.html, (2020).
[34] J.A.M.J. Brandon José Leal Pérez, Rajat Bhardwaj, Earl Goetheer, Martin van Sint Annaland, Fausto Gallucci, Methane pyrolysis in a molten gallium bubble column reactor for sustainable hydrogen production: Proof of concept & techno-economic assessment, International Journal of Hydrogen Energy, 46 (2021) 4917-4935.

[35] Y. Itoh, K. Ozaki, R. Maezawa, Hydrolyzable-emulsifier-containing polymer latices as dispersants and binders for waterborne carbon black paint, Journal of Applied Polymer Science, (2013).
[36] M. Barekat, R.S. Razavi, S. Bastani, Effect of Carbon Black Pigment on the Surface Resistivity of the Black Silicone Thermal Control Coating, Advanced Materials Research, 472-475 (2012) 110-113.
[37] M. Steinberg, Fossil fuel decarbonization technology for mitigating, International Journal of Hydrogen Energy, (1999) 771-777.
[38] X.-h. Shao, J.-w. Zheng, Soil Organic Carbon, Black Carbon, and Enzyme Activity Under Long-Term Fertilization, Journal of Integrative Agriculture, 13 (2014) 517-524.
[39] C.R. A. Abánades, D. Salmieri, Technological challenges for industrial development of hydrogen production based on methane cracking, Energy, 46 (2012) 359-363.
[40] J.W.M. Brett Parkinson, Thomas B. McConnaughy, D. Chester Upham, Eric W. McFarland, , Techno-Economic Analysis of Methane Pyrolysis in Molten Metals: Decarbonizing Natural Gas, Chemical Engineering & Technology, 40 (2017) 1022-1030.
[41] H.F. Abbas, W.M.A. Wan Daud, Hydrogen production by methane decomposition: A review, International Journal of Hydrogen Energy, 35 (2010) 1160-1190.
[42] S.T. D. Paxman, M. Nikoo, M. Secanell, G. Ordorica-Garcia, Initial Experimental and Theoretical Investigation of Solar Molten Media Methane Cracking for Hydrogen Production, Energy Procedia, 49 (2014) 2027-2036.
[43] M.R.A. Mehdi Jafarian∗, Graham J. Nathan, Preliminary evaluation of a novel solar bubble receiver for heating a gas, Solar Energy 182 (2019) 264–277.
[44] M.A.L. Manuela Serban, Christopher L. Marshall, and Richard D. Doctor, Hydrogen Production by Direct Contact Pyrolysis of Natural Gas, (2003).
[45] D.K. Nazanin Rahimi, John Gelinas, Aditya Menon, Michael J. Gordon, Horia Metiu, Eric W. McFarland, Solid carbon production and recovery from high temperature methane pyrolysis in bubble columns containing molten metals and molten salts, Carbon, 151 (2019) 181-191.
[46] L. Weger, A. Abánades, T. Butler, Methane cracking as a bridge technology to the hydrogen economy, International Journal of Hydrogen Energy, 42 (2017) 720-731.

[47] N.G. Guillaume Fau, Philippe Gillard, Johan Steelant, Methane pyrolysis: Literature survey and comparisons of available data for use in numerical simulations, Journal of Analytical and Applied Pyrolysis, 104 (2013) 1-9.
[48] S.F. Abanades, Gilles, Hydrogen production from solar thermal dissociation of methane in a high-temperature fluid-wall chemical reactor, Chemical Engineering and Processing: Process Intensification, 47 (2008) 490-498.
[49] C.J.C.a.M.H. Back, The Thermal Decomposition of Methane. I. Kinetics of the Primary Decomposition to C2H6+H2, Rate Constant for the Homogeneous Unimolecular Dissociation of Methane and its Pressure Dependence, 53 (1975) 3580-3590.
[50] M. Takach, M. Sarajlić, D. Peters, M. Kroener, F. Schuldt, K. von Maydell, Review of Hydrogen Production Techniques from Water Using Renewable Energy Sources and Its Storage in Salt Caverns, Energies, 15 (2022).
[51] H.C. RF. Horng, CH. Lee , HT. Tsai, Characteristics of hydrogen produced by partial oxidation and auto-thermal reforming in a small methanol reformer, Journal of Power Sources, 161 (2006) 1225-1233.
[52] F. Shafizadeh, Introduction To Pyrolysis Of Biomass, Journal of Analytical and Applied Pyrolysis, 3 (1982) 283-305.
[53] S.I. Meramo-Hurtado, P. Puello, A. Cabarcas, Process Analysis of Hydrogen Production via Biomass Gasification under Computer-Aided Safety and Environmental Assessments, ACS Omega, 5 (2020) 19667-19681.
[54] J.R. Rostrup-Nielsen, J. Sehested, J.K. Nørskov, Hydrogen and synthesis gas by steam- and C02 reforming, Advances in Catalysis, Academic Press2002, pp. 65-139.
[55] H.C. H. Zhou, H. Zhao, H. Liu , W. Pan Investigation of H2O and CO2 reforming and partial oxidation of methane: catalytic effects of coal char and coal ash Energy Fuels, 22 (2008) 2341-2345.
[56] R. Siavash Moakhar, S.M. Hosseini-Hosseinabad, S. Masudy-Panah, A. Seza, M. Jalali, H. Fallah-Arani, F. Dabir, S. Gholipour, Y. Abdi, M. Bagheri-Hariri, N. Riahi-Noori, Y.F. Lim, A. Hagfeldt, M. Saliba, Photoelectrochemical Water-Splitting Using CuO-Based Electrodes for Hydrogen Production: A Review, Adv Mater, 33 (2021) e2007285.
[57] Hydrogen Power Generation - Handbook, Mitsubishi Heavy Industries, Ltd. Energy Systems.

[58] J.-F. Brau, Production of Hydrogen for Oil Refining by Thermal Gasification of Biomass: Process Design, Integration and Evaluation, Thesis, (2013).
[59] S.S. Juergen Antrekowitsch, Potential of hydrogen as alternative reducing agent in metallurgical processes, (2010).
[60] M.-s.C. Jue Tang, Feng Li, Cong Feng, Zheng-gen Liu & Yu-sheng Zhou Development and progress on hydrogen metallurgy, International Journal of Minerals, Metallurgy and Materials, 27 (2020) 713–723.
[61] W. Liu, H. Zuo, J. Wang, Q. Xue, B. Ren, F. Yang, The production and application of hydrogen in steel industry, International Journal of Hydrogen Energy, 46 (2021) 10548-10569.
[62] I.F. Jan Rongé, Use of hydrogen in buildings, WaterstofNet, (2021).
[63] W.W. Zeyu Fan, Jing Zhou, Dong Gu, Wei Xiao Catalytic decomposition of methane to produce hydrogen: A review, Journal of Energy Chemistry, 58 (2021) 415-430.
[64] C.N. E. B. Agyekum, A. M. Agwa, S. Kamel, A Critical Review of Renewable Hydrogen Production Methods: Factors Affecting Their Scale-Up and Its Role in Future Energy Generation, Membranes (Basel), 12 (2022).
[65] J.T. Hugill, High purity oxygen for steel making, The Canadian Journal of Chemical Engineering, (1958) 169-174.
[66] W.C. Newell, Application of Oxygen to Steel-Making, Nature, 162 (1948) 518–519.
[67] L.Z. Xiao Li, Jiayuan Yu, Xiaoyan Liu, Xiaoli Zhang, Hong Liu & Weijia Zhou, Water Splitting: From Electrode to Green Energy System, Nano-Micro Letters, 12 (2020).
[68] E.B. Mingquan Yu, Priv.-Doz. Dr. Harun Tüysüz, Principles of Water Electrolysis and Recent Progress in Cobalt-, Nickel-, and Iron-Based Oxides for the Oxygen Evolution Reaction, Angew.Chem.Int.Ed., 61,e202103824(1 of 24). (2022).
[69] J.S. Devendra Pakhare, A review of dry (CO2) reforming of methane over noble metal catalysts, Chem. Soc. Rev., 43 (2014) 7813-7837.
[70] S.W.a.G.Q.M. Lu, Carbon Dioxide Reforming of Methane To Produce Synthesis Gas over Metal-Supported Catalysts: State of the Art, Energy & Fuels, 10 (1996) 896 - 904.

[71] https://netl.doe.gov/research/Coal/energy-systems/gasification/gasifipedia/intro-to-gasification (Access On 03/10/2022).
[72] H. Ishaq, I. Dincer, A new energy system based on biomass gasification for hydrogen and power production, Energy Reports, 6 (2020) 771-781.
[73] N.P.V.a.D.M. Austgen, Hydrogen-Donor Solvents in Biomass Liquefaction, Ind. Eng. Chem. Process Des. Dev. , 24 (1985) 304-311.
[74] H.Y. Wang, A.C. Lua, Hydrogen Production by Thermocatalytic Methane Decomposition, Heat Transfer Engineering, 34 (2013) 896-903.
[75] L.A. J. Dunkleman, Pyrolysis of propane in tubular flow reactors constructed of different materials, Ind. Lab. Pyrolysis American Chemical Society, (1976) 261–273.
[76] Y.T. Q. Sun, G. Gavalas, Methane pyrolysis in a hot filament reactor, EnergyFuels, 14 (2000) 490–494.
[77] D.S. H. Huang, L. Spadaccini, Endothermic heat-sink of hydrocarbon fuels for scramjet cooling, in: Endothermic Heat-Sink Hydrocarbon Fuels Scramjet Cooling. , 38th AIAA/ASME/SAE/ASEE Joint Propulsion Conference and Exhibit, Indianapolis, (2002) 3871.
[78] D.K. J. Chakraborty, High pressure pyrolysis of n-heptane, J. Anal. Appl.Pyrolysis, 86 (2009).
[79] S.B. K. Tabayashi, The early stages of pyrolysis and oxidation of methane Combust. Flame 34 (1979) 63–83.
[80] Y.H. G. Liu, L. Wang, X. Zhang, Z. Mi, Supercritical thermal cracking of N-dodecane in presence of several initiative additives: products distribution andkinetics Energy Fuels, 22 (2008) 3960–3969.
[81] M.H. T. Bruno, A. Laesecke, E. Lemmon, R. Perkins, Thermochemical and thermophysical properties of JP-10, Advance Science Technology, 45 (2006) 1–67.
[82] R.S. S. Garner, K. Brezinsky, The high-pressure pyrolysis ofsaturated and unsaturated C7 hydrocarbons, Proc. Combust. Inst. , 32 (2009) 461-467.
[83] W.F. Y. Xing, W. Xie, Y. Guo, R. Lin, Thermal cracking of JP-10 underpressure, Ind. Eng. Chem. Res., 47 (2008) 10034–10040.
[84] S.K. S. Zeppieri, F. Dryer, Modeling concepts for larger carbon numberalkanes: a partially reduced skeletal mechanism for n-decane oxidation andpyrolysis, Proc. Combust. Inst., 28 (2000) 1587–1595.
[85] S.L. A.Basile, A.Iulianelli, Membrane Reactors For Energy Applications And Basic Chemical Production, Woodhead Publishing Series In Energy, (2015) 31-59.

[86] N. Muradov, Low-carbon production of hydrogen from fossil fuels, Compendium of Hydrogen Energy2015, pp. 489-522.
[87] V.A. D. Chester Upham, Alexander Khechfe, Zachary R. Snodgrass, Michael J. Gordon, Horia Metiu, Eric W. McFarland, Catalytic molten metals for the direct conversion of methane to H2 and C, Research, (2017).
[88] K.E.S.T. Tiina Keipi, Henrik Konttinen, Jukka Konttinen, Thermo-catalytic decomposition of methane: The effect of reaction parameters on process design and the utilization possibilities of the produced carbon, Energy Conversion and Management, 126 (2016) 923-934.
[89] E.W.M. Thomas C. Farmer, Michael F. Doherty, Membrane bubble column reactor model for the production of hydrogen by methane pyrolysis, International Journal of Hydrogen Energy, 44 (2019) 14721 -14731.
[90] D.W.A. G. Kreysa, I. Schultz Decarbonisation of Fossil Energy via Methane Pyrolysis, The Future Role of Hydrogen in Petrochemistry and Energy Supply DGMK Conference, (2010).
[91] M.M.N. Randy Vander Wal, Carbons as Catalysts in Thermo-Catalytic Hydrocarbon Decomposition: A Review, Journal of Carbon Research, 6 (2020).
[92] D.S. J. Dufour, J. Galvez, J. Moreno, C. Garcia, Life cycle assessment of processes for hydrogen production. Environmental feasibility and reduction of greenhouse gases emissions, International Journal of Hydrogen Energy, 34 (2009) 1370-1376.
[93] T. Lipman, An Overview of Hydrogen Production and Storage Systems with Renewable Hydrogen Case Studies, Clean Energy States Alliance (2011).
[94] A.A.I. Anis Fakeeha, Hesham Aljuraywi, Yazeed Alqahtani, Ahmad Alkhodair, Suliman Alswaidan, Ahmed E. Abasaeed, Samsudeen O. Kasim, Sofiu Mahmud, Ahmed S. Al-Fatesh, , Hydrogen Production by Partial Oxidation Reforming of Methane over Ni Catalysts Supported on High and Low Surface Area Alumina and Zirconia, Processes, 8 (2020).
[95] Z. Salameh, Renewable Energy System Design, Academic Press, (2014) 201-298.
[96] H. Al-Haj Ibrahim, Introductory Chapter: Pyrolysis.
[97] B.L.C. M. S. Khan, Survey of Recent Methane Pyrolysis Literature, Industrial and Engineering Chemistry, 62 (1970) 54-59.
[98] M. Poletto, A.J. Zattera, R.M. Santana, Thermal decomposition of wood: kinetics and degradation mechanisms, Bioresour Technol, 126 (2012) 7-12.

[99] W.M. JH. Horn Thermal carbon black process, United States Patent US3523010, (1970).
[100] G.V.C.P. A.V. Bridgwater, Fast pyrolysis processes for biomass, Renewable and Sustainable Energy Reviews, 4 (2000) 1-73.
[101] G.D. Eoin Butler, Dietrich Meier, Kevin McDonnell, A review of recent laboratory research and commercial developments in fast pyrolysis and upgrading, Renewable and Sustainable Energy Reviews, 15 (2011) 4171–4186.
[102] J.L.P. W. J. Burlant, Pyrolysis of Polyacrylonitrile, Journal of Polymer Science, XXII (1956) 249-256
[103] S.R.C. D. S. Scott, J. Piskorz, and D. St. A. G. Radlein, Fast Pyrolysis of Plastic Wastes, Energy & Fuels, 4 (1990) 407-411.
[104] F. Safizadeei and Y. L. Fu, Pyrolysis Of Cellulose, Carbohydiate Research, 29 (1973) 113-122.
[105] Y.S. Allan G. W. Bradbury, Fred Shafizadeh, A Kinetic Model for Pyrolysis of Cellulose, Journal of Applied Polymer Science, 23 (1979) 3271-3280.
[106] T.H.F. P. R. Solomon, R. J. Pugmire, Progress in coal pyrolysis, Fuel 72 (1993) 587-597.
[107] S.-C.Z. Gary L. Messing, Gopal V. Jayanthi, Ceramic Powder Synthesis by Spray Pyrolysis, Journal of the American Ceramic Society, 76 (1993) 2707-2726.
[108] M.D. Christophe Gueret, Francis Billaudi, Methane pyrolysis: thermodynamics, Chemical Engineeing Science, 52 (1997) 815-827.
[109] T.W.C. Jing Xia Qian, Linga Reddy Enakonda, Da BinLiu, Gerard Mignani, Jean-MarieBasset, LuZhou, Methane decomposition to produce COx-free hydrogen and nano-carbon over metal catalysts: A review, International Journal of Hydrogen Energy 45 (2020) 7981-8001.
[110] B.L.C. M. S. Khan, Survey of recent Methane pyrolysis literature, Ind. Engng Chem., 62 (1970) 54-59.
[111] K.I. Omar, The pyrolysis of methane, Chem. Engng Res, 6 (1982) 29-34.
[112] R.S. Nuria Sánchez-Bastardo, Holger Ruland, , Methane Pyrolysis for CO2-Free H2 Production: A Green Process to Overcome Renewable Energies Unsteadiness, Chemie Ingenieur Technik, 92 (2020) 1596-1609.
[113] E.H.K. Jinho Boo, No-Kuk Park, Changkook Ryu, Yo-Han Kim, Jinmo Park, Dohyung Kang Methane Pyrolysis in Molten Potassium Chloride: An Experimental and Economic Analysis, energies, 14 (2021).

[114] Christophe Gueret, Michel Daroux, Francis Billaudi, Methane pyrolysis: thermodynamics, Chemcol Engineermg Science, Vol. 52, No. 5, pp. 815-827, 1997. .
[115] Alberto Abánades, Natural Gas Decarbonization as Tool for Greenhouse Gases Emission Control Frontiers in Energy Research, June 2018 , Volume 6 , Article 47, 1-7.
[116] M.T. Clarke Palmer, Henrik H. Kristo ff ersen, John Gelinas, Michael J. Gordon, Eric W. McFarland, and Horia Metiu, Methane Pyrolysis with a Molten Cu−Bi Alloy Catalyst, ACS Catalysis, (2019) 8337−8345.
[117] R.U. J.L. Pinilla, R.K. Karn, I. Suelves, M.J. La´zaro, R. Moliner, A.B. Garcı´a, J.N. Rouzaud, High temperature iron-based catalysts for hydrogen and nanostructured carbon production by methane decomposition, International Journal of Hydrogen Energy, 36 (2011) 7832-7843.
[118] M.I. K. Murata, M. Miki, T. Yamaguchi, , Formation of filamentous carbon and hydrogen by methane decomposition over Al2O3-supported Ni catalysts Reaction Kinetics and Catalysis Letters, 85 (2005) 21-28.
[119] T.L. W. Qian, F. Wei, Z. Wang, Y. Li, Enhanced production of carbon nanotubes: combination of catalyst reduction and methane decomposition, Applied Catalysis A: General, 258 (2004) 121-124.
[120] G.Y.H. Kang Kyu Lee, Ki June Yoon, Byung Kwon Lee, , Thermocatalytic hydrogen production from the methane in a fluidized bed with activated carbon catalyst, Catalysis Today, 93-95 (2004) 81-86.
[121] R.K. M. Borghei, A. Rashidi, N. Izadi, Kinetics of methane decomposition to COx-free hydrogen and carbon nanofiber over Ni-Cu/MgO catalyst, International Journal of Hydrogen Energy, 35 (2010) 9479-9488.
[122] O.D.B. G. Bonura, L. Spadaro, F. Arena, F. Frusteri, A basic assessment of the reactivity of Ni catalysts in the decomposition of methane for the production of "COx-free" hydrogen for fuel cells application Catalysis Today, 116 (2006) 298-303.
[123] D.Y.E. M.A. Ermakova, Ni/SiO2 and Fe/SiO2 catalysts for production of hydrogen and filamentous carbon via methane decomposition, Catalysis Today, 77 (2002) 225-235.
[124] G. Fau, N. Gascoin, J. Steelant, Hydrocarbon pyrolysis with a methane focus: A review on the catalytic effect and the coke production, Journal of Analytical and Applied Pyrolysis, 108 (2014) 1-11.

[125] S.A. Sylvain Rodat, Jean-Louis Sans, Gilles Flamant, A pilot-scale solar reactor for the production of hydrogen and carbon black from methane splitting, International Journal of Hydrogen Energy, 35 (2010) 7748-7758.
[126] R. Moliner, I. Suelves, M. Lazaro, O. Moreno, Thermocatalytic decomposition of methane over activated carbons: influence of textural properties and surface chemistry, International Journal of Hydrogen Energy, 30 (2005) 293-300.
[127] Z. Bai, H. Chen, W. Li, B. Li, Hydrogen production by methane decomposition over coal char, International Journal of Hydrogen Energy, 31 (2006) 899-905.
[128] S.A. S. Rodat, J. Coulie, G. Flamant, , Kinetic modelling of methane decomposition in a tubular solar reactor, Chemical Engineering Journal, 146 (2009) 120-127.
[129] L.Y. Fang Liu, Chen Song, Chemical looping hydrogen production using activated carbon and carbon black as multi-function carriers, International Journal of Hydrogen Energy, 43 (2018) 5501-5511.
[130] A. Bo, O. To, O. Pc, Effect of Temperature on Regeneration of Deactivated Catalytic Reforming Catalyst (Pt/Al2O3), Journal of Chemical Engineering & Process Technology, 08 (2017).
[131] V.V.R. P. R. Gunjal, Catalytic Reaction Engineering, Industrial Catalytic Processes for Fine and Specialty Chemicals, pp. (2016) 263-314.
[132] H.A. Jakobsen, Chemical Reactor Modeling, Springer-Verlag Berlin Heidelberg (2008).
[133] E.R. Lionel J.J. Catalan, Coupled hydrodynamic and kinetic model of liquid metal bubble reactor for hydrogen production by noncatalytic thermal decomposition of methane, Internatioanl Journal of Hydrogen, 45 (2020) 2486-2503.
[134] J.L. H. B. Palmer, and K. C. Hou, On the Kinetics and Mechanism of the Thermal Decomposition of Methane in a Flow System, (1968).
[135] H.B. B. Eisenberg, Kinetics of methane pyrolysis, Chemical Engineering Progress Symposium Series 63 (1967) 3–17.
[136] I.B. H.A. Jakobsen, H.F. Svendsen, K.W. Hjarbo, Interaction Between Reaction Kinetics and Flow Structure in Bubble Column Reactors, (2001) 543-550.
[137] B. Lautrup, Physics of Continuous Matter Exotic and everyday phenomena in the macroscopic world, The Niels Bohr Institute, Revision 7.7 (2004).
[138] A.A.K.a.J.B. Joshi, Bubble Formation and Bubble Rise Velocity in Gas-Liquid

Systems: A Review, American Chemical Society, (2005).
[139] J.S.F. R. J. Andreini, And R. W. Callen, Characterization of Gas Bubbles Injected into Molten Metals Under Laminar Flow Conditions, (1977).
[140] T.S. T. Fehling, E. Baake, Paolo Di Barba, Fabrizio Dughiero, Michele Forzan, Elisabetta Sieni, Numerical modeling of bubble dynamics in liquid metal exposed to electromagnetic fields for hydrogen production, International Journal of Applied Electromagnetics and Mechanics, 53 (2017) S111-S120.
[141] A. Bahramian, S. Elyasi, A Numerical Model for Bubble Column Reactors: Prediction of the Fractional Gas Holdup by the Implementation of the Drift-Flux Model, Journal of Chemical Engineering & Process Technology, 10 (2019).
[142] S.E. C. Zhang, G. Gerbeth, Experimental study of single bubble motion in a liquid metal column exposed to a DC magnetic field, International Journal of Multiphase Flow, 31 (2005) 824-842.
[143] T. Ziegenhein, D. Lucas, Observations on bubble shapes in bubble columns under different flow conditions, Experimental Thermal and Fluid Science, 85 (2017) 248-256.
[144] A.A. T. Geißler, A. Heinzel, K. Mehravaran, G. Müller, R. K. Rathnam, C. Rubbia, D. Salmieri, L. Stoppel, S. Stückrad, A. Weisenburger, H. Wenninger4, Th. Wetzel, Hydrogen production via methane pyrolysis in a liquid metal bubble column reactor with a packed bed, Chemical Engineering Journal, 299 (2016) 192-200.
[145] T.C. Farmer, E.W. McFarland, M.F. Doherty, Membrane bubble column reactor model for the production of hydrogen by methane pyrolysis, International Journal of Hydrogen Energy, 44 (2019) 14721-14731.
[146] N. Zaghloul, S. Kodama, H. Sekiguchi, Hydrogen Production by Methane Pyrolysis in a Molten-Metal Bubble Column, Chemical Engineering & Technology, 44 (2021) 1986-1993.
[147] B.B. Alchagirov, A.M. Chochaeva, Temperature dependence of the density of liquid tin, High Temperature, 38 (2000) 44-48.
[148] N.G.D. D. Darmana, J. A. M. Kuipers, Detailed modeling of hydrodynamics, mass transfer and chemical reactions in a bubble column using a discrete bubble model, Chemical Engineering Science, 60 (2005) 3383-3404.
[149] C.T.P. J. F. Branco, R. A. Figueiredo, Heat Conduction In The Hollow Sphere With A Power-Law Variation Of The External Heat Transfer Coefficient, Int. Comm. HeatMass Transfer, (2000).

CHAPTER 3

A NUMERICAL INVESTIGATION OF METHANE PYROLYSIS IN A MOLTEN CATALYST BATH–A SINGLE BUBBLE APPROACH

Chapter preview

In this chapter, a numerical model of a single rising and pyrolysing bubble within a molten bath column is developed through the simultaneous solution of the principle governing equations of mass, momentum, and energy. The developed numerical model provides us with an assessment opportunity of the effects of variations in bubble size, bubble rise velocity, liquid height, pressure, gas temperature, molten bath temperature, and initial bubble composition on the conversion of the methane within a single bubble. Also, the results of a sensitivity analysis of methane conversion to the abovementioned parameters are presented.

The following section is presented in a paper format, and already has been submitted to the *International Journal of Hydrogen Energy*.

Statement of Authorship

Title of Paper	A Numerical Investigation of Methane Pyrolysis in a Molten Catalyst Bath–A Single Bubble Approach
Publication Status	☐ Published ☐ Accepted for Publication ☐ Submitted for Publication ■ Unpublished and Unsubmitted w ork w ritten in manuscript style
Publication Details	In this paper, we enhance the methane pyrolysis technique within a molten-catalyst bath. The effects of the main controling factors are simulated and analysed. The results will be used for the cutting-edge industrial sectors, which are persuing to establish facilities for producing hydrogen as a clean fuel.

Principal Author

Name of Principal Author (Candidate)	Nazgol Mehrabian		
Contribution to the Paper	Conceptulization, methodology, validation/verification, designing, writing original draft, investigation, data curation, writing-review and editing, formal analysis		
Overall percentage (%)	70%		
Certification:	This paper reports on original research I conducted during the period of my Higher Degree by Research candidature and is not subject to any obligations or contractual agreements with a third party that would constrain its inclusion in this thesis. I am the primary author of this paper.		
Signature		Date	12/05/2022

Co-Author Contributions

By signing the Statement of Authorship, each author certifies that:

i. the candidate's stated contribution to the publication is accurate (as detailed above);

ii. permission is granted for the candidate in include the publication in the thesis; and

iii. the sum of all co-author contributions is equal to 100% less the candidate's stated contribution.

Name of Co-Author	Graham 'Gus' Nathan		
Contribution to the Paper	Conceptulization, methodology, validation/verification, design, review and refinement of documents and figures.		
Signature		Date	13/5/2022

Name of Co-Author	Ahmad Seyfaee		
Contribution to the Paper	Conceptulization, methodology, validation/verification, design, review, refinement of documents		
Signature		Date	14/05/2022

Please cut and paste additional co-author panels here as required.

Co-Author Contributions

By signing the Statement of Authorship, each author certifies that:

i. the candidate's stated contribution to the publication is accurate (as detailed above);

ii. permission is granted for the candidate in include the publication in the thesis; and

iii. the sum of all co-author contributions is equal to 100% less the candidate's stated contribution.

Name of Co-Author	Mehdi Jafarian		
Contribution to the Paper	Conceptulization, methodology, validation/verification, design, review and refinement of the ducument.		
Signature		Date	18/05/2022

Name of Co-Author			
Contribution to the Paper			
Signature		Date	

Please cut and paste additional co-author panels here as required.

A Numerical Investigation of Methane Pyrolysis in a Molten Catalyst Bath–A Single Bubble Approach

Nazgol Mehrabian, Ahmad Seyfaee, Graham J. Nathan, Mehdi Jafarian*

Centre for Energy Technology, School of Mechanical Engineering, The University of Adelaide, Adelaide, SA 5005, Australia

*Corresponding email: mehdi.jafarian@adelaide.edu.au

Abstract

A dynamic one-dimensional numerical model of methane pyrolysis within a rising and pyrolysing bubble in a column of molten $Ni_{0.27}Bi_{0.73}$, as a molten catalyst, is presented. The model predicts both the behavior of the rising bubble in the column and the chemical reactions within it, accounting for any variations in bubble diameter and rising velocity, which have previously been assumed to be constant. The conservation equations of energy, mass and momentum are solved simultaneously using the implicit Gauss–Seidel numerical method. The model accounts for the main parameters contributing to methane pyrolysis reaction, namely the bubble size, column height, residence time, molten bath temperature, pressure, bubble composition and temperature. The reliability of the model was assessed by comparison with the available experimental data from the literature and a reasonable agreement was found. The current calculations revealed that more than 97% of the overall methane conversion occurs at the interface of the bubble and the molten bath. A sensitivity analysis was also undertaken. For the studied conditions, a 400 K increase in the temperature of the molten bath from 1013 to 1413 K and a rise in the pressure of the system from 0.1 to 8 MPa enhances the overall conversion by >80%. However, a wide range of variations in the initial gas temperature from 313 to 1313 K and the initial bubble radius from 0.6 to 2.6 mm improves the conversion by approximately 10%. Furthermore, increasing the initial methane mole fraction within the injected gas from 0% to 100% decreases the overall methane conversion by ~12%.

Keywords: Hydrogen; Pyrolysis; Molten Catalyst; Carbon Capture; bubble column; Methane

Graphical Abstract/ Table of Contents

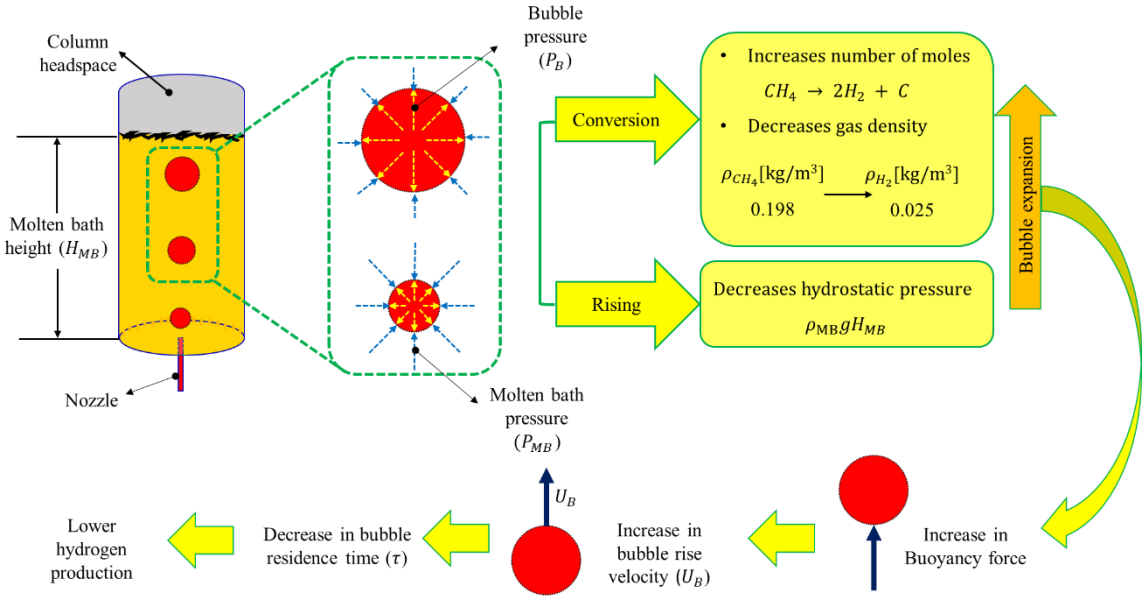

Nomenclature

A_0 : pre-exponential factor [$1/\mathrm{s}$]
A_c : Nozzle cross-sectional area [m]
Ar : Archimedes number [-]
a, b : Numerical parameters [-]
C : Concentration [$\mathrm{mole/m^3}$]
C_d : Drag coefficient [-]
c_p : Specific heat capacity [$\mathrm{J/kg.K}$]
E_a : Activation energy [$\mathrm{J/mol}$]
g : Gravity [$\mathrm{m/s^2}$]
h : Convective heat transfer coefficient [$\mathrm{W/m^2.K}$]
H : Height [mm]
ΔH : Reaction enthalpy [$\mathrm{J/mol}$]
k : Conductive heat transfer coefficient [$\mathrm{W/m.K}$]
Mo : Morton number [-]
Nu : Nusselt number [-]
p : Pressure [Pa]
P_c : Critical pressure of gas [Pa]
p_s : Nozzle perimeter [m]
r : Bubble radius [mm]
Re : Reynolds number [-]
R_g : Universal gas constant [$\mathrm{J/mol/K}$]
T : Temperature [K]
t : Time [s]
U : Rise velocity [$\mathrm{m/s}$]
V : Volume [$\mathrm{m^3}$]
X : Conversion of methane [-]
y_i : Mole fraction of species [-]
Z : Compressibility factor of gas [-]
z_B : Axial distance from the bottom of the column [mm]
z_P : Axial distance through the nozzle pipe [mm]

Greek letters

μ : Dynamic viscosity [Pa. s]
ρ : Density [$\mathrm{kg/m^3}$]
σ : Surface tension [$\mathrm{N/m}$]
Ω : Collision integral [-]
τ : Residence time of the bubble [s]

Subscripts

B : Bubble
c : Critical
equ : Equilibrium
f : Final
g : Gas
HS : Headspace
$intf$: Interface
m : mean
MB : Molten bath
mix : Mixture
nz : Nozzle
rxn : Reaction

3.1 Introduction

There is growing demand for technologies that enable low-cost production of hydrogen without any net CO_2 emissions, often termed 'net-zero' hydrogen production [1-4]. New technologies are needed because Steam Methane Reforming (SMR), which is currently the most cost-effective commercial process for H_2 production (at ~$1.5 (per kg H_2)) [5, 6] and used to produce ~96% of the global hydrogen production, also generates some 9-10 tones of CO_2 per tones of H_2 [7, 8]. While these emissions can be mitigated via Carbon Capture and Storage (CCS), this increases the cost of SMR-derived H_2 to ~$2.5 (per kg H_2) and still typically only achieves 90% CO_2 avoidance [9], thereby failing to meet the requirement for net-zero H_2 production. Auto-thermal reforming is another potential approach for H_2 production that increases the capture efficiency of CO_2 [10]. However, this technology costs ~$3.6 (per kg H_2) since it requires an air separation unit to produce pure O_2 as a feedstock [11, 12]. The current levelized cost of H_2 production with nearly zero-carbon emissions using Photo-Electrochemical (PEC) [13, 14] and Photovoltaic-Electrolytic (PV-E) methods is estimated to be $11.4 and $12.1 per kg H_2, respectively [15-17]. While these costs are reducing rapidly, there remains a need for other technologies with the potential to reduce the price differential for CO_2-free hydrogen and natural gas if hydrogen is to make a substantial contribution to CO_2 mitigation. Hence, there is a need for the development of alternative technologies with the potential to achieve cost-effective, zero-carbon production of hydrogen.

An emerging technology option for net-zero hydrogen with strong potential is methane pyrolysis ($CH_4 \rightarrow 2H_2 + C$) [15, 18-20]. This technology avoids direct emission of CO_2 by generating a carbon product. The storage of solid carbon is technically less

challenging than CO_2 sequestration [21], which requires specific sites and geology [22]. Moreover, carbon black is a co-product of hydrogen in pyrolysis, which can be used as a raw material for several valuable products, such as paints [23], rubber [24], tires, and fertilizers [25, 26]. However, it is worth noting that the reaction conditions affect the carbon product type and its value [27]. The aforementioned factors have led those generating energy transition policies to conclude that the methane pyrolysis technology has alternative value drivers from the SMR, PEC and PV-E technologies, although the technology must still be optimized [28-31]. Hence, the overall aim of the current study is to investigate methane pyrolysis as a potential method for hydrogen production.

While methane starts to dissociate at temperatures above 673 K, its complete conversion to H_2 and C requires temperatures above 1273 K [28] in atmospheric pressure. Coke formation is prominent in the methane pyrolysis reactions on solid based catalyst systems [32-35], which necessitates periodic decoking of the catalyst by burning the carbon [36, 37]. This, in turn, not only increases the cost of the process, but also produces CO_2 as a by-product. Catalyst deactivation through sintering of the unwanted solid-state reactions between the metallic catalyst and the oxide occurs at elevated temperatures [38]. Therefore, significant effort has been allocated to developing those catalysts, e.g., those employing nickel (Ni) and iron (Fe) [19], which enable reasonable methane conversion at temperatures less than 1273 K [34, 39]. Nonetheless, practical application of these solid-state catalysts is limited due to their fast deactivation through the coke formation on their active sites [20, 38, 40].

A developing technique for methane pyrolysis is to perform the reaction in low-melting temperature metals, e.g., tin (melting temperature = 500 K) [41] and gallium (melting point = 300K) [42, 43] or alloys, e.g., GaInSn (melting point = 278 K) [42].

This technique results in thermal decomposition of CH_4 within a bubbling column of molten metal [30, 44, 45]. Due to the lower density of the insoluble carbon, it floats to the surface of the molten bath to be separated physically [30, 37], in parallel with the collection of hydrogen gases. Furthermore, a bubbling gas flow regime enables high heat and mass transfer rates [46, 47]. This process is illustrated schematically in Figure 3.1a and b. Despite these potential advantages, the pyrolysis of methane in a molten bath has received far less attention than its solid catalyst counterparts, so the full extent of the potential benefits and limitations of this technology are yet to be identified.

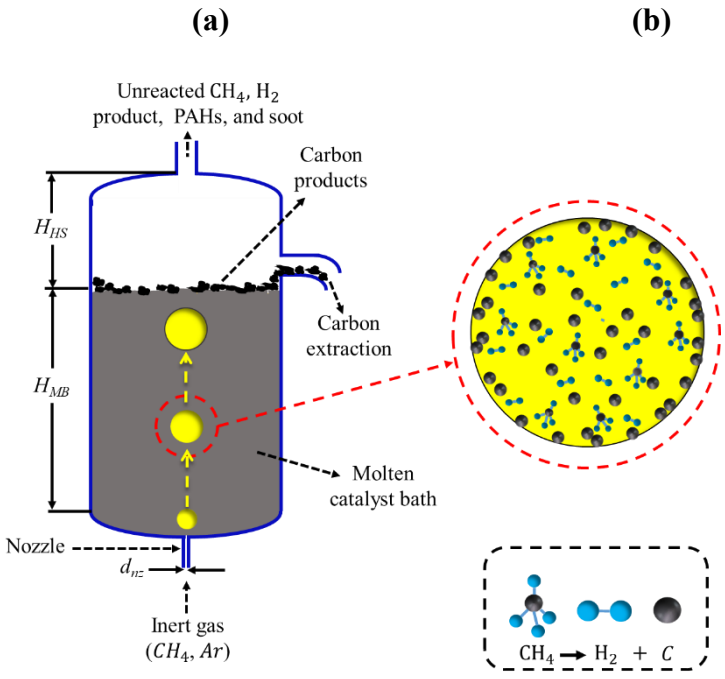

Figure 3.1. Schematic presentation of (a) a single rising bubble within a molten bath bubble column reactor for the pyrolysis of methane, (b) a cross section through the bubble, showing the relative positions of major components within it.

It has been deduced that the CH_4 from the gas within a rising and pyrolysing bubble in a molten metal bath (Figure 1b) diffuses toward the bubble-liquid interface, where it cracks into H_2 and solid carbon through multi-step reactions. The extent of the

catalytic effect within the molten media has been controversial because some previous studies have reported that the use of a catalytic material in the molten bath can decrease the methane decomposition temperature to less than 1273 K [44, 48-50], whilst no catalytic effect was seen by others [28, 51]. Moreover, the catalytic influence of the carbon layer has also been investigated during the pyrolysis reactions [28, 51, 52]. Hence, the proper design and optimization of the molten metal pyrolysis reactors requires a deep understanding of both the hydrodynamics of the bubbles [28, 33, 36, 53-56] and of the heat/mass transfer and reaction kinetics [37, 44, 57-60]. For example, an increase in column height leads to a longer residence time of bubbles within the bath, which increases both the conversion efficiency [36] and the parasitic pressure drop, which has an energy penalty. However, the design and construction of such systems is expensive due to the specific materials requirements because of the corrosivity of molten baths at high temperatures. Moreover, the opacity of the molten metals inhibits detailed and in situ measurements within the columns. In this context, modelling is an effective way to advance the understanding of methane pyrolysis within a molten bath. Therefore, the current study aims to advance understanding of methane pyrolysis through development of a mathematical model of a single rising and pyrolysing bubble within a molten bath.

Few previous numerical simulations are available for methane cracking reactions within a single bubble in a molten bath column. Plevan *et al.* [28] developed a 1-D thermochemical simulation for a single rising and pyrolysing methane bubble in a molten tin bath. They subdivided the column into four zones consisting of a preheater, an orifice, the liquid phase, and the gas phase. Each zone was modelled separately to account for their different temperatures and estimate the methane conversion through the column. They assumed that the gas flowrate does not change the bubble rise

velocity, but influences the frequency of bubble formation, based on the assumption that the bubble rise velocity has a constant value of 0.2 m/s. They found that the conversion increases with the temperature and with a reduction in the gas flowrate. Furthermore, a column height of 1150 mm was found to be insufficient to achieve a high conversion within the column for temperatures up to 1173 K. However, the impact on these results of the assumption that velocity is constant remains to be evaluated.

In another study, Geibler *et al.*[51] developed a 1-D model of methane conversion in a molten tin bath. Their model considered the whole column and did not subdivide it into zones, in contrast with that of Plevan *et al.* [28]. However, they also assumed a constant bubble size and residence time (i.e., a constant bubble rise velocity), together with a spherical shape and neglected the convection within the bubble gas phase. This model, despite showing a good agreement for temperatures in the range 1093 — 1208 K, departs from the experimental data for higher temperatures of 1208 K to 1273 K. However, the extent to which these differences are influenced by the key simplifying assumptions of constant values for the bubble rise velocity and bubble size are also yet to be evaluated.

In the light of the above discussions, the aim of the present work is to evaluate the influence of any variations in bubble size and rising velocity on the calculated rate of methane pyrolysis within a molten bath. In particular, we aim to assess the influence of changes to bubble diameter and rise velocity on the transport phenomena, the heat transfer between the gas and the molten bath and the chemical reactions both inside the methane gas bubble and at the interface of the bubble and the molten bath. We also aim to assess the sensitivity to operational parameters, consisting of the bubble size,

the molten bath height, the gas and bath temperatures, and the methane mole fraction within the injected gas in terms of the methane conversion.

3.2 Method

3.2.1 Model description

The following assumptions were employed to develop the current model:

a) the temperature of the molten bath is both uniform and constant.

b) the bubble size is less than 7.5 mm, ensuring that the bubble is close to spherical [42].

c) the initial velocity of the bubble is equal to its local terminal velocity. This is because bubbles have been measured as accelerating rapidly to their terminal velocity within a molten bath, due to the significant buoyancy force on the bubble, originating from the substantial difference between the densities of the bubble itself and the molten metal bath [61-63].

d) any interactions between the bubbles and walls are ignored by considering a single bubble, under a bubbly flow regime [64, 65].

e) the liquid metal is saturated with hydrogen and other chemically active components, such that the effects of solubility at the gas-molten bath interface can be ignored. Therefore, the mass fluxes within the bubble are due to chemical reactions alone, either within the gas phase or at the interface between the gas and the molten bath.

f) heat is convected from the molten bath to the bubble through their interface.

g) conduction is assumed to be the dominant heat transfer mechanism within the bubble and convection within the bubble is ignored, following earlier works [28, 51].

h) the methane conversion reaction was considered to be of the first order; however, in reality there will be some chain reactions. Moreover, all of the methane at the interface converts to carbon and hydrogen due to the ultrafast reactions at the interfaces [66, 67].

i) the impact of the carbon layer on the conversion at the bubble surface was ignored. That is, based on the current calculations, for a bubble with a radius of 0.6 mm (the smallest size of the bubble in this study) and 2.6 mm (the maximum size of the bubble in this study), if all the methane content of the bubble converts to carbon and hydrogen (X_{CH_4} = 100%) and product carbon remains uniformly at the gas and bath interface, the percentage of the ratio of the carbon layer thickness at the gas-molten bath interface to the bubble radius will be less than 5×10^{-6} and 2×10^{-6}, respectively. Moreover, due to the occurrence of the methane conversion in the gas phase as well as the gas-liquid interface, it is likely that carbon distributes within the gas phase of the bubble instead of forming a layer at the bubble interface.

j) As an estimation, the surface tension of the $Ni_{0.27}Bi_{0.73}$ was assumed to be the same as the bismuth ($345 \times 10^{-3}\ \frac{kg}{s^2}$).

k) In calculations, the heat transfer via radiation was ignored.

3.2.2 Bubble rise velocity

Two semi-empirical equations (Eqs. 3.1 and 3.2) [68, 69] were used to estimate the bubble rise velocity of a spherical bubble for which the set of coefficients varies, depending on the Reynolds number (Eq. 3.3) of the bubble (Re_B), as follows:

$$U_B = \frac{4{r_B}^2 \rho_{MB} g}{18\mu_{MB}} \left(1 + \frac{\frac{Ar}{96}}{(1+0.079Ar^{0.794})^{0.755}}\right)^{-1}, \text{ at } Re_B \leq 130 \quad (3.1).$$

$$U_B = \sqrt[3]{\frac{g\mu_{MB}}{\rho_{MB}}} \left(\frac{4a^2 Mo^{0.46b}}{3C_d}\right)^{\frac{1}{(2-2b)}} Ar^{\frac{(2b+1)}{(6-6b)}}, \quad \text{at } Re_B > 130 \text{ and } C_d = 0.95 \quad (3.2).$$

$$Re_B = \frac{2\rho_{MB} U_B r_B}{\mu_{MB}} \quad (3.3).$$

In these equations, the symbols C_d, r_B, μ_{MB}, ρ_{MB} and U_B are the drag coefficient, bubble radius, dynamic viscosity of the molten bath, density of the molten bath, and the bubble rise velocity, respectively. Also, a and b are the numerical parameters (Table 3.1), that are selected based on the Archimedes (Ar) and Morton (Mo) numbers, given by Eqs. 3.4 and 3.5, respectively [70]:

$$Ar = \frac{8g{r_B}^3 \rho_{MB}(\rho_{MB} - \rho_B)}{{\mu_{MB}}^2} \quad (3.4),$$

$$Mo = \frac{g{\mu_{MB}}^4(\rho_{MB} - \rho_B)}{{\rho_{MB}}^2 {\sigma_{MB}}^3} \quad (3.5).$$

Table 3.1: Parameters a and b in Eq. 3.2 as a function of the bubble's Archimedes and Morton numbers [68].

Condition	Parameter
$12.332 \leq Ar < 3.158 \times Mo^{-0.46}$	$a = 1$ $b = 0$
$3.158 \times Mo^{-0.46} \leq Ar < 29.654 \times Mo^{-0.46}$	$a = 1.14$ $b = -0.176$
$29.654 \times Mo^{-0.46} \leq Ar < 506.719 \times Mo^{-0.46}$	$a = 1.36$ $b = -0.28$
$506.719 \times Mo^{-0.46} \leq Ar$	$a = 0.62$ $b = 0$

3.2.3 Energy and mass conservation equations

The unsteady-state energy conservation equation for a single bubble based on the bubble surface is given as follows:

$$-\frac{1}{r^2}\frac{\partial}{\partial r}\left(r^2 k_g \frac{\partial T_B}{\partial r}\right) + R_{rxn}\,\Delta H_{rxn} = \rho c_p \frac{\partial T_B}{\partial t} \qquad (3.6).$$

In this equation, T_B and k_g are the bubble temperature and the thermal conductivity of the gas within the bubble, respectively. Moreover, c_p is the heat capacity, r is the radial direction and t is the time. Also, R_{rxn} is the rate of methane conversion in the gas phase (Eq. 3.7) and ΔH_{rxn} is the enthalpy of the endothermic cracking reaction of CH_4 to C and H_2, as follows:

$$R_{rxn} = A_0 C_i \; exp\left(-\frac{E_a}{R_g T_B}\right) \qquad (3.7).$$

In addition, C_i is the concentration of component $'i'$, A_0 is the pre-exponential factor, E_a is the activation energy, and R_g is the universal gas constant (8.314 J/mol. K). The

values of the pre-exponential factor (A_0) and the activation energy (E_a) are given in Table 3.2.

Table 3.2. Kinetic constants for methane cracking reaction, for both the internal volume away from the surface layer (non-catalytic) and at the gas-molten bath interface (catalytic) in an $Ni_{0.27}Bi_{0.73}$ column.

	Activation energy [kJ/ mol]	Pre-exponential factor $[1/s]$	Reference
Gas-molten bath interface (catalytic)	208	7.88×10^{4}	[44]
Inside bubble (non-catalytic)	422.9	$1.26\times10^{+14}$	[71]

The initial condition and boundary conditions for Eq. 3.6 are given as follows:

$$T(r,t) = T_g\,, \qquad \text{at} \qquad t = 0 \tag{3.8}$$

$$\frac{\partial T}{\partial r}|_{r=0} = 0\,, \qquad \text{at} \qquad t \geq 0 \tag{3.9}$$

$$k_g \frac{\partial T}{\partial r} = h_{MB}(T_{MB} - T_B)|_{r=r_B}\,. \qquad \text{at} \qquad t \geq 0 \tag{3.10}$$

In these equations, r_B is the bubble radius and h_{MB} is the heat transfer coefficient at the interface of the gas and the molten bath, estimated according to the following equation [28]:

$$h_{MB} = \frac{k_{MB}}{2r_B}(2 + 0.6\,{Re_{MB}}^{0.5}{Pr_{MB}}^{1/3}) \tag{3.11}$$

In this equation, k_{MB} and Pr_{MB} are the conduction and Prandtl number of the molten bath, respectively.

Eq. 3.12 shows the rate of mass conservation of species within the bubble. That is, any mass fluxes within the bubble are due to chemical reactions alone, either within the gas phase or at the interface between the gas and the molten bath.

$$\frac{1}{r^2}\frac{\partial}{\partial r}\left(D_{i,mix}\, r^2 \frac{\partial C_i}{\partial r}\right) + R_{rxn} = \frac{\partial C_i}{\partial t} \quad (3.12).$$

Here too, $D_{i,mix}$ is the diffusion coefficient of component i in the mixture. The initial and boundary conditions for Eq. 3.12 are as follows:

$$C_i = C_{i,0}\,, \qquad \text{at} \qquad t = 0 \quad (3.13),$$

$$\frac{\partial C_i}{\partial r}|_{r=0} = 0\,, \qquad \text{at} \qquad t \geq 0 \quad (3.14),$$

$$D_{i,mix}\frac{\partial C_i}{\partial r}|_{r=r_B} = sR_{rxn,\,CH_4}, \text{ at } t \geq 0 \begin{bmatrix} s=0, \quad if \;\; i = inert\; gas \\ s=1, \;\; if \;\; i = CH_4 \\ s=2, \quad if \;\; i = H_2 \end{bmatrix} \quad (3.15).$$

The symbol, $C_{i,0}$ is the initial composition of component $'i'$ within the bubble.

The diffusion coefficient for component $'i'$ in the gas mixture, $D_{i,mix}$, within the bubble is a function of a two-component diffusion coefficient in the gas mixture and was calculated following an earlier work [72]:

$$D_{i,mix} = \frac{1-y_i}{\frac{y_j}{D_{i,j}}+\frac{y_k}{D_{i,k}}} \quad (3.16).$$

Here too, y_i, y_j, and y_k are the mole fractions of components $'i'$, $'j'$, and $'k'$ in the gas mixture, respectively. $D_{i,j}$ and $D_{i,k}$ are the diffusion coefficients in a two-component gas mixture. The diffusion coefficient of the two-component gas mixture was estimated based on Eq. 3.17 [73, 74]:

$$D_{i,j} = \frac{\left(1.8583\times10^{-7}\right) {T_g}^{3/2}}{P_B\, \Omega^D_{i,j}\,(T)} \sqrt{\frac{1}{M_{w,i}}+\frac{1}{M_{w,j}}} \quad (3.17).$$

In this equation, P_B is the pressure within the bubble, the function $\Omega_{i,j}^{D}(T)$ is the collision integral, which imitates the collision between components $'i'$and $'j'$ [72], and M_w is the molecular weight of each component.

Eq. 3.18 was utilised to calculate the overall methane conversion:

$$X_{CH_4} = \frac{n_{CH_4,0} - n_{CH_4,t}}{n_{CH_4,0}} \quad (3.18).$$

In this equation, $n_{CH_4,0}$ and $n_{CH_4,t}$ are the number of moles of CH_4 at the start and at time, $'t'$, respectively. Since there is a radial distribution of CH_4 within the bubble, $n_{CH_4,t}$ was calculated by Eq. 3.19:

$$n_{CH_4,t} = \int_{r=0}^{r=r_B} 4\pi\, C_{CH_4,t}\, r^2 dr \quad (3.19).$$

The fractions of the methane conversion inside the bubble, $X_{CH_{4,g}}$, and at the interface of the bubble and molten bath at time t, $X_{CH_{4,intf}}$, are given by:

$$X_{CH_{4,intf}} = \frac{-\int_{t-1}^{t} 4\pi\ {r_B}^2\, D_{CH4,mix} \frac{\partial C_{CH4}}{\partial r}|_{r=r_B}\, dt}{n_{CH4,cons\,(t)}} \quad (3.20),$$

$$X_{CH_{4,g}} = 1 - X_{CH_{4,intf}} \quad (3.21).$$

Here, $n_{CH4,cons\,(t)}$ is the total number of moles of CH_4 consumed at time t: at the nozzle and at $t = 0$, $n_{CH4,cons} = 0$. Hence, the calculated $X_{CH_{4,intf}}$ and $X_{CH_{4,g}}$ are plotted for $t \geq 0$.

At each height within the bath, the pressure within the bubble, P_B, was correlated with the static pressure and the surface tension, σ, of the bath over the bubble using Eq. 3.22:

$$P_B = \frac{2\sigma}{r_B} + \rho_{MB} g H_{MB} + P_0 \quad (3.22).$$

In this equation, P_0 is the pressure on top of the molten bath surface, and H_{MB} is the height of the molten bath at the top of the bubble.

The bubble volume (V_B) was estimated as follows:

$$V_B = \frac{nZR_gT_B}{P_B} \quad (3.23).$$

In this equation, n and Z are the number of moles and the compressibility factor, which is calculated as follows [75]:

$$Z = 1 + 0.257\left(\frac{P_B}{P_c}\right) - 0.533\left(\frac{P_B}{P_c}\right)\left(\frac{T_c}{T_B}\right) \quad (3.24).$$

Here, the subscripts $'B'$and $'c'$ stand for the bubble and the critical value, respectively. The initial bubble radius was calculated from Tate's law equation (Eq. 3.25) [51], and then the radius at the other locations within the column was estimated based on Eq. 3.26:

$$r_{B,in} = \sqrt[3]{\frac{3r_{noz}\sigma}{2(\rho_{MB}-\rho_g)g}} \quad \text{at} \quad t = 0 \quad (3.25),$$

$$r_B = \sqrt[3]{\frac{3V_B}{4\pi}}. \quad \text{at} \quad t > 0 \quad (3.26).$$

In these equations, r_{noz} is the nozzle diameter.

3.2.4 Computational methodology

The above-mentioned sets of partial differential equations were discretized and solved simultaneously using the finite element method with the implicit Gauss-Seidel iteration. Figure 3.2 shows the algorithm employed for the simultaneous solution of the sets of equations using an in-house developed MATLAB code. The model was

initiated by providing the gas composition and temperature, together with the height and temperature of the molten bath. Each subsequent time step then uses the temperature and gas composition distribution from the previous time step. The conservation equations of energy and mass were solved simultaneously to calculate the new distributions, and then compared with the previous iteration. This process was repeated until the condition of convergence is satisfied. Afterwards, the bubble mole fraction, species concentrations, number of moles, the size, and the bubble's physical properties and rise velocity were calculated. Next, the concentration of each component was calculated based on the new size and location of the bubble within the molten bath. Finally, the bubble location was updated, and the calculations repeated until the bubble reaches the surface of the bath.

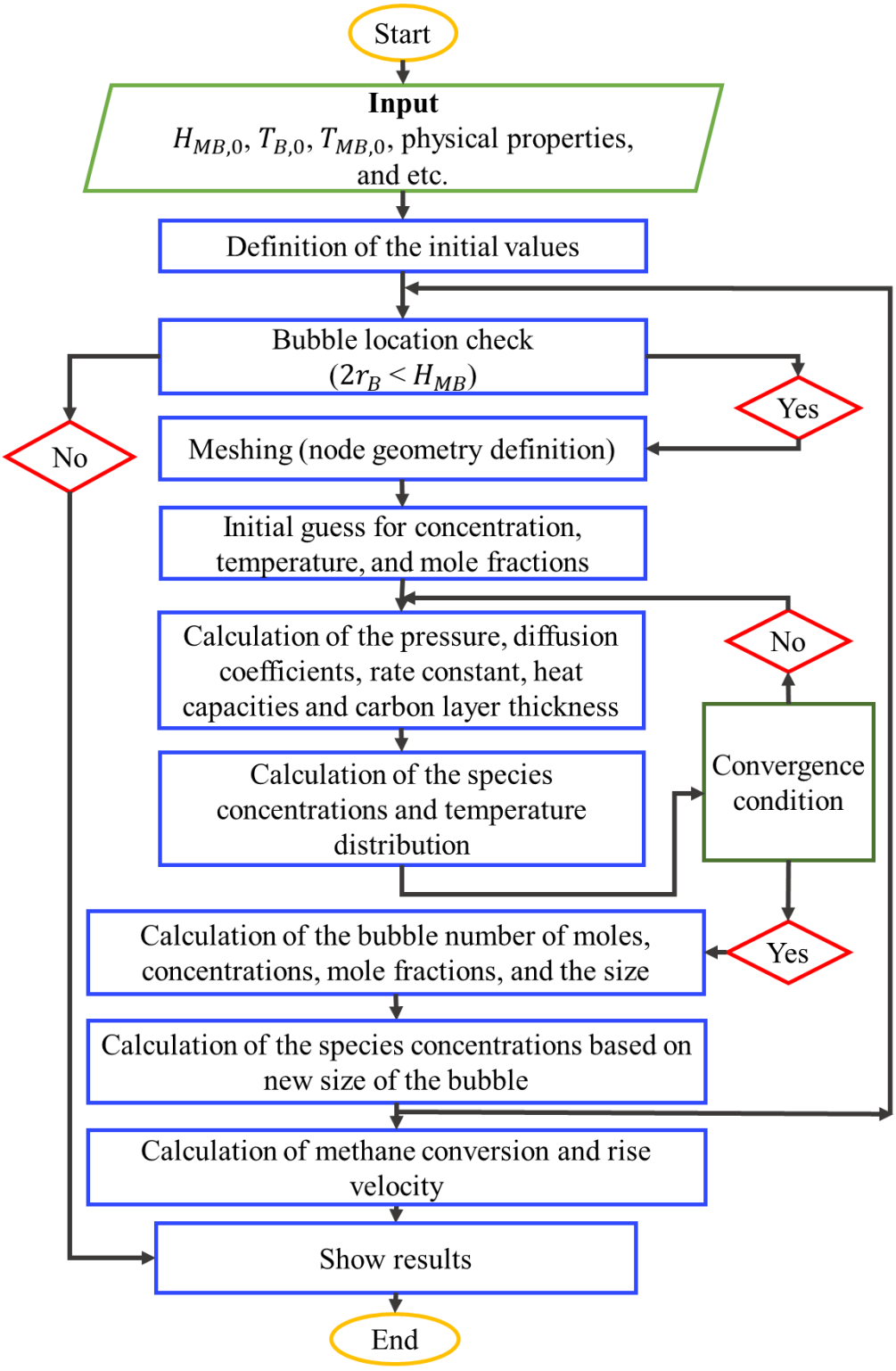

Figure 3.2. Flow chart of the process by which the set of equations was solved numerically at each time step.

3.3 Results and discussion

3.3.1 Model validation

Direct validation of the pyrolysis of a single rising and pyrolysing bubble in a molten bath is not possible due to the limited availability of experimental data under relevant conditions. Therefore, a process of indirect verification was performed by comparing the bubble rise velocity and total calculated conversion using the most relevant available experimental data. Figure 3.3 presents a comparison of the calculated bubble rise velocity as a function of the bubble radius with the experimental measurements reported by Anderini *et al.* [76] for a single argon bubble in a column of molten tin at a temperature of 535 K, under atmospheric pressure. As shown, the calculated results provide a good agreement with the experimental data (with an error of ±3%).

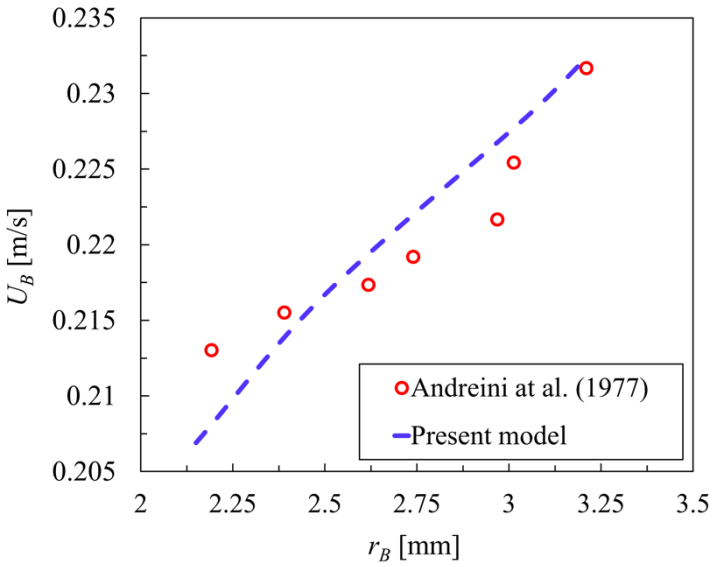

Figure 3.3. The values of the bubble rise velocity as a function of the bubble radius for a system of argon and tin at a temperature of 535 K, as calculated from the present model together with the experimental data reported Anderini *et al.* [76].

Figure 3.4 presents the calculated mean values of the methane conversion, $X_{CH_4,m}$, into C and H_2 as a function of the molten bath height in comparison with the available experimental data reported by Upham *et al.* [44] for a molten $Ni_{0.27}Bi_{0.73}$ bath and the conditions summarized in Table 3.3. Since no measurements of the bubble size were reported in this work, we used Tate's law (Eq. 3.25) to estimate the initial bubble radius to be 2.1 mm. In this case ($r_B = 2.1$ mm): methane conversion exponentially varies with molten bath height.

As depicted in Figure 3.4, with this initial size of the bubble, the experimental data and model predictions agree within less than 10% error, where the molten bath height is more than 100 mm.

It is noteworthy that the selected experiments [37, 44] introduced the methane into the column through pipes that were inserted vertically downwards within the molten bath, which results in pre-heating of the inlet gas. According to this approach and based on the calculations, the injected gas temperature at the nozzle tip is much higher than at room temperature. For this reason, the initial gas temperature of the bubble leaving the nozzle was calculated as shown in Table 3.3. The employed heat transfer equations for the estimation of the temperature of the bubble, leaving the submerged nozzle, are given in Supplementary Information-A. However, the conversion within the submerged pipe is neglected because of the short residence time of the gas within it.

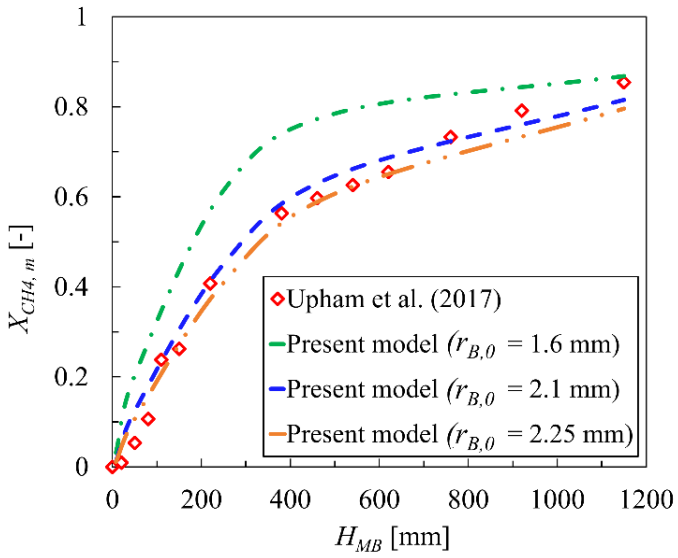

Figure 3.4. Comparison of the calculated mean methane conversion for three initial bubble radii (1.6, 2.1, and 2.25 mm) (dash lines) with experimental data (diamonds) as a function of the molten bath of $Ni_{0.27}Bi_{0.73}$ height, based on the experimental conditions presented in Table 3.3 [44].

Table 3.3. Experimental conditions reported by Upham *et al.* [44] and Rahimi *et al.* [37] for pyrolysis in a molten metal bubble column.

Parameters	Upham [44]	Rahimi [37]
Molten bath type	$Ni_{0.27}Bi_{0.73}$	$Ni_{0.27}Bi_{0.73}$
Molten bath height [mm]	1100	110, 240, 350, 660
Molten bath temperature [K]	1313	1273
Calculated bubble radius [mm]	2.1	2.8

Column height [mm]	1150	300, 430, 1000
Column radius [mm]	6	11
Nozzle position	Vertically downward	Vertically downward
Nozzle radius [mm]	1.5	1
Headspace temperature [K]	1213	1273
Headspace length [mm]	50	80
Conversion in headspace section	-	2.7 ± 0.5 % @ 1273K
Conversion for case with additional 110 mm layer of molten salt	-	2%
Gas mixture	80% CH_4, 20% Ar	70% CH_4, 30% Ar
Calculated Temperature of the bubble introduced into the bath from nozzle [K]	1313	995
Feed gas flowrate [sccm]	10	10

The model predictions were also compared with the experimental data reported by Rahimi *et al.* [37] in Figure 3.5 for the conditions listed in Table 3.3. This experiment employed a layer of molten salt on top of the molten metal to separate any drops of metal from the bubbles. The initial radius of the bubble was estimated to be 1.8 mm using Tate's law, following the approach described above, this also being due to the

absence of an experimental measurement of this parameter. However, better agreement is found for an assumed initial radius of 2.8 mm. One possible explanation for this difference is the impact of the molten salt layer on top of the molten $Ni_{0.27}Bi_{0.73}$, which affects the size and rise velocity of the bubble through the column, as well as the residence time. It can be seen that there is a good agreement for case $'iii'$, which does not consider the molten salt layer above the molten catalyst bath. However, by decreasing the height of the molten $Ni_{0.27}Bi_{0.73}$ and increasing the length of the molten salt on top of that, the departure of the calculated methane conversion from the experimental results increases.

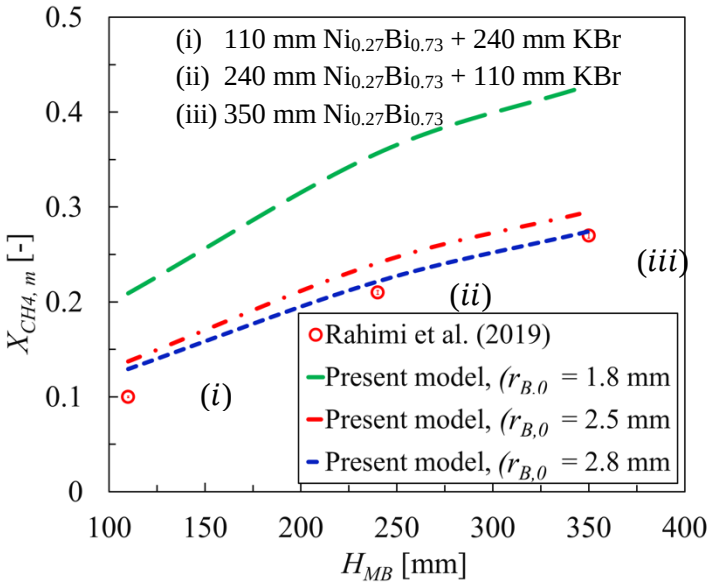

Figure 3.5. A comparison of the calculated and measured methane conversion as a function of the height of the bubbling column containing $Ni_{0.27}Bi_{0.73}$ with a layer of molten salt (KBr) on top of the molten metal. The input parameters were based on the conditions presented in Table 3.3 [37].

Further confidence in the numerical method has been obtained by comparing the predicted temperature distribution within a non-reacting bubble of radius 0.1 and 6 mm in a molten tin column at 1073 K with the data obtained from the analytical solution of the heat transfer equation. Both the analytical and numerical calculated temperatures match within less than $\pm 1\%$ error. This gives additional verification that the equations have been implemented correctly in the model (see Supplementary Information-B).

3.3.2 Impact of bubble size and rise velocity

Figure 3.6 presents the calculated variations in bubble radius, r_B, and rise velocity, U_B, as a function of the bubble distance from the bottom of the bath of molten $Ni_{0.27}Bi_{0.73}$, z_B, for the conditions of Upham's experiments (Table 3.3). As expected, the calculated bubble radius, while it is rising from the bottom towards the bath surface, increases with height from ~2.1 mm at z_B= 0 mm to approximately 3 mm at z_B= 1100 mm. This is consistent with the change in the static pressure above the bubble ($\rho_{MB} g H_{MB} + P_0$), decreasing from 195 kPa at z_B=0 mm to 102 kPa at z_B=1100 mm. In addition, the process of methane decomposition into carbon and hydrogen increases the bubble radius by increasing the number of gas moles within the bubble. That is, one mole of CH_4 decomposes into two moles of H_2 gas ($CH_4 \rightarrow 2H_2 + C$) [45]. Furthermore, the buoyancy force increases with an increase in bubble radius and changes the bubble rise velocity by approximately 44% from 0.21 m/s at z_B= 0 mm to 0.30 m/s at z_B= 1100 mm. The residence time scales inversely with the rise velocity. Hence, an increase in rise velocity will decrease the time for both surface interaction with the molten bath and for heat transfer between the gas within the bubble and the molten

bath. In other words, decreasing the bubble radius provides more time for the heat transfer to achieve the required temperature for methane pyrolysis. Meanwhile, the characteristic length of conduction heat transfer within the bubble decreases with the bubble radius, leading to a more uniform temperature distribution within the bubble. This highlights the importance of accounting for changes to the bubble size and rise velocity within a molten bath column, despite both being assumed to be constant in previous models [28, 41, 51]..

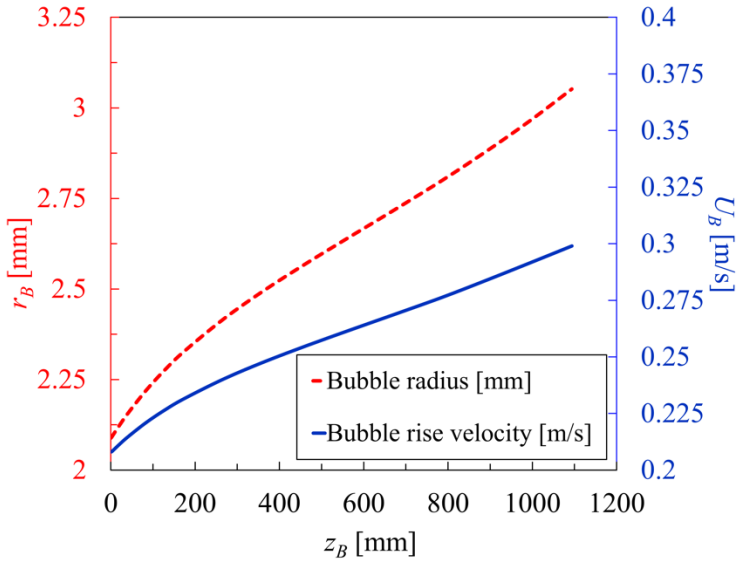

Figure 3.6. Calculated variations in bubble radius (left vertical axis) and rise velocity (right vertical axis) as a function of the distance of the bubble from the bottom of the molten bath under conditions reported in Table 3.3 [44]

3.3.3 Sensitivity analysis

A sensitivity analysis was undertaken to assess the impact on methane conversion of the temperature of the bath and inert gas, bubble radius, molten bath height, and mole

fraction of the injected gas, using Upham's experiments as the reference conditions. Table 3.4 presents the range over which each parameter was varied.

Table 3.4. The range of conditions over which parameters were varied for the sensitivity analysis of the rising and pyrolysing bubble within a molten $Ni_{0.27}Bi_{0.73}$ bath.

	Variables	Reference conditions	Variation range
Bubble	Input temperature [K]	1313	313-1313
	radius [mm]	2.1	0.6-2.6
	Gas composition	80% CH_4-20% Ar	10-100% CH_4
Molten bath	Temperature [K]	1313	1013-1413
	Height [mm]	1100	50-4000

3.4.3.1 Effect of the bath temperature

The axial variation of the calculated mean methane conversion, $X_{CH_4,m}$, as a function of the bubble distance from the bottom of the column (z_B) within the molten bath is shown in Figure 3.7a for a series of molten bath temperatures, T_{MB}. Figure 3.7b presents the dependence on temperature of the final mean conversion of methane, $X_{CH_4,m,f}$, when the bubble reaches the surface of the molten bath. As expected, the conversion is highly sensitive to the bath temperature owing to the exponential dependence of reaction rates on temperature (Eq. 3.7), both within the bubble (in the

gas phase) and over the bubble and molten bath interface. This behavior has also been observed previously [28, 37, 51]. For example, the maximum overall conversion increases from 0.6% at T=1013 K, to approximately 82% and 94% for temperatures of 1313 K and 1413 K, respectively. Moreover, $X_{CH_4,m,f}$ varies non-linearly with the molten bath temperature, such that the dependence becomes less sensitive at high bath temperatures than at low ones. For example, an increase in T_{MB} from 1113 K to 1213 K leads to a 79.2% increase in $X_{CH_4,m,f}$, while $X_{CH_4,m,f}$ only increases by approximately 13.2% points as T_{MB} is increased from 1313 K to 1413 K. That is because, by increasing the temperature to more than 1400 K, methane conversion approaches the equilibrium value, which is ~98%.

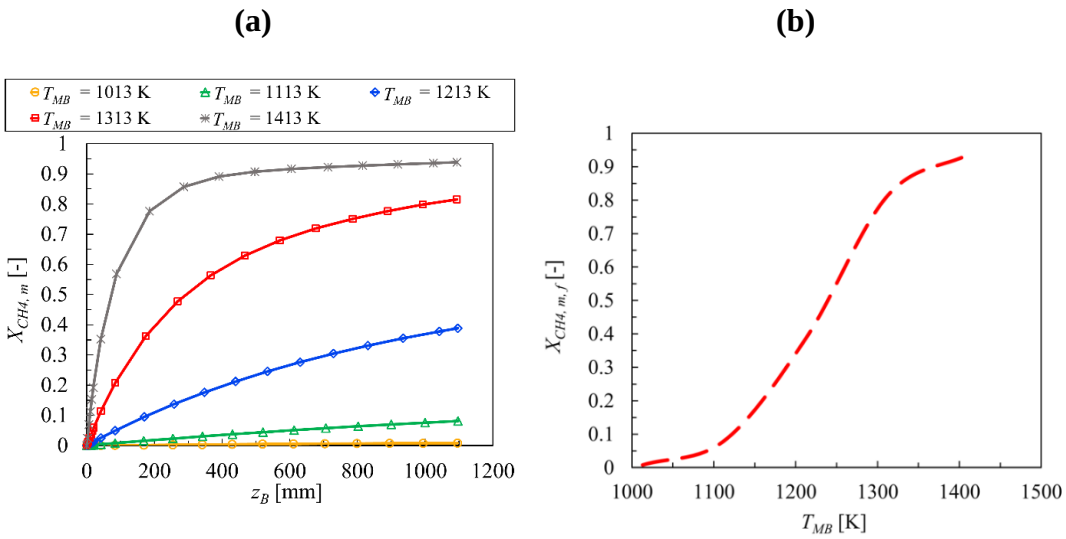

Figure 3.7. Calculated mean values of methane conversion a) in a bubble as a function of the axial position in a 1100 mm height column of $Ni_{0.27}Bi_{0.73}$ for a series of molten bath temperatures; b) at the top of the column as a function of the molten bath temperature. Other conditions are shown in Table 3.3 [44].

Figure 3.8a-c presents the calculated methane mole fraction distribution as a function of time and bubble radius while it rises and pyrolyses through a column of 1100 mm molten $Ni_{0.27}Bi_{0.73}$ for three molten bath temperatures of 1013, 1213, and 1413 K. This shows that the calculated concentration of methane is approximately uniform through the bubble at any given condition. In addition, there is little difference in both the bubble residence time and radius for the three temperatures. As abovementioned, increasing the temperature from 1013 K to 1413 K has a large effect on methane consumption and, consequently, on the hydrogen production. For a bath temperature of 1013 K, as Figure 3.8a shows, the mole fraction of methane, for the reference conditions, decreases by only 0.7% from 0.8 to 0.793. and by increasing the bath temperature to 1413 K, Figure 3.8c, y_{CH_4} decreases by 96.4% to a final value of ~0.03 from 0.8, which is consistent with higher methane conversion.

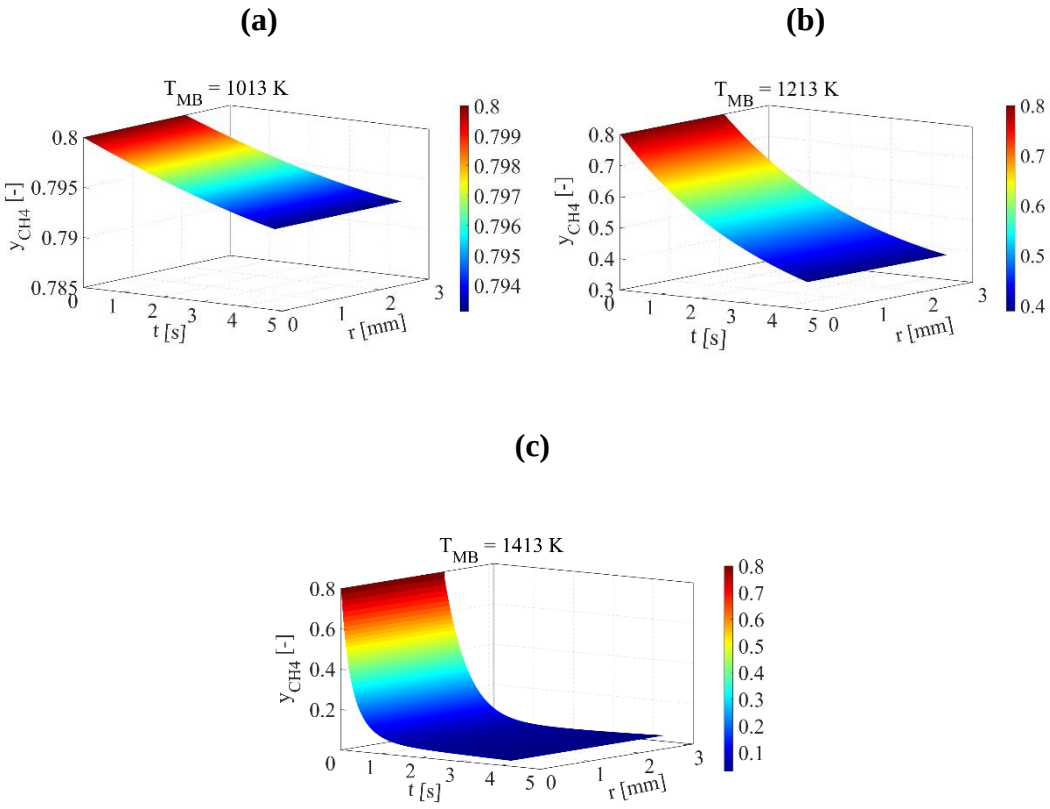

Figure 3.8. Methane mole fraction distribution as a function of time and radial distance within a bubble while it rises and pyrolyses within a column of 1100 mm of molten $Ni_{0.27}Bi_{0.73}$ for columns at temperatures of a) 1013 K, b)1213 K, and c) 1413 K. Other conditions are shown in Table 3.3 [44]. (Note the difference in scale for each Figure.)

Figure 3.9 presents the calculated portion of the total mole consumption that occurs at the bubble's interface with the molten bath, $X_{CH_{4,intf}}$, as a function of the time (while it rises within the column) for the conditions of Upham's experiment (Table 3.3) and for a series of molten bath temperatures. It can be seen that, more than 97.5% of the overall mole consumptions, at each time step, occurs at the bubble's surface, and less than 2.5% takes place within the bubble. Also, decreasing the molten bath temperature

from 1313 K to 1113 K results in an increase in the portion that occurs at the gas-molten bath interface. This implies that bubble's surface has a significant catalytic impact on the overall conversion for the studied conditions, and that the reaction is kinetically controlled. This is consistent with previous studies that show using a catalytic molten bath increases the hydrogen production via methane pyrolysis within a bubble column [37, 44]. Moreover, as the bubble approaches the surface of the molten bath, $X_{CH_{4,intf}}$ increases. That is attributed to the decreasing of the methane concentration within the bubble, as it rises within the bath, and the faster conversion rate of methane at the gas-molten bath interface, which leads to the diffusion of methane towards the surface of the bubble and less conversion within the gas phase.

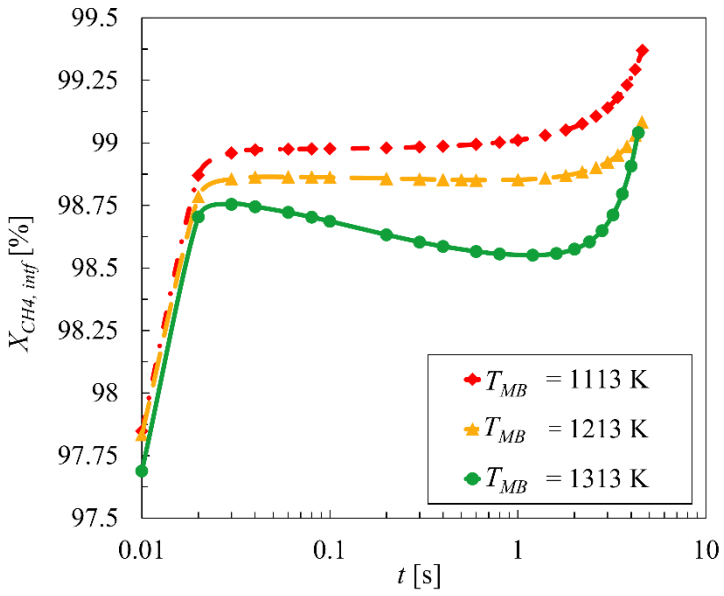

Figure 3.9. Calculated fraction of methane consumption (in percentages) at the bubble's interface with the molten $Ni_{0.27}$ $Bi_{0.73}$ bath for a series of molten bath temperatures, as a function of the time that the bubble rises within the column. Other conditions are presented in Table 3.3 [44].

3.4.3.2 Effect of the temperature of the injected gas

Figure 3.10a and b show the estimated methane conversion as a function of the gas bubble's distance from the bottom of the molten $Ni_{0.27}Bi_{0.73}$ column, and the significance of the initial temperature of the injected gas mixture of CH_4 and Ar over the range 313 — 1313 K. Figure *3.10*b illustrates the final conversion of methane, $X_{CH_{4,m,f}}$, as a function of the inlet gas temperature, $T_{g,0}$. It can be seen that $X_{CH_{4,m,f}}$ increases almost logarithmically with an increase in $T_{g,0}$. For instance, at $T_{g,0}$ = 313 K, conversion is about 0.71 and it increases to ~0.82 at $T_{g,0}$ = 1313 K. That is, at higher values of $T_{g,0}$, methane decomposes faster than at low ones.

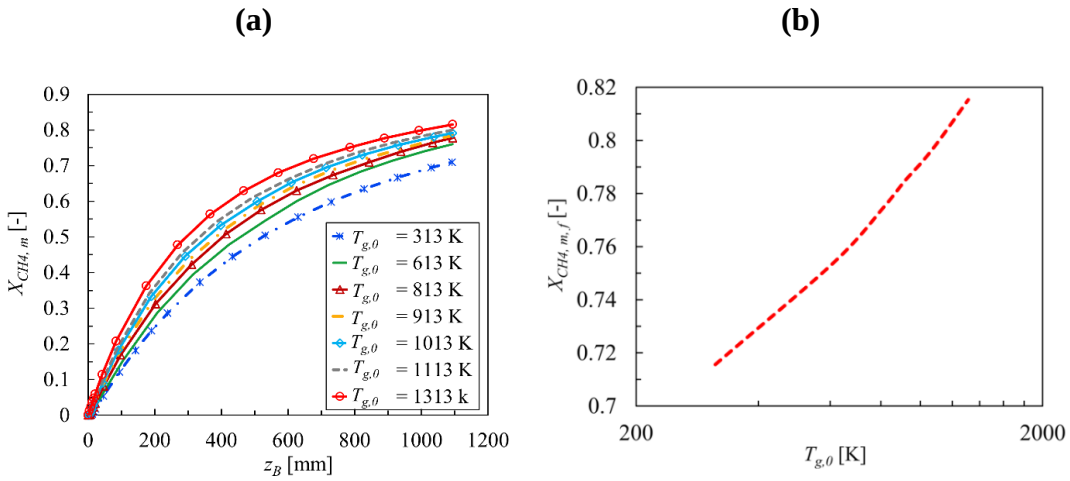

Figure 3.10. Calculated mean methane conversion a) within a rising and pyrolysing bubble as a function of its distance from the bottom of the column for various initial temperatures of the gas mixture for the reference case (80% of methane and 20% of argon), and b) at the top of the molten bath as a function of the initial temperature of the gas mixture. The other parameters were selected based on the conditions in Table 3.3 [44].

Figure 3.11 shows the distribution of temperature within the bubble in the radial direction as a function of time for the case where the initial temperature of the injected gas is 1113 K. The calculations show that the gas temperature under the studied conditions ($T_{g,0}$=1113 K) of initial radius of 2.1 mm in a column of 1100 mm molten $Ni_{0.27}Bi_{0.73}$ reaches the molten bath temperature (1313 K) in about 0.06 s. However, it causes an approximately 2% decrease in the overall methane conversion compared with the case where the injected gas is at the molten bath temperature, 1313 K.

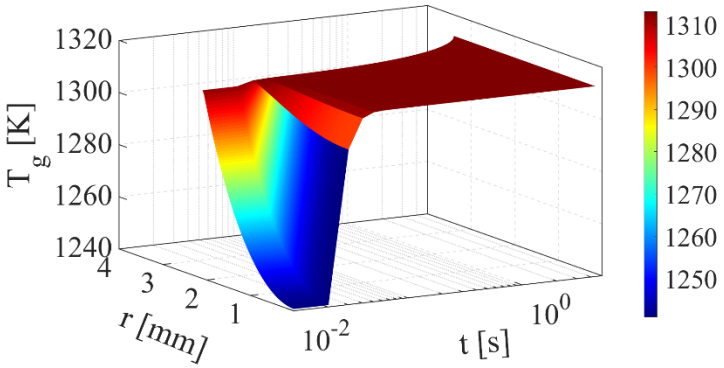

Figure 3.11. Temperature distribution of the gas mixture of methane and argon (reference case) as a function of time over the radius of a bubble ($r_{B,0} = 2.1$ mm) when the initial temperature of the gas is 1113 K. The other operational parameters were based on the conditions reported in Table 3.3 [44].

Figure 3.12 shows the ratio of time that it takes the gas content of the bubble to reach the molten bath temperature, and the bubble residence time in the column, τ, as a percentage shown as a function of the initial temperature of the injected gas. It can be seen that the percentage of the ratio of the heating time to the bubble residence time within the molten bath decreases logarithmically from ~2.8% to ~1.8% by increasing the initial temperature of the gas from 313 K to 1113 K, respectively. Despite the quick

increase in the temperature of the bubble's gas content over the radius to 1313 K, the initial gas temperature has an impact on the overall methane conversion.

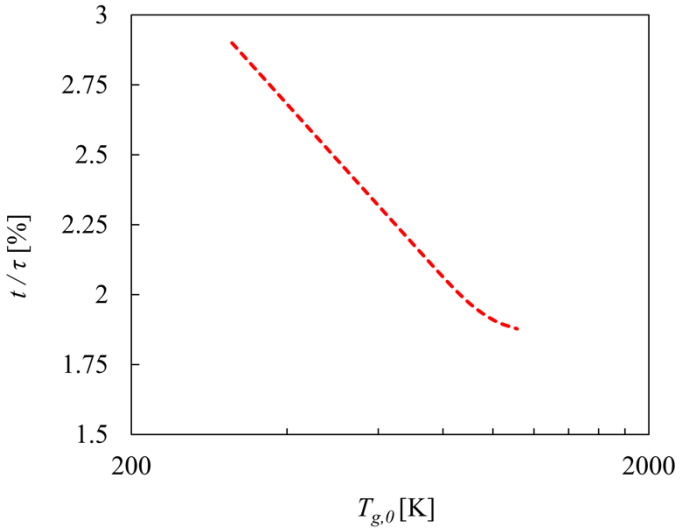

Figure 3.12. Ratio of the heating time of the bubble's gas content to its residence time within the molten bath as a percentage of the function of the initial temperature of the injected gas. The other operational parameters were based on the conditions reported in Table 3.3 [44].

Figure 3.13 shows the calculated portion of the total methane consumption occurring at the bubble's interface with the molten bath, $X_{CH_{4,intf}}$, as a function of the time for a series of initial gas temperatures. Graphs show that by increasing the initial temperature of the injected gas to the molten bath from 313 K to 1313 K, $X_{CH_{4,intf}}$ increases slightly from less than 98.5% to more than 99% at the top of the column. Consequently, the consumption percentage within the gas phase of the bubble decreases from ~1.5% to ~0.7%. This could be due to both the temperature and the methane distributions within the bubble.

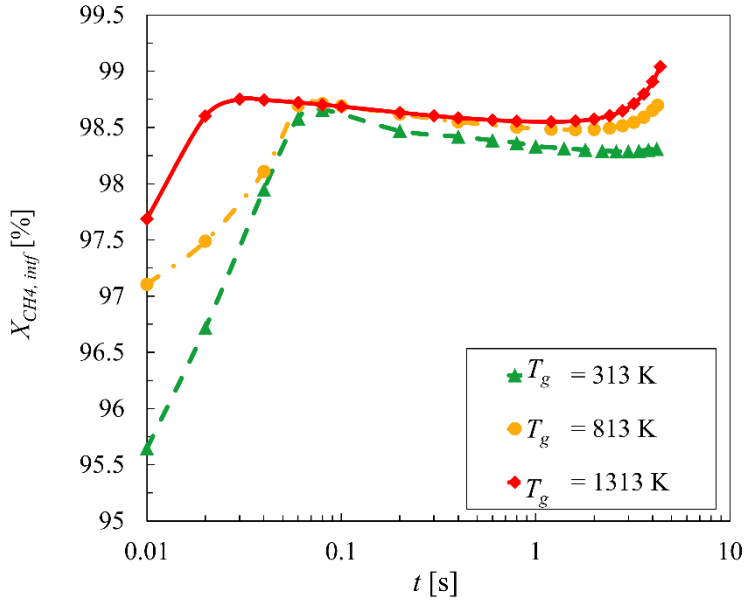

Figure 3.13. Calculated fraction of methane consumptions (in percentages) at the bubble's interface with the molten $Ni_{0.27}$ $Bi_{0.73}$ bath for a series of initial gas temperatures, as a function of the time that the bubble rises within the column. Other conditions are presented in Table 3.3 [44].

3.4.3.3 Effect of the bubble size

Figure 3.14a presents the sensitivity of the estimated mean methane conversion, $X_{CH_{4,m}}$, within a rising and pyrolysing bubble as a function of the bubble's distance from the bottom of the column (z_B) for a series of initial bubble radius values ($r_{B,0}$ = 0.6 - 2.6 mm) and for the conditions reported in Table 3.3. It shows that as the bubble's radius decreases, hydrogen production increases. Figure 3.14b also shows the final methane conversion, $X_{CH_{4,m,f}}$, as a function of the initial radius of the bubble. For the studied range of the bubble's radius, conversion decreases about 15% when the bubble size increases ~2.5X. This is consistent with the trend of increase in the bubble's rise velocity, and hence decrease in its residence time. Also, with the

increased ratio of the surface area to the volume of the bubble by reducing $r_{B,}$ the heat transfer from the molten bath both to the surface and within the bubble increases. That is consistent with previous studies that show that by using a Mott sparger instead of a single orifice, despite using a lower temperature (1023 K instead of 1273 K), conversion increases to 51% from 32%, respectively [77]. That is because, when using a Mott sparger instead of a single orifice, the bubble size decreases, which, in turn, leads to a greater surface area of the bubble being in contact with the molten bath and hence increasing the conversion rate at the bubble-molten bath's interface.

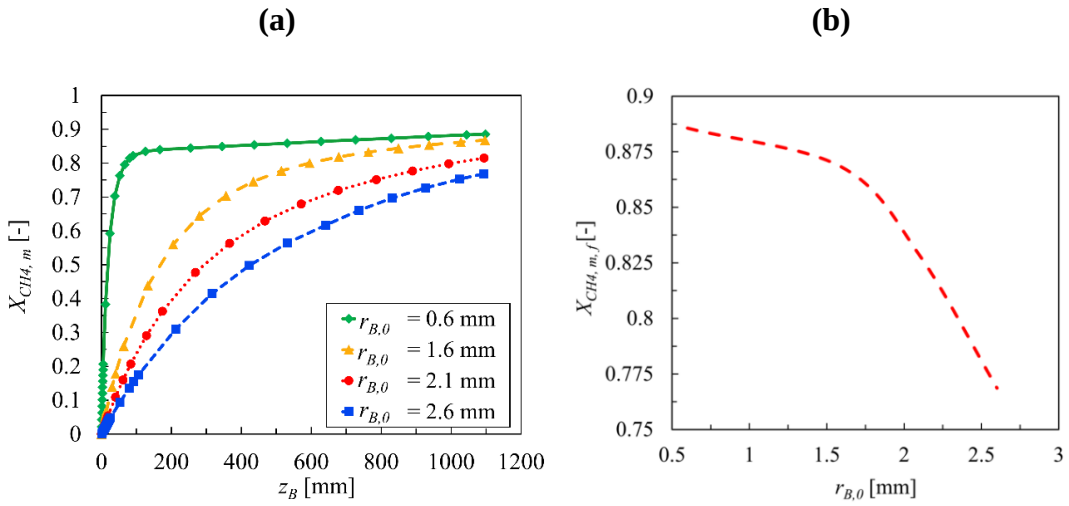

Figure 3.14. Calculated conversion of methane a) within a rising and pyrolysing bubble as a function of the axial distance of the bubble from the bottom of a 1100 mm height molten bath column of $Ni_{0.27}Bi_{0.73}$ for a series of initial bubble radii, and b) at the top of the molten bath as a function of the initial bubble's radius. The other parameters were selected based on the conditions reported in Table 3.3 [44].

Figure 3.15 presents the calculated fractions of methane consumption that occurs at the interface of the bubble with the molten bath, $X_{CH_4,intf}$, as a function of the time that the bubble rises within the column for a series of the initial bubbles' radii. As

shown, the portion of methane mole consumption either within the gas or at the gas-molten bath interface is sensitive to the bubble's radius mainly at the beginning and the end of the bubble rise within the column. However, this sensitivity diminishes in the middle of the column and the estimated $X_{CH_{4,intf}}$ becomes independent of each individual bubble's radius. By decreasing the initial size of the bubble from ~2.6 to 1.6 mm, at the start of the rise, conversion occurring at the interface increases from approximately 97.2% to more than 98%. Commensurate with this, methane mole consumption within the gas phase of the bubble, $X_{CH_{4,g}}$, decreases from > ~2.7% to > ~1.7%. That is because the gas-molten bath interface increases when the bubble radius is decreased.

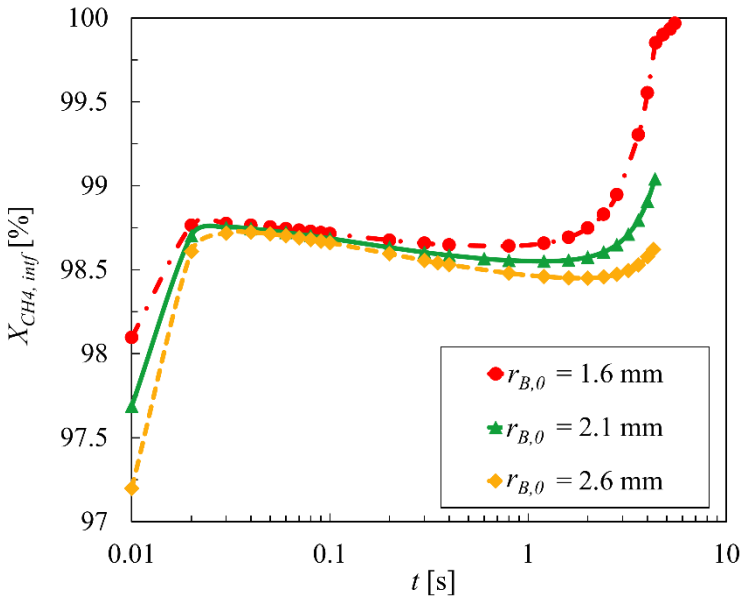

Figure 3.15. The calculated fraction of the total methane consumption that occurs at interface of the bubble with the catalyst as a function of the time that the bubble rises within the column for a series of the initial bubble's radii. Other factors are listed in Table 3.3 [44].

The axial variations of the mean methane mole fraction, $y_{CH_4,m}$, within a bubble as a function of the time that a bubble with various initial radii rises within a 1100 mm height of a molten bath column at 1313 K is shown in Figure 3.16a. As seen, for a bubble with an initial radius of 1.2 mm, it takes about 17.5 s to reach to the top of the molten bath and the methane content decreases from 0.8 to ~0.05 (~88.5% conversion of methane to hydrogen and carbon). However, if the initial radius of the bubble increases to 1.6 mm, the bubble spends less time in the column, approximately 5.5 s, and methane conversion decreases to ~86.5%. The residence time and conversion of methane decrease to 4.3 s to ~77%, respectively, by increasing the initial bubble radius to 2.6 mm. As the size of the bubble decreases, the interface of the bubble and the bath increases. That is, the methane conversion or hydrogen production increases as the bubble size is decreased. Moreover, the radial distribution of the methane mole fraction for a case where the initial bubble radius is equal to 1.6 mm is presented in Figure 3.16b. It can be seen that the methane distribution remains almost uniform within the bubble as it rises from the nozzle to the bath surface.

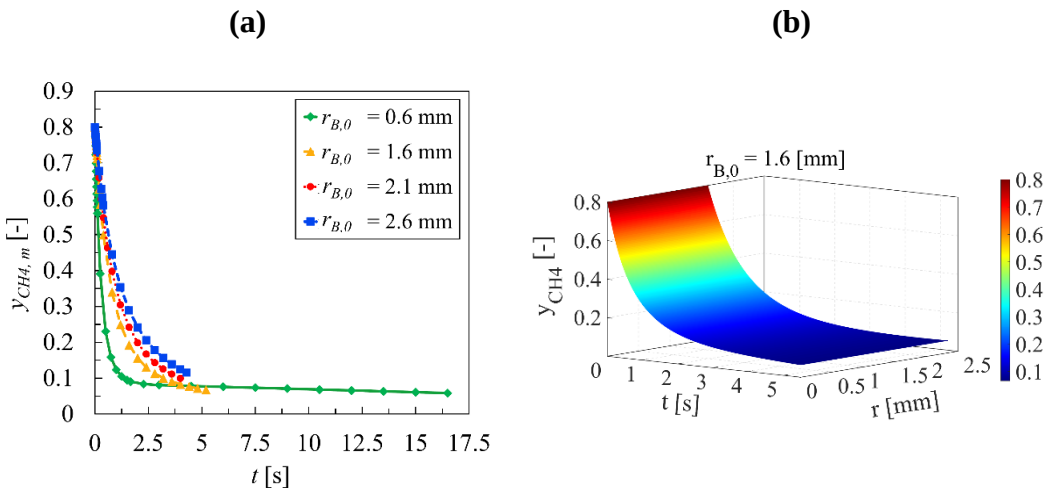

Figure 3.16. Distribution of the mean methane mole fraction within the bubble a) as a function of the time that the bubble spends within the molten bath with various initial radii, and b) as a function of the rise time over the radius of a bubble with $r_{B,0}$ = 1.6 mm. The rest of the parameters were selected based on the conditions in Table 3.3 [44].

3.4.3.4 Sensitivity to the height of the molten bath

Figure 3.17a presents the sensitivity of the calculated mean value of methane conversion to the height of the molten bath, H_{MB}, as a function of the distance of the rising and pyrolysing bubble within the column. As seen in Figure 3.17b, the final estimated mean value of methane conversion, $X_{CH_4,m,f}$ increases asymptotically with an increase in the molten bath height. It is highly sensitive to the height of the molten bath column for heights less than about 1000 mm, but only weakly sensitive for heights greater than this. In the range of $50 \leq H_{MB} \leq 2000$ mm, the higher the molten bath height, the greater the time spent by the bubble in contact with the bath, and this results in an increase in methane conversion. However, for the studied

conditions and ranges, as Figure 3.17b shows, methane conversion is no further sensitive to the molten bath height when it is greater than 2000 mm.

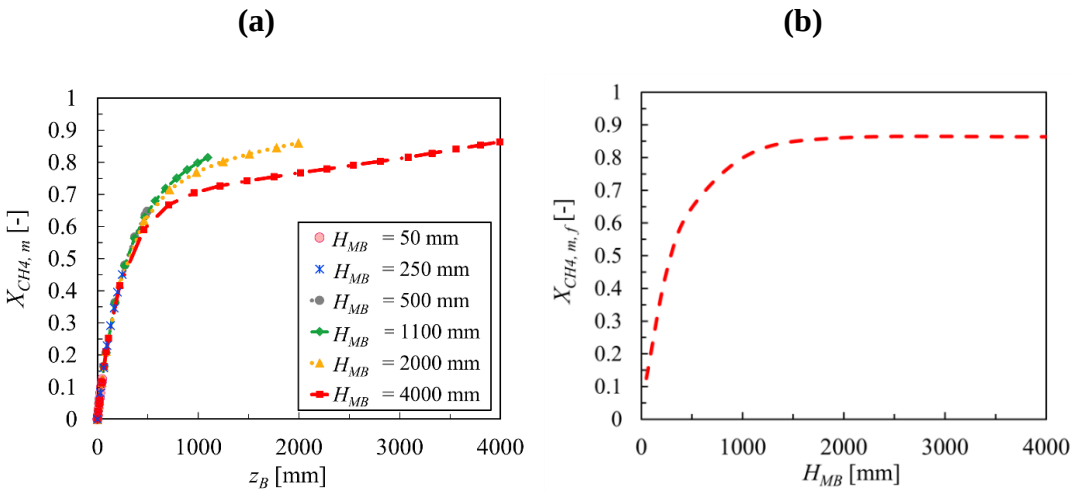

Figure 3.17. Calculated mean value of methane conversion a) within the bubble as a function of the distance of the bubble from the bottom of the column for a series of column heights, and b) at the top of the bath as a function of the height of the molten bath. Other conditions are as summarised in Table 3.3 [44].

The estimated distributions of the methane mole fraction within the bubble as a function of time, over the radius of the bubble while it rises and expands through the molten bath for three heights of column, 50, 1100, and 2000 mm, are shown in Figure 3.18a-c, respectively. As Figure 3.18a illustrates, in a column with 50 mm height of molten $Ni_{0.27}Bi_{0.73}$, the mole fraction of methane within the bubble decreases by only ~ 19% from 0.8 to ~0.65. Moreover, as shown, the bubble radius growth is small in this column, varying from 2.1 mm at the bottom of the column, z_{MB} = 0 mm, to 2.7 mm at the top of the molten bath at $z_{MB} \cong 50$ mm. However, by increasing the molten bath height to 1100 and 2000 mm, Figure 3.18b and c, the methane mole fraction decreases to less than 0.2, whilst the bubble radius increases from an initial value of

2.1 mm to approximately 3 and 4 mm, respectively. Furthermore, by increasing the molten bath height from 50 mm to 1100, and 2000 mm, the time that the bubble spends in contact with the bath increases from 0.2 s to 4.4 s, and 7.9 s, respectively, as shown in Figure 3.19. Therefore, the height of the molten bath is a factor that impacts methane conversion significantly, as previous studies have shown [37, 44] and it must be considered in any prediction of methane conversion or hydrogen production estimation.

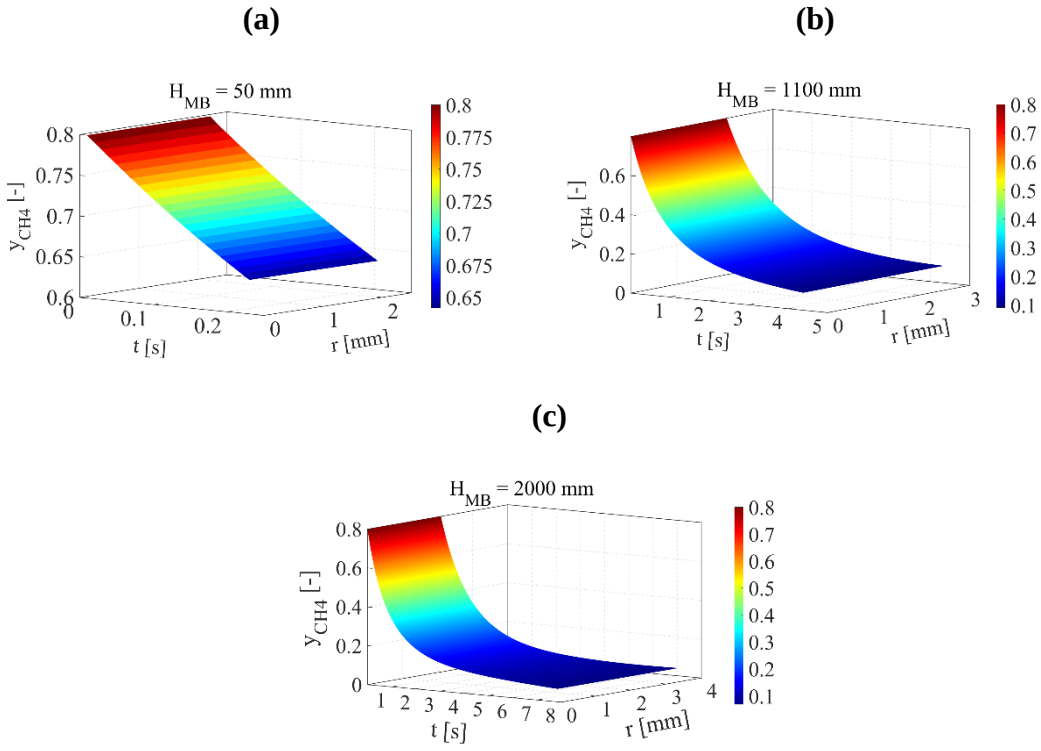

Figure 3.18. The calculated distribution of the mole fraction of methane within a bubble as a function of the time and over the bubble radius, where the molten bath height is equal to a) 50 *mm*, b) 1100 *mm*, and c) 2000 *mm* . The other factors are based on Table 3.3 [44].

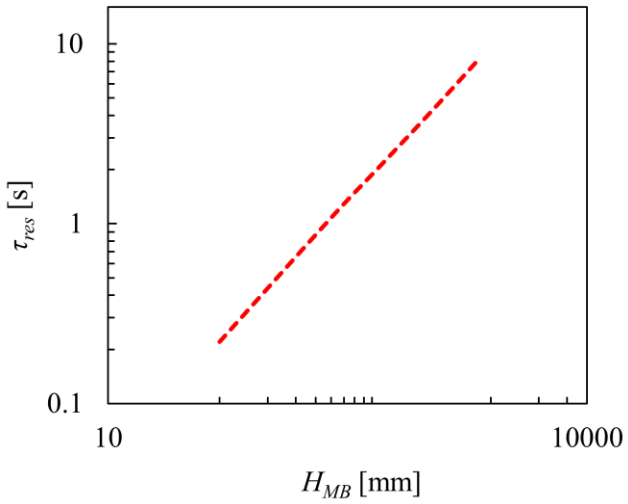

Figure 3.19. Bubble residence time within column as a function of the molten bath height for the range 50 – 2000 mm.

Figure 3.20 presents the percentage of the methane consumption that occurs at the surface of the bubble, $X_{CH_4,intf}$, as a function of the time, whilst it rises within the column for a series of the height of the molten bath, H_{MB}. As can be seen, by increasing the column height from 50 to 2000 mm, the percentage of the methane consumption at the bubble's surface decreases from >98% to <97.5% at the start of the rise and then it increases at the top of the column. That is, the pressure within a bubble with the same size rises with any increase in the height of the column and that results in a less forward reaction of methane decomposition, impacting the conversion within and at the bubble's surface. However, by increasing the height of the column, the contact time between the bubble and the molten bath elevates and, consequently, the overall conversion increases, but the percentage within and at the interface of the bubble at the bottom of the column varies.

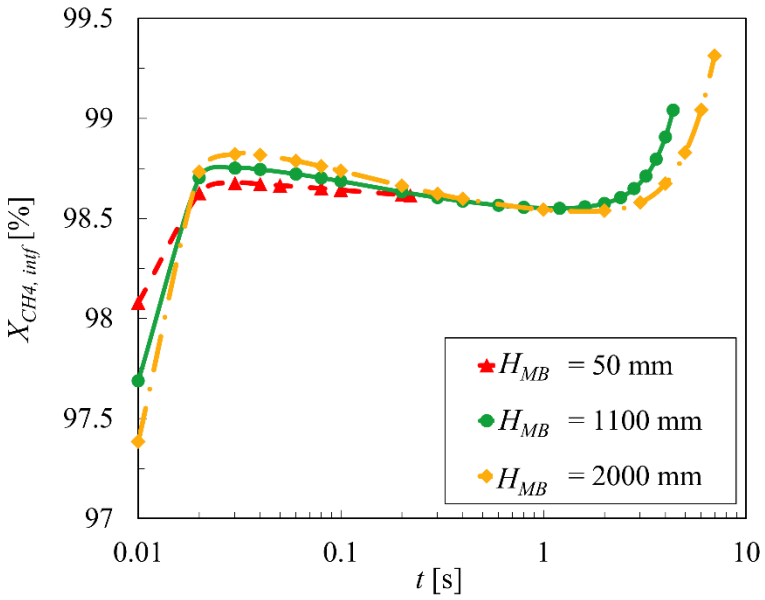

Figure 3.20. Calculated percentage of the portion of the total methane mole consumption that occurs at the interface of the bubble with the molten bath as a function of the time whilst it rises within the column for various heights of the molten bath. Other conditions are presented in Table 3.3 [44].

3.4.3.5 Sensitivity to the initial mole fraction of methane

The sensitivity of the calculated mean value of methane conversion, $X_{CH_4,m}$, to the initial mole fraction of methane within the bubble is presented in Figure 3.21a for the various blends of CH_4 and Ar. Figure 3.21b shows the calculated final mean value of methane conversion, $X_{CH_4,m,f}$, as a function of the ratio of methane in the gas mixture. As seen, with a decrease in the methane mole fraction from 100% to 10%, methane conversion increases approximately 12% from 0.80 to 0.91. That is because, by decreasing the initial mole fraction of methane, the partial pressure of methane within the gas bubble decreases and, based on Le Chatelier's principle, it favors the forward

reaction for further H_2 production. Consequently, more methane will be converted and hydrogen production increases [32, 77].

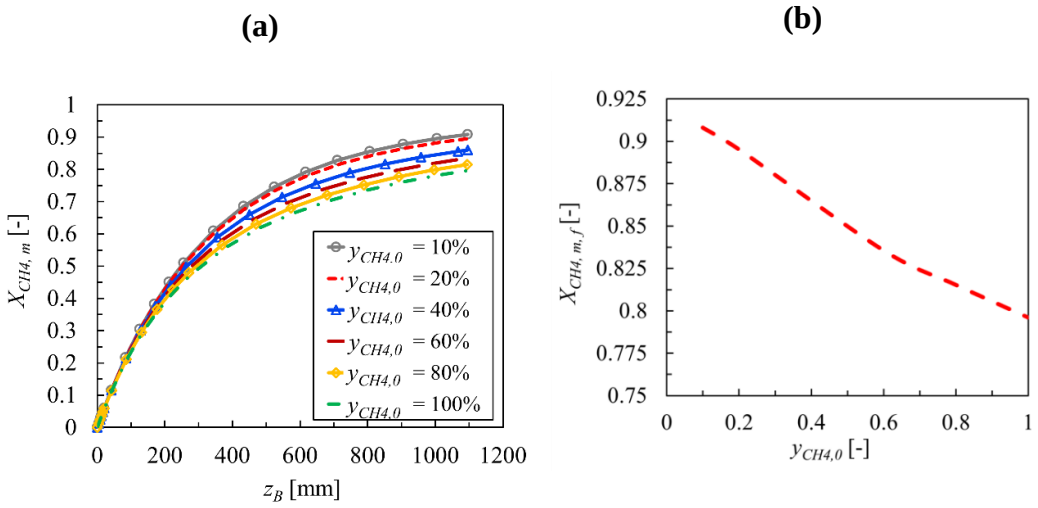

Figure 3.21. Calculated mean methane conversion a) within a bubble as a function of the distance of the bubble from the bottom of the column (z_B) for a series of initial mole fractions of CH_4 within the injected gas mixture of methane and argon, and b) at the top of the molten bath as a function of the initial mole fraction of methane in the injected gas. Other conditions are shown in Table 3.3 [44].

Figure 3.22 presents the estimated history of the fractions of the overall methane consumption at the interface of the bubble and the molten bath, $X_{CH_4,intf}$, as the bubble rises from the bottom to the surface of the molten bath for a series of initial compositions of the bubble. It can be seen that, in all assessed cases, the sensitivity is marginal, such that more than 97.5% of the conversion has occurred at the bubble-molten bath interface. Also, as the initial mole fraction of methane increases from 0.2 to 1.0, no variation is predicted in the initial values of $X_{CH_4,intf}$ at the bottom of the column. Nonetheless, the effect becomes more significant near the surface of the

column. Such that, $X_{CH_4,intf}$ decreases from 99.8% to ~99% as the initial mole fraction of methane is decreased from 1.0 to 0.2.

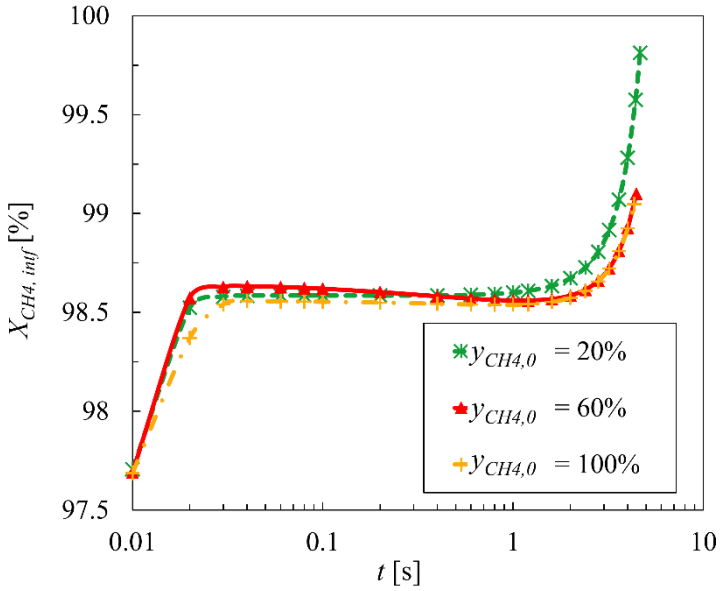

Figure 3.22. Calculated fraction of the methane consumption portion at the interface of the bubble with molten bath as a function of time, as it rises from the bottom to the surface of the molten bath for a series of initial mole fractions of CH_4 in the mixture of injected gas (argon as inert gas). Other parameters are summarized in Table 3.3 [44].

3.4.3.6 Sensitivity to the pressure

Figure 3.23a shows the calculated mean value of methane conversion as a function of the distance of the bubble from bottom of the column for a series of the pressures. As can be seen, by increasing the pressure of the column from 0.1 MPa to 8 MPa, conversion of methane within the column decreases. Figure 3.23b shows the calculated mean final value of conversion as a function of the column's pressure. As seen, the overall methane conversion decreases from >80% where the pressure is ~0.1

MPa to approximately 20% for a column with a pressure of 8 MPa. That could be as a result of the pressure on the diffusion of the methane to the surface of the bubble. By increasing the pressure, the bubble size less expands across the column. Moreover, as more forward reaction of methane decomposition occurs, concentration within the bubble increases and due to the smaller size of the bubble in a column with a high pressure, less methane diffuses to the gas-molten bath interface, hence, the overall methane conversion decreases. In assurance to the impact of the pressure on the bubble size variation, Figure 3.24 depicts the variation of the radius of the bubble through the column for a series of the pressure. For a column with a pressure of 0.1 MPa the bubble's final radius approaches to ~3 mm; however, by increasing the pressure to 8 MPa the bubble size enhancement reduces to a radius of <2.2 mm.

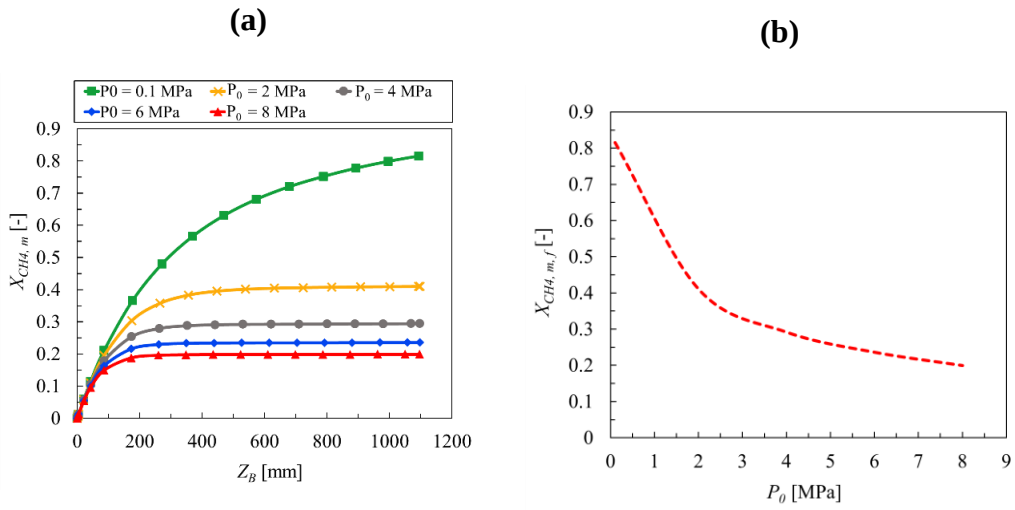

Figure 3.23. Calculated mean methane conversion a) within a bubble as a function of the distance of the bubble from the bottom of the column (z_B) for a series of the pressure, and b) at the top of the molten bath as a function of the pressure. Other factors are based on Table 3.3 [44].

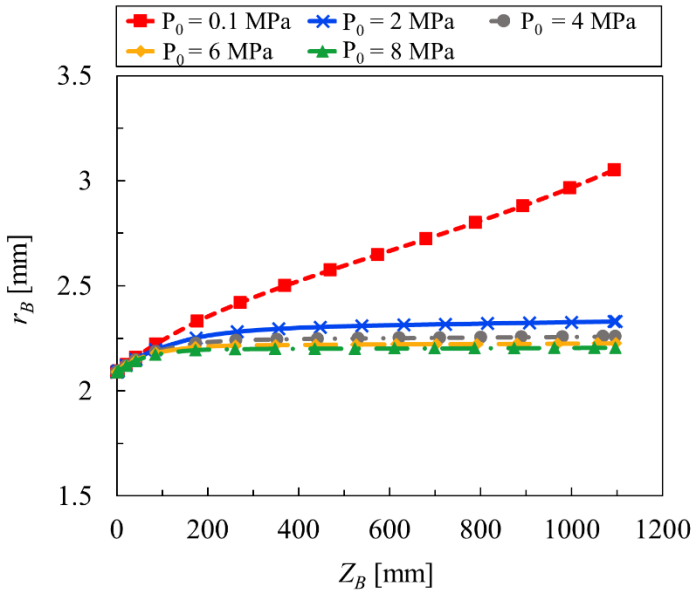

Figure 3.24. Calculated bubble radius as a function of the bubble's distance from bottom of the column for a series of the pressure. Other factors are based on Table 3.3 [44].

3.4 Conclusions

In conclusion, the reliable prediction of methane conversion within a rising and pyrolysing bubble in a column for hydrogen production requires that the variations of bubble size and rise velocity be considered. That is because they have a significant impact on the bubble residence time in the molten bath and, consequently, the amount of overall methane conversion. In the current study, for the reference case, the bubble radius increases from approximately 2.2 mm at the bottom of the column to 3 mm at the top of a 1100 mm molten $Ni_{0.27}Bi_{0.73}$ bath, while the bubble's rise velocity increases asymptotically, from 0.21 m/s to 0.30 m/s. Moreover, the current calculations showed that more than 97% of the total methane consumption occurs at the bubble's surface and less than 3% takes place within the gas phase of the bubble

for the selected conditions. This means that the presence of a catalyst in the molten bath has a substantial effect on the methane conversion. Furthermore, a sensitivity analysis to the parameters, including the molten bath temperature, initial gas temperature, the molten bath height, bubble size, and the gas composition revealed that:

1. By increasing the temperature of the bath from 1013 K to 1413 K, conversion increases by approximately 85%.
2. The initial temperature of the gas mixture influences the methane conversion logarithmically. The gas mixture within the bubble reaches the molten bath temperature soon after release from the nozzle, in less than 0.1 s for the studied range. Hence, an increase in the initial gas temperature from 313 K to 1313 K, increases the methane conversion from approximately 0.72 to 0.82.
3. The bubble size has an inverse influence on the methane conversion. In the studied range, by decreasing the radius of the bubble from 2.6 to 0.6 mm, methane conversion increases from approximately 0.77 to 0.89, respectively.
4. Methane conversion increases asymptotically by increasing the molten bath height. By increasing the molten bath height from 50 mm to 2000 mm, methane conversion increases by approximately 85.5%. It could be as a result of an increase in the bubble residence time within the bath from increasing the height of the molten bath. However, for the conditions assessed here, increasing the height of the column to values of more than 2000 mm up to 4000 mm, almost no variation in the conversion was seen.
5. Methane conversion decreases with an increase in the initial methane mole fraction in the injected gas mixture. That is because reduction of the methane

mole fraction within the gas mixture decreases its partial pressure, and it favors greater methane conversion based on Le Chatelier's principle.

6. Increasing of the bubble column's pressure from 0.1 MPa to 8 MPa, results in a decrease in methane conversion from >80% to approximately 20%. That could be due to the impact of the pressure on the bubble's size and reduction of the methane diffusion to the surface of the bubble.

Author declaration

The authors have no conflicts of interest to declare. All co-authors have seen and agree with the content of the manuscript.

Acknowledgments

This work is funded by the Future Fuels CRC, supported through the Australian Government's Cooperative Research Centers Program. We gratefully acknowledge the cash and in-kind support from all our research, government, and industry participants. Moreover, this work is supported by Discovery Grant DP180102045 from the Australian Research Council.

3.5 References-Chapter 3

[1] M.P. Ankica Kovač, Doria Marciuš, Hydrogen in energy transition: A review, International Journal of Hydrogen Energy, 46 (2021) 10016-10035.

[2] I.D. Haris Ishaq, Curran Crawford, A review on hydrogen production and utilization: Challenges and opportunities, International Journal of Hydrogen Energy, 47 (2022) 26238-26264.

[3] J.J.D. B. E. Lebrouhi, B. Lamrani, K. Benabdelaziz, T. Kousksou, , Global hydrogen development - A technological and geopolitical overview, International Journal of Hydrogen Energy, 47 (2022) 7016-7048.

[4] M.Y. Tahir Khan, Muhammad Waseem, , Review on recent optimization strategies for hybrid renewable energy system with hydrogen technologies: State of the art, trends and future directions, International Journal of Hydrogen Energy, 47 (2022) 25155-25201.

[5] S. Dillich, T. Ramsden, M. Melaina, Hydrogen production cost using low-cost natural gas, DOE Hydrogen and Fuel Cells Program, (2012).

[6] J.S. Omar Faye, Ubong Eduok, A critical review on the current technologies for the generation, storage, and transportation of hydrogen, International Journal of Hydrogen Energy, 47 (2022) 13771-13802.

[7] U. Bossel, Does a Hydrogen Economy Make Sense?, Proceedings of the IEEE, 94 (2006) 1826-1837.

[8] D. Paxman, S. Trottier, M. Nikoo, M. Secanell, G. Ordorica-Garcia, Initial Experimental and Theoretical Investigation of Solar Molten Media Methane Cracking for Hydrogen Production, Energy Procedia, 49 (2014) 2027-2036.

[9] G. Collodi, G. Azzaro, N. Ferrari, S. Santos, Techno-economic Evaluation of Deploying CCS in SMR Based Merchant H2 Production with NG as Feedstock and Fuel, Energy Procedia, 114 (2017) 2690-2712.

[10] J.P. Jeongdong Kim, Meng Qi, Inkyu Lee, Il Moon, Process Integration of an Autothermal Reforming Hydrogen Production System with Cryogenic Air Separation and Carbon Dioxide Capture Using Liquefied Natural Gas Cold Energy, Industrial & Engineering Chemistry Research, 60 (2021) 7257-7274.

[11] G.D.A. Duane B. Myers, Brian D. James, John S. Lettow, C.E. (Sandy) Thomas, & Reed C. Kuhn, Cost and Performance Comparison Of Stationary Hydrogen Fueling

Appliances in: N.C.-.-. Proceedings of the 2002 U.S. DOE Hydrogen Program Review (Ed.), (2002).
[12] J.R. Rostrup-Nielsen, J. Sehested, J.K. Nørskov, Hydrogen and synthesis gas by steam- and C02 reforming, Advances in Catalysis, Academic Press, (2002), 65-139.
[13] R. Van de Krol, M. Grätzel, Photoelectrochemical Hydrogen Production, https://doi.org/10.1007/978-1-4614-1380-6 (2012).
[14] R. Siavash Moakhar, S.M. Hosseini-Hosseinabad, S. Masudy-Panah, A. Seza, M. Jalali, H. Fallah-Arani, F. Dabir, S. Gholipour, Y. Abdi, M. Bagheri-Hariri, N. Riahi-Noori, Y.F. Lim, A. Hagfeldt, M. Saliba, Photoelectrochemical Water-Splitting Using CuO-Based Electrodes for Hydrogen Production: A Review, Adv Mater, 33 (2021) e2007285.
[15] M.R. Shaner, H.A. Atwater, N.S. Lewis, E.W. McFarland, A comparative technoeconomic analysis of renewable hydrogen production using solar energy, Energy & Environmental Science, 9 (2016) 2354-2371.
[16] T.F.M. Mohamed Nasser, Shinichi Ookawara, Hamdy Hassan, A review of water electrolysis–based systems for hydrogen production using hybrid/solar/wind energy systems, Environmental Science and Pollution Research, (2022).
[17] M.A. Furat Dawood, G. M. Shafiullah, Hydrogen production for energy: An overview, International Journal of Hydrogen Energy, 45 (2020) 3847-3869.
[18] K.W. Wei Xi, Yongli Shen, Mengke Ge, Ziliang Deng, Yunfeng Zhao, Qiue Cao, Yi Ding, Guangzhi Hu, Jun Luo, Dynamic co-catalysis of Au single atoms and nanoporous Au for methane pyrolysis, Nature Communications, 11 (2020).
[19] D.A.K. I-Wen Wang, Bingying Gao, Hanjing Tian, Jianli Hu, Methane Pyrolysis for Carbon Nanotubes and COx-Free H2 over Transition-Metal Catalysts, Energy Fuels, 33 (2019) 197−205.
[20] M.T. Clarke Palmer, Henrik H. Kristo ff ersen, John Gelinas, Michael J. Gordon, Eric W. McFarland, and Horia Metiu, Methane Pyrolysis with a Molten Cu−Bi Alloy Catalyst, ACS Catalysis, (2019) 8337−8345.
[21] O.D. Bert Metz, Heleen de Coninck, Manuela Loos, Leo Meyer, IPCC Special Report on Carbon Dioxide Capture and Storage, Cambridge University Press, (2005).
[22] D.W.A. G. Kreysa, I. Schultz Decarbonisation of Fossil Energy via Methane Pyrolysis, The Future Role of Hydrogen in Petrochemistry and Energy Supply DGMK Conference, (2010).

[23] Y. Itoh, K. Ozaki, R. Maezawa, Hydrolyzable-emulsifier-containing polymer latices as dispersants and binders for waterborne carbon black paint, Journal of Applied Polymer Science, (2013).
[24] M. Barekat, R.S. Razavi, S. Bastani, Effect of Carbon Black Pigment on the Surface Resistivity of the Black Silicone Thermal Control Coating, Advanced Materials Research, 472-475 (2012) 110-113.
[25] M. Steinberg, Fossil fuel decarbonization technology for mitigating, International Journal of Hydrogen Energy, (1999) 771-777.
[26] X.-h. Shao, J.-w. Zheng, Soil Organic Carbon, Black Carbon, and Enzyme Activity Under Long-Term Fertilization, Journal of Integrative Agriculture, 13 (2014) 517-524.
[27] C.b. pricing, https://m.echemi.com/productsInformation/pd20150901230-carbon-black.html, (2020).
[28] T.G. M. Plevan, A. Abánades, K. Mehravaran, R. K. Rathnam, C. Rubbia, D. Salmieri, L. Stoppel, S. Stückrad, Th. Wetzel, Thermal cracking of methane in a liquid metal bubble column reactor: Experiments and kinetic analysis, International Journal of Hydrogen Energy, 40 (2015) 8020-8033.
[29] E.W.M. Thomas C. Farmer, Michael F. Doherty, Membrane bubble column reactor model for the production of hydrogen by methane pyrolysis, International Journal of Hydrogen Energy, 44 (2019) 14721 -14731.
[30] N.R. Dohyung Kang, Michael J. Gordo, Horia Metiu, Eric W. McFarland, Catalytic methane pyrolysis in molten MnCl2-KCl, Applied Catalysis B: Environmental 254 (2019) 659–666.
[31] Y.J.L. Yong-Gyu Noh, Jina Kim, Yu Kwon Kim, JungSeub Ha, Shankara S. Kalanur, Hyungtak Seo, Enhanced efficiency in CO2-free hydrogen production from methane in a molten liquid alloy bubble column reactor with zirconia beads, Chemical Engineering Journal, 428 (2022).
[32] S.A. Sylvain Rodat, Jean-Louis Sans, Gilles Flamant, A pilot-scale solar reactor for the production of hydrogen and carbon black from methane splitting, International Journal of Hydrogen Energy, 35 (2010) 7748-7758.
[33] A.R. Abánades, Renu Kumar Geißler, Tobias Heinzel, Annette Mehravaran, Kian Müller, George Plevan, Michael Rubbia, Carlo Salmieri, Delia Stoppel, Leonid Stückrad, Stefan Weisenburger, Alfons Wenninger, Horst Wetzel, Thomas,

Development of methane decarbonisation based on liquid metal technology for CO2-free production of hydrogen, International Journal of Hydrogen Energy, 41 (2016) 8159-8167.
[34] H.Y. Wang, A.C. Lua, Hydrogen Production by Thermocatalytic Methane Decomposition, Heat Transfer Engineering, 34 (2013) 896-903.
[35] G.Y.H. Kang Kyu Lee, Ki June Yoon, Byung Kwon Lee, , Thermocatalytic hydrogen production from the methane in a fluidized bed with activated carbon catalyst, Catalysis Today, 93-95 (2004) 81-86.
[36] M.A.L. Manuela Serban, Christopher L. Marshall, and Richard D. Doctor, Hydrogen Production by Direct Contact Pyrolysis of Natural Gas, (2003).
[37] D.K. Nazanin Rahimi, John Gelinas, Aditya Menon, Michael J. Gordon, Horia Metiu, Eric W. McFarland, Solid carbon production and recovery from high temperature methane pyrolysis in bubble columns containing molten metals and molten salts, Carbon, 151 (2019) 181-191.
[38] G. Fau, N. Gascoin, J. Steelant, Hydrocarbon pyrolysis with a methane focus: A review on the catalytic effect and the coke production, Journal of Analytical and Applied Pyrolysis, 108 (2014) 1-11.
[39] C.A. Jarrett Riley, Ranjani Siriwardane, Robert Stevens, Technoeconomic analysis for hydrogen and carbon Co-Production via catalytic pyrolysis of methane, International Journal of Hydrogen Energy, 46 (2021) 20338-20358.
[40] M. Msheik, S. Rodat, S. Abanades, Methane Cracking for Hydrogen Production: A Review of Catalytic and Molten Media Pyrolysis, Energies, 14 (2021).
[41] S.T. D. Paxman, M. Nikoo, M. Secanell, G. Ordorica-Garcia, Initial Experimental and Theoretical Investigation of Solar Molten Media Methane Cracking for Hydrogen Production, Energy Procedia, 49 (2014) 2027-2036.
[42] C. Zhang, Liquid Metal Flows Driven by Gas Bubbles in a Static Magnetic Field (2009).
[43] J.A.M.J. Brandon Jose Leal Perez, E.G. Rajat Bhardwaj, Martin van Sint Annaland,, F. Gallucci, Methane pyrolysis in a molten gallium bubble column reactor for sustainable hydrogen production: Proof of concept &techno-economic assessment, International Journal of Hydrogen Energy, 46 (2021) 4917-4935.
[44] V.A. D. Chester Upham, Alexander Khechfe, Zachary R. Snodgrass, Michael J. Gordon, Horia Metiu, Eric W. McFarland, Catalytic molten metals for the direct conversion of methane to H2 and C, Research, (2017).

[45] S. Schneider, S. Bajohr, F. Graf, T. Kolb, Verfahrensübersicht zur Erzeugung von Wasserstoff durch Erdgas-Pyrolyse, Chemie Ingenieur Technik, 92 (2020) 1023-1032.
[46] M. Jafarian, Y. Chisti, G.J. Nathan, Gas-lift circulation of a liquid between two inter-connected bubble columns, Chemical Engineering Science, 218 (2020).
[47] M.R.A. Mehdi Jafarian∗, Graham J. Nathan, Preliminary evaluation of a novel solar bubble receiver for heating a gas, Solar Energy 182 (2019) 264–277.
[48] H.F. Abbas, W.M.A. Wan Daud, Hydrogen production by methane decomposition: A review, International Journal of Hydrogen Energy, 35 (2010) 1160-1190.
[49] P.B. A. Hornés, M. Fernández-García, A. Guerrero-Ruiz, A. Martínez-Arias, Catalytic and redox properties of bimetallic Cu–Ni systems combined with CeO2 or Gd-doped CeO2 for methane oxidation and decomposition. , Appl Catal B: Environ 111–112:96–105 (2012).
[50] D.P. N. Shah, GP. Huffman Hydrogen production by catalytic decom-position of methane., Energy Fuels, 15 (2001) 1528–1534.
[51] M.P. T. Geißler, A. Abánades, A. Heinzel, K. Mehravaran, , C.R. R. K.Rathnam, D. Salmieri, L. Stoppel, S. Stückrad, A. Weisenburger, H. Wenninger, Th. Wetzel, Experimental investigation and thermo-chemical modeling of methane pyrolysis in a liquid metal bubble column reactor with a packed bed, International Journal of Hydrogen Energy, 40 (2015) 14134-14146.
[52] F.S. Nazim Muradov, Ali T-Raissi, Catalytic activity of carbons for methane decomposition reaction, Catalysis Today, 102-103 (2005) 225-233.
[53] D.H.N.a.D.M.N. R. L. Datta, The properties and behaviour of gas bubbles formed at the circular orifice, Trans. Inst. Chem. Eng., 28 (1950) 14-26.
[54] S.A. Sylvain Rodat, Julien Coulié, Gilles Flamant, Kinetic modelling of methane decomposition in a tubular solar reactor, Chemical Engineering Journal, 146 (2009) 120–127.
[55] M.H. T. Bruno, A. Laesecke, E. Lemmon, R. Perkins, Thermochemical and thermophysical properties of JP-10, Advance Science Technology, 45 (2006) 1–67.
[56] J.W.M. Brett Parkinson, Thomas B. McConnaughy, D. Chester Upham, Eric W. McFarland, , Techno-Economic Analysis of Methane Pyrolysis in Molten Metals: Decarbonizing Natural Gas, Chemical Engineering & Technology, 40 (2017) 1022-1030.

[57] Y.T. Q. Sun, G. Gavalas, Methane pyrolysis in a hot filament reactor, EnergyFuels, 14 (2000) 490–494.
[58] D.S. H. Huang, L. Spadaccini, Endothermic heat-sink of hydrocarbon fuels for scramjet cooling, in: Endothermic Heat-Sink Hydrocarbon Fuels Scramjet Cooling. , 38th AIAA/ASME/SAE/ASEE Joint Propulsion Conference and Exhibit, Indianapolis, (2002) 3871.
[59] K.E.S.T. Tiina Keipi, Henrik Konttinen, Jukka Konttinen, Thermo-catalytic decomposition of methane: The effect of reaction parameters on process design and the utilization possibilities of the produced carbon, Energy Conversion and Management, 126 (2016) 923-934.
[60] E.R. A. Abánades, E. M. Ferruelo, F. Hernández, A. Cabanillas, J. M. Martínez-Val, J. A. Rubio, C. López, R. Gavela, G. Barrera, C. Rubbia, D. Salmieri, E.Rodilla, D.Gutiérrez, Experimental analysis of direct thermal methane cracking, International Journal of Hydrogen Energy, 36 (2011) 12877-12886.
[61] P.B.G. Md. Tariqul Islam, Ji Cheng, Mohammad Salah Uddin, Single bubble rising behaviors in Newtonian and non-Newtonian fluids with validation of empirical correlations: A computational fluid dynamics study, Engineering Reports, (2019).
[62] Y.J. Xiaokang Yan, Lijun Wang , Yijun Cao, Drag coefficient fluctuation prediction of a single bubble rising in water, Chemical Engineering Journal, 316 (2017) 553–562.
[63] N.G.D. D. Darmana, J. A. M. Kuipers, Detailed modeling of hydrodynamics, mass transfer and chemical reactions in a bubble column using a discrete bubble model, Chemical Engineering Science, 60 (2005) 3383-3404.
[64] M.L. Liang Hu, Wenyu Chen, Haibo Xie, Xin Fu, Bubbling behaviors induced by gas-liquid mixture permeating through a porous medium, Physics of Fluids, 28 (2016).
[65] F.I. Giorgio Besagni, Thomas Ziegenhein, Two-Phase Bubble Columns: A Comprehensive Review, Chem Engineering, 2 (2018).
[66] S.Y. Satoshi Nihonyanagi, and Tahei Tahara, Ultrafast Dynamics at Water Interfaces Studied by Vibrational Sum, Chemical Reviews, 117 (2017) 10665 − 10693.
[67] R. Kusaka, S. Nihonyanagi, T. Tahara, The photochemical reaction of phenol becomes ultrafast at the air-water interface, Nat Chem, 13 (2021) 306-311.

[68] A.V. Nguyen, Prediction of Bubble Terminal Velocities in Contaminated Water (1998).
[69] H.S. A.V. Nguyen , G. Zobel, H.J. Schulze An improved formula for terminal velocity of rigid spheres (1997).
[70] D.D. Arun K. Saha, Rajesh Srivastava, P.K. Panigrahi, K. Muralidhar, Fluid Mechanics And Fluid Power-Contemporary research .pdf>, Springer, (2017).
[71] H.B.P.a.T.J. Hirt, The activation energy for the Pyrolysis of methane, (1963).
[72] a.J.H.L.V. John H. Lienhard IV A Heat transfers textbook, (2017).
[73] J.H. Lienhard, A Heat Transfers Textbook, (2017).
[74] R. E.Treybal, Mass Transfer Operations, New York: McGraw-Hill, (1980).
[75] S. Sanaye, J. Mahmoudimehr, Technical Assessment of Isothermal and Non-Isothermal Modelings of Natural Gas Pipeline Operational Conditions, Oil & Gas Science and Technology – Revue d'IFP Energies nouvelles, 67 (2012) 435-449.
[76] J.S.F. R. J. ANDREINI, AND R. W. CALLEN, Characterization of Gas Bubbles Injected into Molten Metals under laminar flow condition, (1977).
[77] J.A.M.J. Brandon José Leal Pérez, Rajat Bhardwaj, Earl Goetheer, Martin van Sint Annaland, Fausto Gallucci, Methane pyrolysis in a molten gallium bubble column reactor for sustainable hydrogen production: Proof of concept & techno-economic assessment, International Journal of Hydrogen Energy, 46 (2021) 4917-4935.

3.6 Supplementary information

A- (Calculation of the gas temperature passing through a submerged nozzle)

The temperature of the gas passing through a submerged nozzle in the molten bath was calculated via Eq. A-1, as follows:

$$-\rho c_p U_g \frac{\partial T}{\partial z_P} + \frac{h\, p_s}{A_c}\left(T_g - T_{wall}\right) = 0\ . \qquad \text{(A-1)}$$

In this equation, ρ, c_p, U_g, p_s and A_c are the density, heat capacity, gas velocity, nozzle perimeter and the cross-sectional area of the nozzle. T_g and T_{wall} are the gas and the nozzle wall temperatures, respectively. z_P stands for the axial distance along the nozzle pipe. A temperature equal to the molten bath was employed as the nozzle wall temperature, T_{wall}. Also, the initial temperature of the gas in the nozzle was assumed to be 298 K. Based on the calculations via Eq. A-1, as Figure A-1a and b show, the gas achieves the molten bath temperature by passing about 900 mm inside the nozzle for the conditions of Upham *et al*'s [44] experiment and it reaches 1000 K at the nozzle tip for Rahimi *et al*'s [37] experimental conditions.

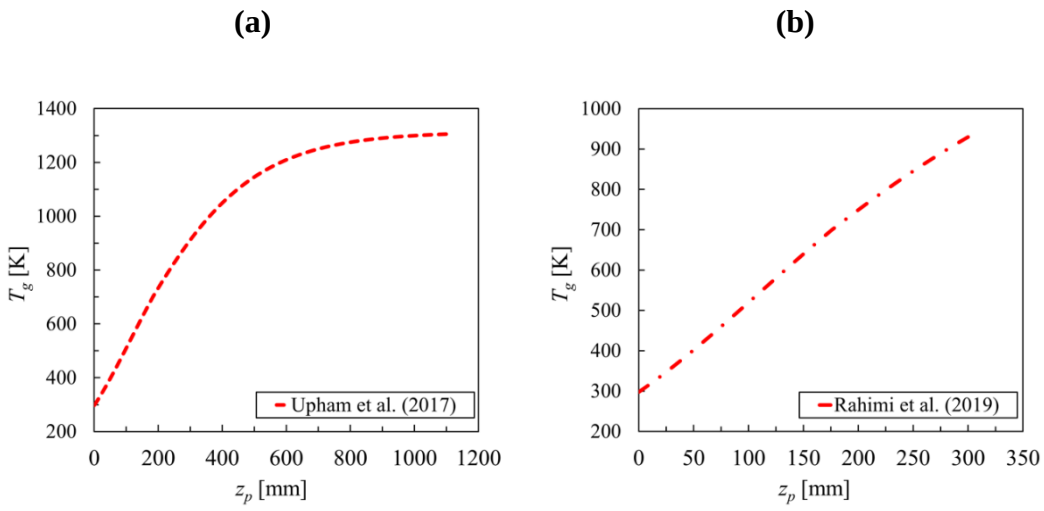

Figure A-1. Calculated temperature of the gas passing through the nozzle as a function of the length of time the submerged nozzle is in the molten bath for both selected experimental setups based on a) Upham *et al*'s, and b) Rahimi's experimental conditions [44].

B- (Analytical solution of the energy balance equation)

The heat transfer equation in a non-reacting bubble is given by Eq. B-1, as follows:

$$-\frac{1}{r^2}\frac{\partial}{\partial r}\left(r^2 k\frac{\partial T}{\partial r}\right) = \rho c_p \frac{\partial T}{\partial t} \ . \quad \text{(B-1)}$$

The abovementioned equation in a non-reacting bubble was solved analytically through the following calculation steps:

$$T = R(r)Q(t) \ . \quad \text{(B-2)}$$

$$\frac{\partial T}{\partial t} = R(r)Q'(t) \ . \quad \text{(B-3)}$$

$$\frac{\partial T}{\partial r} = R'(r)Q(t) \ . \quad \text{(B-4)}$$

$$\frac{\partial^2 T}{\partial r^2} = R^{"}(r)Q(t) \ . \quad \text{(B-5)}$$

where T is the temperature and it is a function of r and t. Then, the equation transforms to the following format:

$$\frac{Q\prime(t)}{Q(t)} = \frac{R"(r)}{R(r)} + \frac{2}{r}\frac{R\prime(r)}{R(r)} \ . \quad \text{(B-6)}$$

$$\frac{R"(r)}{R(r)} + \frac{2}{r}\frac{R\prime(r)}{R(r)} = M \ . \quad \text{(B-7)}$$

$$Q'(t) - MQ(t) = 0 \ . \quad \text{(B-8)}$$

$$rR"(r) + 2R'(r) - MrR(r) = 0 \ . \quad \text{(B-9)}$$

$$(rR(r))" - M(rR(r)) = 0 \ . \quad \text{(B-10)}$$

If we consider that:

$$S(r) = rR(r) \ . \quad \text{(B-11)}$$

then Eq. B-10 will be as follows:

$$S" - MS = 0 \ . \quad \text{(B-12)}$$

$$S(r) = \frac{\sin\sqrt{-Mr}}{\sqrt{-M}} \ . \quad \text{(B-13)}$$

To solve Eq. B-1 numerically, a meshing on the bubble was considered and based on the northern and southern meshes of each one, the solution is as follows:

$$4k\pi r_s^2 \ \frac{T_S - T_p}{\Delta r} + 4k\pi r_s^2 \ \frac{T_N - T_p}{\Delta r} = 4\pi\rho C_p r^2 \Delta r \frac{\partial T}{\partial t} \ . \quad \text{(B-14)}$$

in which subscripts $'S'$, and $'N'$ show the southern and northern meshes of each mesh $'P'$. To simplify the equation, multipliers are given as follows:

$$a_s = \frac{kr_s^2}{\Delta r} \ . \quad \text{(B-15)}$$

$$a_n = \frac{kr_n^2}{\Delta r} \ . \quad \text{(B-16)}$$

$$a_0 = \frac{\rho C_p r^2 \Delta r}{\Delta t} \ . \quad \text{(B-17)}$$

$$T_P^{t+\Delta t} = \frac{a_s T_S^{t+\Delta t} + a_s T_N^{t+\Delta t} + a_0 T_P^t}{a_s + a_n + a_0} \ . \quad \text{(B-18)}$$

The analytical solution results were compared with the numerical results, as shown in Figure B-1 a and b. It can be seen that there is a very good agreement between the analytical and numerical solution results for cases where the inial radius of the bubble is 0.1 mm: within less than 1% error. In the case that the bubble initial radius, $r_{B,0}$, is 6 mm, there is a deviation between the analytical and numerical calculation results where , $r < 1.5$ mm; however, this deviation is less than 20% and it decreases when the radial distance is increased.

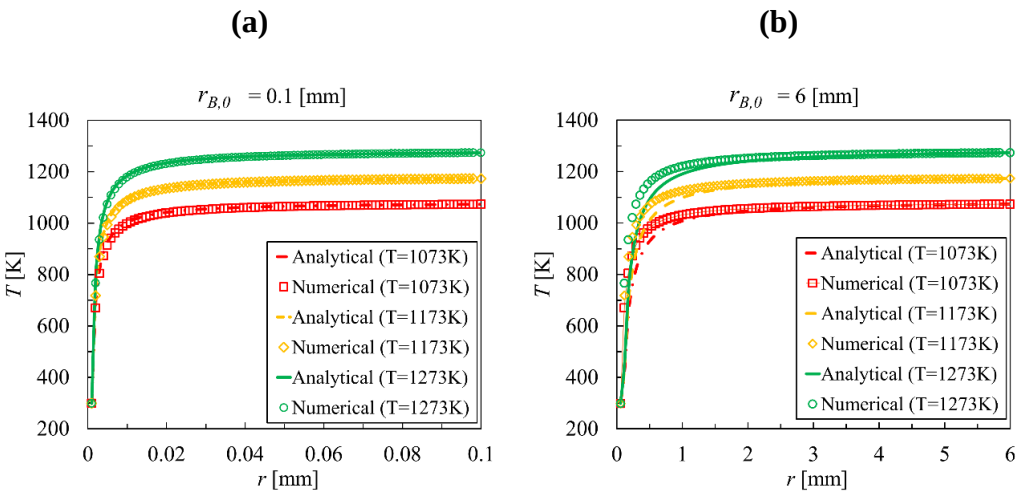

Figure B-1. Temperature distribution in the radial direction for a bubble with an initial radius of a) 0.1 mm and b) 6 mm, for comparison of the numerical and analytical solution techniques for the energy balance equation in a rising and non-reacting bubble within a molten tin column.

CHAPTER 4

CONCLUSIONS AND FUTURE WORK

The threat of global warming has inclined the world either to capture and sequestrate emitted CO_2 resulting from burning fossil fuels or to use low emission/clean energy sources (e.g., hydrogen, renewable energies) as an alternative to conventional fuels (e.g., hydrocarbons and fossil fuels) to reduce and mitigate the CO_2 emissions. Hydrogen (H_2), as a clean fuel, burns without emissions of gaseous carbon products (e.g., CO_x) and hence seems to be a promising substitute for the current fossil fuels to address a huge portion of the world's air pollution challenge. Currently, the majority of H_2 is produced via steam methane reforming (SMR), as the most cost-effective method for industrial scale H_2 production. The main drawback of SMR is the level of CO_2 emissions. In this field, methane pyrolysis has manifested itself as a promising technique for hydrogen production without CO_2 emissions. To save time and resources for the scale-up of the methane pyrolysis within a molten catalyst bath as a competitor for industrial-scale SMR, the underlying phenomena of the process should be well understood, and the relative importance of fundamental factors should be mathematically explained. In the following subsections, the significance of the current study and some suggestions for future work are presented.

4.1 Significance of the present work

A 1-D numerical model of a rising and pyrolysing bubble was developed through simultaneous solution of the principal governing equations of mass, momentum, and energy. The model was validated against some of the experimental results available in the literature. The impact of the operating parameters, namely the molten bath temperature, initial gas composition, gas temperature, bubble column height, bubble size, and pressure were studied. The results showed that the bubble size and rise velocity inversely influence the residence time of the bubble within the column and consequently the final conversion of methane and hydrogen production. For the studied conditions, the bubble's radius increased from 2.2 mm to approximately 3 mm in a molten $Ni_{0.27}Bi_{0.73}$ bath with a height of 1100 mm. Meanwhile, the bubble rise velocity increased from 0.21 to 0.30 m/s.

In accordance with the catalytic effect of the molten bath on the decomposition reaction, calculations were undertaken to find out the fraction of the hydrogen conversion occurring on the internal surface of the bubble compared with the space inside it. The results revealed that for the studied conditions, methane consumption at the gas-molten bath interface (i.e., internal surface of the bubble) is more than 97%, which it is consistent with methane consumption within a bubble being less than ~3%. Moreover, a sensitivity analysis to the independent parameters showed that:

1. By changing the molten bath temperature from ~1000 K to ~1400 K about 85% enhancement was achieved for the overall methane conversion.
2. The injected gas rapidly reached the molten bath temperature, in less than 0.1s. Despite that, the overall methane conversion decreased approximately 10%,

from 0.82 to 0.72, where the initial temperature of the injected gas was decreased from 1313 K to 313 K, respectively.

3. By increasing the bubble size from 0.6 to 2.6 mm, methane conversion decreased from ~0.89 to ~0.77 (12%). It could be because of the bubble radius's impact on its rising velocity. A smaller bubble spends more time in contact with the molten bath due to its lower rising velocity compared with a larger one. By increasing the bubble residence time, the gas content will have more time for heat and mass transfer, and consequently more methane will be converted to H_2 and C.
4. The molten bath height influenced the overall methane conversion. By increasing the height, the methane content of the bubble spends more time in contact with the molten media, which resulted in an increase in the conversion. An increase of the molten bath height from 50 to 2000 mm caused a rise of about 85.5% in the total conversion of methane. However, an increase in the height of the molten bath from 2000 mm to 4000 mm had almost no impact on the overall conversion.
5. A decrease in the initial methane mol fraction within the injected gas from 1.0 to 0.1, showed an increase in the methane conversion from ~0.8 to more than 0.9. That could be due to a decrease in the partial pressure of methane within the bubble according to Le Chatelier's principle.
6. By decreasing the column pressure from 8 MPa to 0.1 MPa, methane conversion increased from 0.2 to more than 0.8: that could be attributed to the impact of the pressure on the bubble's size and the reduction in the methane diffusion to the surface of the bubble.

4.2 Recommendations for future work

The work presented in this thesis was focused on the impact of some main affecting parameters on methane conversion within a single rising and pyrolysing bubble in a molten catalyst bath. Further studies are required to develop greater understanding about the phenomena and concepts in order to commercialise this technique. Some gaps to be addressed in future work are as follows:

1. The behavior of the product carbon within the bubble. It is still unknown whether or not it forms a layer at the bubble's surface or disperses within the bubble. It is of importance to know its performance because it may have an impact on the methane diffusion to the gas-molten bath interface, where most of the conversion occurs.
2. The interactions of multiple bubbles within a column. It is necessary to investigate how these interactions affect the bubble size, the rise velocity and consequently the overall methane conversion.
3. The impacts of some other inert gases (e.g., N_2, He). Each inert gas may have a different effect on the methane diffusion to the gas-molten bath interface and methane conversion.
4. The effect of the non-hydrogen-saturated molten metal bath on methane conversion, overall bubble size, and the contribution of the surface reactions. The unsaturated molten bath could affect the methane diffusion within the bubble to the gas-molten metal interface, where most of the conversion occurs.
5. The effect of applied pressure on methane conversion and the temperature profile under a constant bubble size.